ADDIS ABABA UNIVRSITY

ADDIS ABABA INSTITUTE OF TECHNOLOGY

School Of Mechanical and Industrial Engineering

Investigations of Dynamic and Thermo-mechanical Wheel-Rail Contact Effects on the Rail

A Thesis Submitted to the School of Graduate Studies of Addis Ababa Institute of Technology in Partial Fulfillment of the Requirement for the Degree of Masters of Science in Mechanical Railway Engineering.

By

Getu Ejeta

Advisor

Mr. Habtamu Tkubet

March 23, 2015

ADDIS ABABA UNIVERSITY

Addis Ababa Institute of Technology

School of Mechanical and Industrial Engineering

(Stream: Mechanical Railway Engineering)

Master's Program Final Thesis Acceptance Approval Form

Thesis Topic: Investigations of Dynamic and Thermo-mechanical Wheel-Rail Contact Effects on the Rail

By: Getu Ejeta

Approved By Board Of Examiners:

Mr. Habtamu Tkubet Advisor	Signature	20/05/11 Date
Mr. Tolossa Deberie Internal Examiner	Signature	19/05/2015 Date
Dr. Daniel Tilahun External Examiner	Signature	20/05/2015 Date
Dr. Birhanu Beshah Railway Head Center	Birhanu Beshah(PhD) Head,Railway Engineering Centre Signature	21/05/15 Date

Director of Postgraduate Program

Addis Ababa University Addis Ababa Institute of Technology

Declaration

I, the undersigned, declare that this thesis report entitled- "**Investigations of Dynamic and Thermo-mechanical Wheel-Rail Contact Effects on the Rail"** is the result of my own research carried out under the supervision of Mr. Habtamu Tkubet. It has not been presented as a thesis in any other university and all source of material used for this thesis are duly acknowledged.

Getu Ejeta _____ Date_____

This is to certify that the above declaration made by the candidate is correct to the best of my knowledge.

Mr. Habtamu Tkubet _____ Date_____

[Advisor]

Acknowledgement

First, I would like to give my magnificence and respect to the Almighty God for his giving me strength, patience and invaluable cares throughout the course of my life and completion of this work and frontward too.

Next and for most, I wish to express my genuine thankfulness to my advisor Mr. Habtamu Tkubet for his valuable assistance, consistent guidance, support and encouragement in bringing this thesis work to a successful completion.

Truthful extended acknowledgement go to my friends Ashebir Worku and Ayantu Temesgen for their kindly support in the course of the study that makes me miss of the missing and gain this achievement.

Last but not least, I express my special appreciation to my dearest families for their endless love, support and reassurance throughout of the work that I can never be repaid.

Abstract

The purpose of the study is to investigate the dynamic and thermo mechanical effects of the rail due to the wheel-rail contact. The guidance of railway vehicles are done by the rails with the carrying wheel loads coming from the axles. But, different loads coming to it may cause damages, especially the heads at the joints and the webs. The friction and thermal power penetrant at the continuous rail surfaces, the cracking of the head ends, deformation of fish plate, high impact force, the contact probe energy generation and vibrations due to discrete contact area and rail heads dip down to a joint even on both sides are some of the problems.

Therefore, this study focused on two loading effects on the rail. The first is the investigation of dynamic effects and the second is thermo-mechanical effects of the contacts between vehicles and rail track during braking. In dynamic analysis, the modal and mechanical transient effects are investigated. Since, a modal analysis is performed on a pre-stressed structure; the static loading effect was first validated. The results for the first five mode shapes of natural frequencies and maximum deformations are: (42.136, 212.22, 259.08, 371.5, 617.67) Hz and (1.1506e-002, 1.1544e-002, 1.1039e-002, 6.3931e-002, 5.0965e-002)m respectively for the continuous rail, and (80.326, 263.43, 335.32, 513.47, 774.65)Hz and (1.116e-002, 1.089e-002, 1.194e-002, 5.4382e-002, 4.8243e-002)m for the jointed rail respectively. In the transient, the total deformations are: 1.4297e-005m & 1.4577e-005m and the Von-mises stresses are: 14.923 Mpa & 20.739 Mpa for the continuous and the jointed rail respectively. Also, the transient total velocity, total acceleration, the joint probe impact forces and the energy probe (for both kinetic and potential) are investigated. Thus, the maximum deformation and von-mises stress of the rail at the joint for the transient is larger than at continuum part.

In thermo-mechanical analysis, the transient thermal effects on the rail, in addition to the static mechanical loads were explored. In this case, the rail body temperature that is generated during braking was imported to the mechanical loading and the combined effects were explained. The thermo-mechanical braking effects developed on the three rail track level conditions: during the downgrade braking, at the straight track braking and at the curved track braking. The maximum temperature rises for the three cases (℃) are: 49.373, 42.576, 378.77 and the thermo-mechanical von mises stresses (Mpa) are:57.42,43.42 and 41.87. As shown in results, the combined thermal and mechanical effects are the highest at the downhill braking.

Keywords: Rail, dynamic, mode shape, thermo-mechanical

Table of Contents

List of table

List of figure

Nomenclature

a, b: semi-axes of wheel-rail elliptical contact

E_w, E_r : Young's modulus of elasticity of the wheel and the rail, respectively (N/m2)

v_w, v_r : Poisson's ratio for the wheel and the rail, respectively

R_1^w : Principal rolling radius of the wheel (m)

R_2^w : Transverse radius of curvature of the wheel profile at the contact point (m)

R_1^r: Principal rolling radius of the rail (m)

R_2^r: Transverse radius of curvature of the rail profile at the contact point (m)

E_k: kinetic energy

E_p: potential energy

W_a : Half axle load,

W_w : Wheel weight,

K_H : Hertzian contact stiffness,

K_p: Rail pad stiffness,

C_p : Rail pad damping coefficient,

K_b : Ballast stiffness ,

C_b: Ballast damping coefficient.

F_{stat}: Static wheel load,

R_w : Wheel radius,

R_r : Transversal railhead radius

l : Distance between two supports [m]

EI: Bending stiffness of rail (static) [Nm2]

m : Mass of the rail per unit length [kg/m]

k : Modulus of foundation stiffness,

I: Moment of inertia of the rail

T_∞: Temperature of the surrounding

u : Velocity field

V_s: Sliding velocity

Q: Heating power per unit volume

M_r: Lumped mass matrix on rail

z_r: Nodal displacement

q_r: Forces vector on the rail

f: wheel-rail contact force

X_w: Wheel displacement

X_r: Rail displacement

r: Rail roughness

N: Normal load at the wheel-rail contact

M: Mass of the tramcar

I_i : Polar inertial moment of rotating parts

F_b: Maximum instantaneous braking force [N]

F_c: Curve resistance forces in [N].

Ω: Heat partitioning parameter

P: Peak pressure in GPa

μ: Wheel-rail friction coefficient

t_c : Traction coefficient

w: Average wear rate in nm/cycle

CHAPTER-ONE: INTRODUCTION

1.1. Background and Justification of the Study

The railway is one of the safest, high speed, and durable mode of transport. Long before railway transport developed into the effective and complex system as generally understood today, rails were used to guide horse-drawn vehicles and by 1767 iron rails had been introduced [1]. By the mid-1800s, the general form of rail and wheel had developed into something very similar to those in use today. At the start of the 19th century, mechanically powered rail transport had started to develop, initially by modification and transfer onto wheels of stationary steam engines, which had by that time become commonplace. At the late of 19^{th} century, in 1896, Hertz developed the first scientific description of the wheel/rail contact. He developed an analysis method to describe the elastic contact of glass lenses but, following its publication, it was found that it could also be used to describe contacts within rolling element bearings, between gear teeth, and between rails and wheels which is an elliptical form.

Metal wheels rolling on metal rails are the principal characteristic that distinguishes railways from other forms of transport. Wheel and rail meet at a contact patch that is small (typically about 100 mm^2) [1] and carries the full wheel load through which all steering, traction, and braking forces are transmitted. This contact patch sees a severe working environment. Stresses normal to the plane of contact can reach values several times the wheel or rail tensile strength, and sometimes shear stresses in the plane of contact can exceed the shear yield stress. Rapid temperature rises, caused by relative slip between the wheel and rail, can reach several hundred degrees Celsius in routine operation, and over 1000°C in extreme circumstances. These stress and temperature conditions inevitably lead to wear, deformation, and damage to the wheels and rails; and a major goal of railroads is to arrange service conditions and maintenance procedures to minimize deterioration and hence extend component life. This is important because rails and to a lesser extent wheels constitute a large part of a railroad's asset base.

Since the adoption of steel rather than iron as the material of choice for rails, the wheel/rail system has remained virtually unchanged. However, this does not imply that the system is ideal. The wheel/rail contact area is typically the size of a small coin. The material in and around the contact area is therefore highly stressed. High rates of wear might be expected for

such a contact but, in addition, because the load is applied and removed many times during the passage of each train, there is the possibility of fatigue of the rail surface.

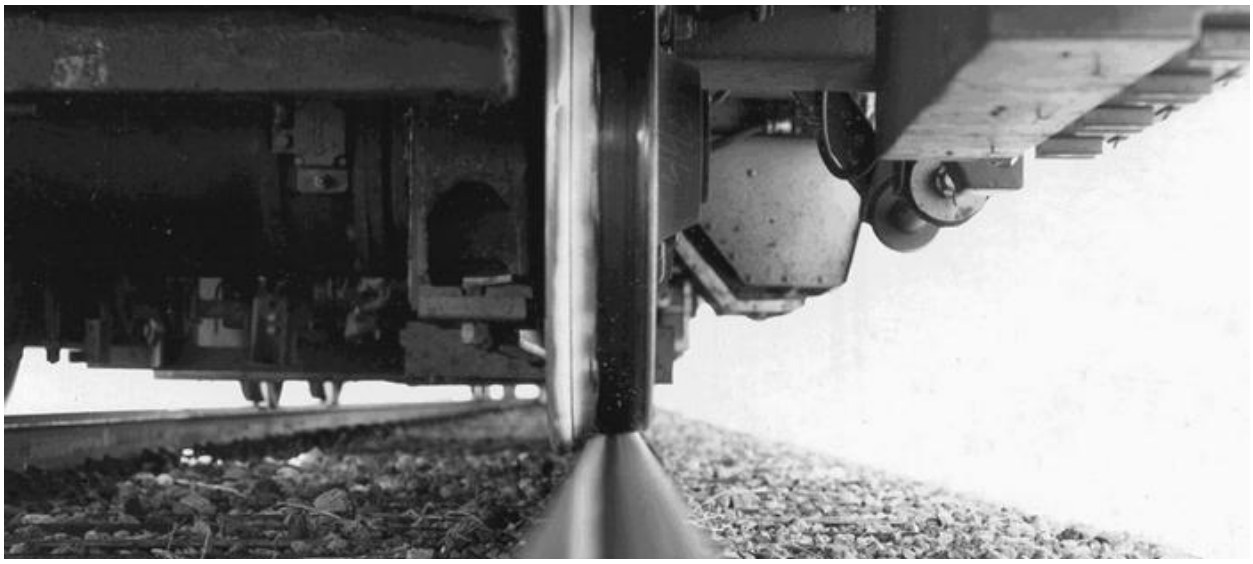

Fig.-1: The first steel wheel rolling on a steel rail [1]

From the start, the wheel-rail contact has been of critical interest to railway engineers. Because of, the performance of rail vehicles is inevitably tied to tiny areas where the wheels meet the rails. This highly-stressed interface is the root to almost all research areas of interest in vehicle-track interaction, especially, for the dynamic performance. The vehicle itself and its guidance, the track, cannot be regarded separately if the dynamic behavior is described. Vehicle and track are coupled by the wheel-rail contact. This enables to support the vehicle, to guide it along the track and to transmit acceleration and braking forces. For the comprehension of the system the geometric and physical properties of the wheel-rail contact is a vital point.

Wheels and rails are subjected to large numbers of repeated contacts. This repeated rolling or sliding contact stresses the material cyclically, and it responds in one of the following four ways [1]:

1. **Perfectly elastic behavior:** This behavior occurs if the contact pressure does not exceed the elastic limit during any load cycle.
2. **Elastic shakedown:** It is in which plastic deformations takes place during the early cycles, but, due to the development of residual stresses and sometimes strain hardening, the steady-state behavior is perfectly elastic. This process is known as shakedown, and the contact pressure below which this is possible is referred to as the elastic shakedown limit.

3. **Plastic shakedown:** It is in which the steady state is a closed elastic-plastic loop, but with no net accumulation of plastic deformation. This behavior is sometimes referred to as cyclic plasticity and the corresponding limit is called the plastic shakedown limit or the ratcheting threshold.
4. **Ratcheting threshold**: The steady state consists of open elastic-plastic loops, and the material accumulates a net unidirectional strain during each cycle, a process known as ratcheting

The most feasible study railway systems are dealing with both static and dynamic effects. Static analysis gives normal contact stress under a specified loading condition. Dynamic assessment is usually performed using vehicle simulation software, which provides detailed information on vehicle dynamics and wheel/rail interaction, including normal forces, tangential forces, displacements, velocities, accelerations, and other dynamic parameters for wheel and rail contact patches. One dynamic effect that would be created at the wheel-rail contact is mechanical effect. Dynamic loads (e.g., at rail-joints or in turnouts points) are much higher, with vertical accelerations reaching values of 100 g (1000 m/s ^{2}). This is a consequence of the high stiffness of the wheel/rail interface.

The most important effect is mechanical train vibrations that are generated at the wheel-rail contact. The instantaneous creation and propagation of rail vibration, wheel vibration and radiated noise will occur during the transit of a tramcar. This vibration is mainly the result of rolling contact. Rolling vibration is caused by vibrations of the wheel and track structures, induced at the wheel-rail contact point by vertical irregularities in the wheel and rail surfaces [18]. A similar mechanism leads to vibrations due to discontinuities in the wheel or rail surface (impact vibrations). Also, the mechanical vibrations occur in sharp curves and are induced by unsteady friction forces at the wheel-rail contact [11]. Vibration refers to the oscillating movement of any object [21].

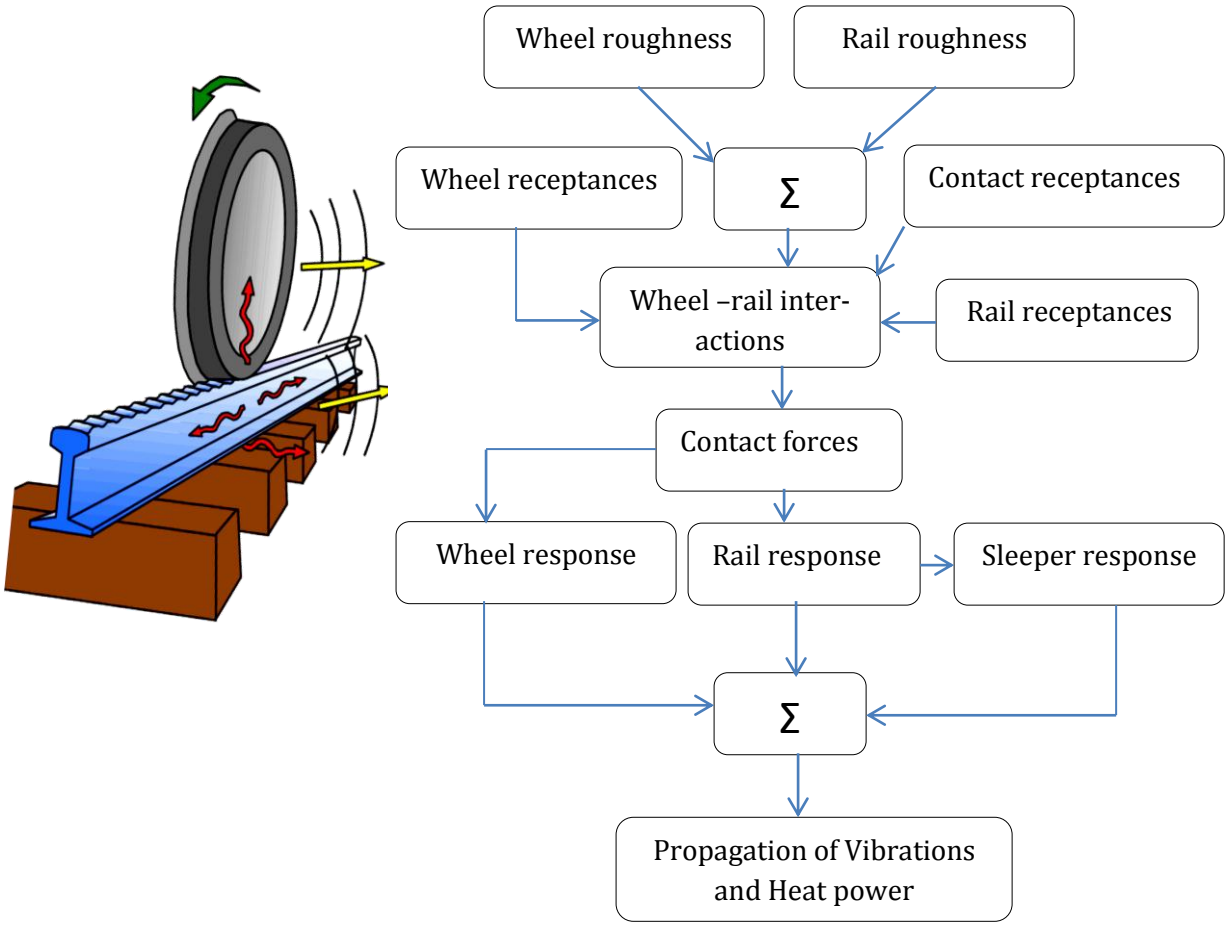

Fig.-2: Track-wheel interaction and vibration propagation diagram, [10]

A moving train creates a moving force and the stress pattern that move with it. This moving stress pattern must impress stress waves into the surrounding ground even in the absence of any imperfections or periodic irregularities in the vehicle or the track. The track itself does not provide uniform support; the rails, themselves of fixed length, are supported on sleepers placed at regular intervals, and the sleepers are in turn surrounded by and resting upon stone ballast. All of these track features can be expected to contribute to the stress field present in the ground below and beside the train [30].

To analyses the dynamic behavior of railway vehicles running on arbitrary tracks under arbitrary maneuvers, usually the vehicle (and if necessary the environment) is represented as a multi-body system. A multi-body system consists of rigid bodies, interconnected via massless force elements and joints. Due to the relative motion of the system's bodies, force elements generate applied forces and torques. Typical examples of such force elements are springs, dampers, and actuators combined in primary and secondary suspensions of railway vehicles. Contrarily, joints give rise to constraint forces by constraining the relative motion of the sys-

tem's bodies. The scope of application begins with simple single-axis rotational joints, and ends with highly complex and specific ones, like the so-called 'wheel–rail joints' guiding bodies along arbitrary tracks. To take the flexibility of lightweight structures into account, an interface between MBS software and Finite Element (FE) software has been implemented in many simulation programs. In the first step, a number of mode shapes of the body to be modeled elastically are analyzed by FE analysis. Then the results are transferred to the multi-body simulation, resulting in a "hybrid" model consisting of rigid and elastic bodies. Finally, on behalf of a dynamic stress analysis of the flexible body's most vulnerable locations, the dynamic forces and accelerations following from time-integration of the system equations can be shifted back to the FE software.

The linear analysis (also called modal analysis) performs an eigenvalue calculation on the matrices that represent the equations of motion. This will indicate the natural frequencies of the various modes of oscillation. The motion can be self-exciting and become unstable, and the eigenvalue analysis can indicate the critical speed at which this instability, or hunting, may occur. In practice, vehicle speed gradually increases until the real part of the complex eigenvalues is not negative, but equal to zero. This speed corresponds to the critical speed of the vehicle.

Generally, rail has three main parts that together can withstand the wheel load. These are: the head, the web and the foot.

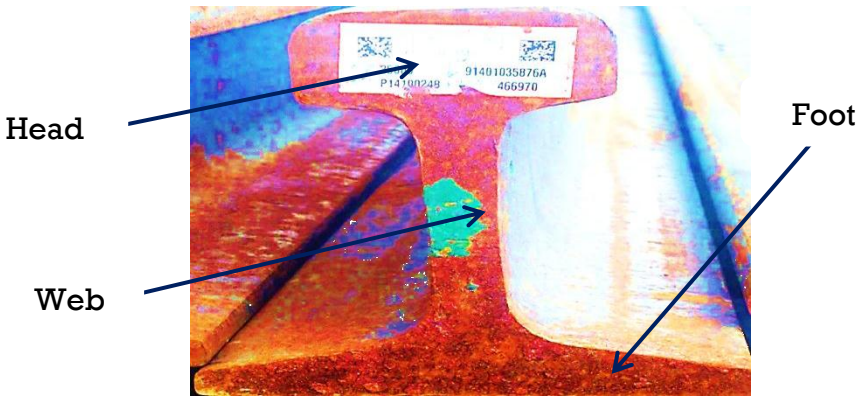

Fig.-3: The typical rail profile

The thermal analysis is a very important stage in the study of braking systems, especially of railway vehicles, where it is necessary to brake huge masses, because the thermal load of a braked railway wheels rolling on the rails that prevails compared to other types of loads. In the braking phase, kinetic energy transforms into thermal energy resulting in intense heating and high temperature states of railway wheels and rails. Thus induced thermal loads deter-

mine thermo-mechanical behavior of the structure of railway rails. In cases of thermal overloads, which mainly occur as a result of long-term braking on down-grade railroads, the generation of stresses and deformations occurs, whose consequences are the appearance of cracks on the rail head and the final total rail defect. The importance to precisely determine the temperature distribution caused by the transfer process of the heat generated during braking due to the friction on contact surfaces of the braking system makes it a challenging research task. Several factors contribute to wheel/rail contact resistance in addition to braking: First, during rolling, the wheel and rail surfaces are elastically deflected such that relative motion can occur. Second, energy can be dissipated by plastic deformation. Third, surface adhesion phenomena can dissipate energy and the temperature may rise at the contact patch.

The temperature rise because of frictional heat at the contact patch is distributed to the wheel and rail according to the heat partitioning parameter. However, the contact surface on the rail is continuously changed and the contact surface on the wheel is essentially the same during sliding. After a short period of sliding, the cold rail absorbs more heat and comparatively less heat flows into the wheel. Therefore, the partition factor is not a constant value and keeps changing in the period of sliding. The heat partitioning parameter is the function of contact patch semi-axis length in rolling direction and the sliding velocity of the vehicle.

Generally, Vehicle-track interaction generates: vibrations, high receptance, noises, and impact force, resonate conditions, frictional force, wear, cracking, heat, spalls and rail corrugations. High frequency interaction between wheel and rail can lead to damage the contacting surfaces of the rails. The other fact is that rail replacement is much more expensive than wheel replacement, and that wheels are more frequently re-profiled or replaced, thus why it would appear more attractive to investigate the loading effects on the rail.

During braking, the frictional effects cause the wheel and braking foundation components. These, thermo-mechanical effects were studied by many researchers. In the other cases, the wheel - rail contact is the area of interest which is affected by the thermo-mechanical loads during braking. But, this effect of the track rail has not been getting the attention of researchers. Even if the effects on the wheel is higher, the rail also much affected by braking loads, especially at the downgrade track level. The temperature of the rail rises because of frictional heat at the contact patch. The thermal stresses and deformations in addition to the mechanical effects are generated. Its consequences are that the appearance of cracks on the rail head and the final total rail defect. Therefore, it is recommendable to deal with the thermo-mechanical

effects on the rail and the heat conduction from the wheel into the colder rail has to be considered.

Therefore, the intention of this research is to investigate the dynamic and thermo-mechanical effects of the contacts between vehicles and rail track. It includes confirming the first cut-off vibration frequencies values and mode shapes with the standards, determining the frictional force and partitioned heat flux, verification of the thermal effect at the down grade, straight track and curved track braking and weighs transient structural (MBD) effects at the rail joints. The model of contacts would be figured with 3D by CATIA VERSION 5-R-16 and simulation finite element analysis is done by using ANSYS-12 workbench.

1.2. Rational of the Problem

Rail provides the running surfaces for the train wheels and guides the wheel-sets in the direction of the track. It accommodates the wheel loads and distributes these loads over the supports. It also stabilizes the Lateral forces from the wheel-sets and longitudinal forces due to traction and braking. These loads may cause damage to the rail heads. At the continuous head it is highly affected by the friction and thermal power penetrant and at the joint it faces the cracking of the head ends, deformation of fish plate, high impact force and vibrations due to discrete contact area and rail heads dip down to a joint even on both sides.

Furthermore, the contact problems leads to rapid crash of the train bodies, dis-comfort of passenger, derailment, floor resonance to the building and high disturbance to the nearby societies. The temperature rises during braking also causes premature wear, rail failure, thermal cracks, rail burns and thermal excited vibrations. But, even if the rail is facing such loads, almost all previous researchers focused on the wheel thermo-mechanical effects.

Therefore, the investigations of dynamic and thermal for the wheel-rail contact effects on the rail are needed especially, at the rail joints and give response for following basic research questions. These are:

① What are the vibration's natural frequencies and mode shapes occurring on the continuous and jointed rail?

② How much is the thermo-mechanical effect on the rail at the wheel-rail contacts during the down grade, straight track and curved track braking?

③ How much is the maximum friction forces and heat power generated at the rail head-wheel tread contact?

④ How much is the transient structural effects on the rail?

1.3. Objective of the study

1.3.1. General Objective

The general objective of this study is to investigate the dynamic and thermo-mechanical wheel-rail contact effects on the rail by using finite element analysis.

1.3.2. Specific objective

The specific objectives of the study are:

- To examine the natural frequencies and mode shapes occur at the continuous and rail joint of wheel-rail contact.
- To investigate the thermo-mechanical effects on the rail at the wheel-rail contacts during downgrade, straight track and curved track braking
- To investigate the transient structural of the rail for the wheel-rail contact at the continuous and jointed rail
- To determine the maximum braking forces and heat power at the rail head-wheel tread contact during braking

1.4. Methodology

This part of thesis is aimed to discuss the scientific procedures used in order to accomplish the research objectives and how the appropriate solutions for the branded problems would be achieved in this paper work.

Research Approaches

In this study, the first method is reviewing the literatures from reference books, internet websites, different articles, related previous researches and journals. The next approach is gathering the wheel-rail geometrical data. Then, the modeling and making analysis for the given data conditions was done for the further discussions.

Data Collection Approaches

The two types of data collections method would be used for this study. The study commenced with the collection of sources of data. Executively, the method of data collection process for the study is conducted in primary perspectives views are the data from the documented design and constructions departments of Ethiopian LRT projects. These data include: geometry of wheel and rail, rail joint component data, rail-pad, concrete dimensions and basalt specifications of the tracks.

Geometrical and Mathematical Model

The geometry of wheel, rail, rail joint components, rail-pad, and concrete are made according to the specifications and standards. The 3D physical modeling and assembly will be done by the CATIA software package. The mathematical models for the manual and analytical methods are developed. The analysis formula and interaction of contact mechanics based on different theories will be practiced. The mechanisms of vibrations are explained using an analogous mechanical model of a friction oscillator excited by a moving wheel base on the rail track. Further, the analyses consider the stiffness and damping effects of the polyethylene rail-pad and ballast to come up with accurate results.

Simulation Modeling and Analysis

The Simulation was done by ANSYS-12 workbench commercial software package. It starts by making material selection from the engineering data, making boundary conditions and load applications. For the analysis, the static load effects, dynamic modal vibrations (natural frequencies) and modes shapes, transient structural and thermo-mechanical effects were investigated. Next, retrieving the results, further discussions, and validation with the concerned standards were done.

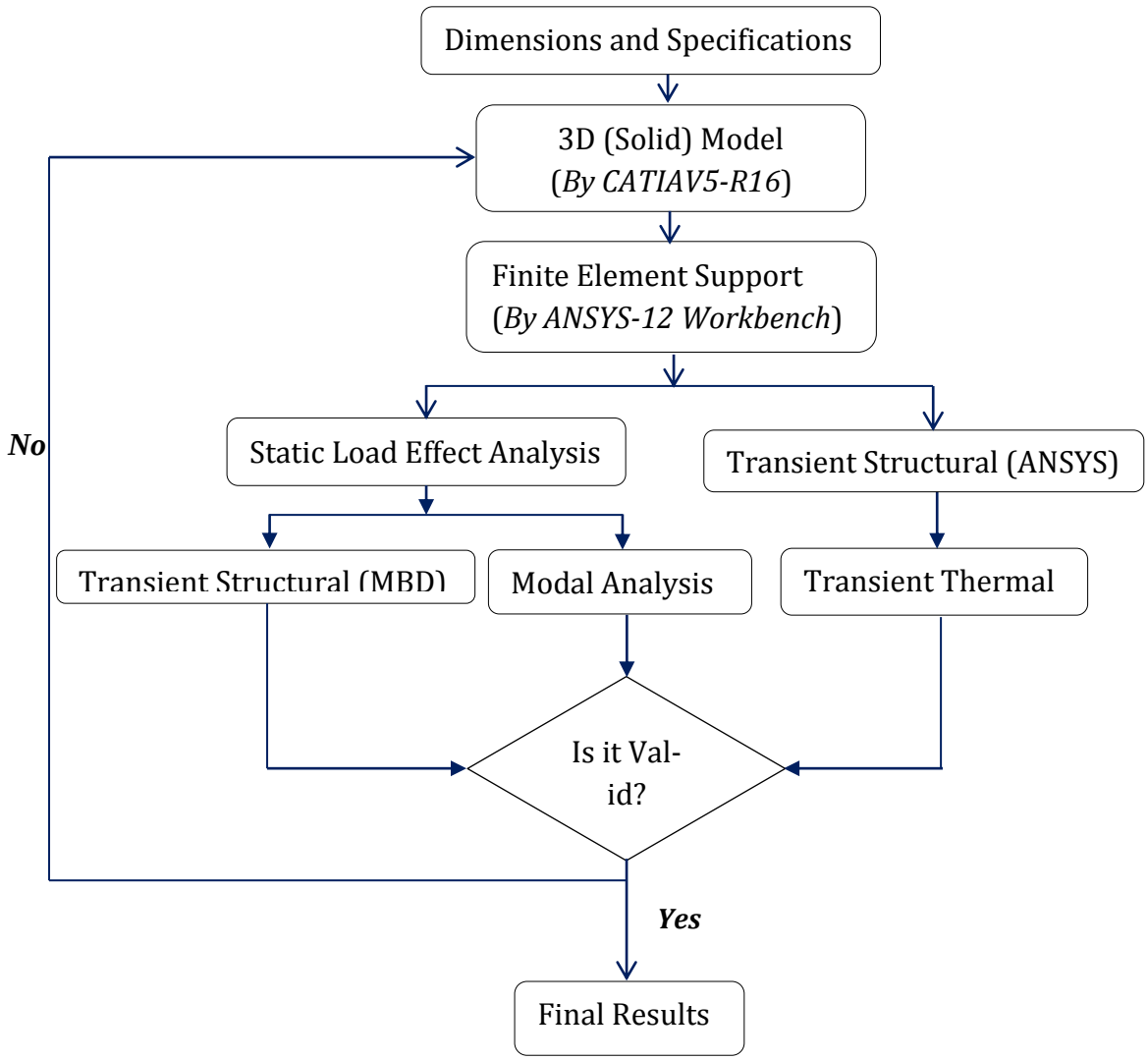

Fig.-4: Modeling and analysis frame works [Author]

1.5. The Scope and Limitation of the Study

It is understandable that the dynamic and thermal effect is formed at each contact components of the train. In this study, the dynamic and thermal effect of the rail during gradient braking at the wheel rail interface; with continuous and jointed rails would be analyzed by considering rail pad and basalt effect (stiffness and damping).

The limitations of the researches are that the thermal transient partitioning between the rail and wheel is difficult to quantify accurately because of the closely coupled nature of the wheel and rail and their proximity to one another. The other problem is the difficulty in getting track data, the document was written by Chine language and the complexity of contact geometry at the rail joints and curvature points is the other challenges.

1.6. Significance of the Study

From this work, the passenger and the AA LRT get positive aids. It provides the first cut-off vibration frequencies values with validation with standards. It shows the thermal stress and temperature rise during braking at the maximum gradient of AA LRT. In addition, the transient MBD effects at the rail joints also displayed. The benefits of this research work is to contribute: the wheel-rail contact tramcar vibration frequencies, maximum friction forces, heat flux generated at the contact patch, vertical displacement, velocity acceleration, critical velocity and maximum temperature rise at the contacting area .

1.7. Expected Outcome

Undoubtedly, the measurable expected outcomes are:

- The natural frequencies and mode shapes occur at the continuous and rail joint of wheel-rail contact.
- The thermo-mechanical effects on the rail at the wheel-rail contacts during braking
- The transient structural (MBD) effects on the rail at the wheel-rail contact for jointed rail
- The maximum friction forces, heat power and temperature gradient at the rail head-wheel tread contact during braking

1.8. Organization of the Thesis

The body of this thesis is divided into five main chapters. The first chapter discusses background and justifications of the study, rational of the problem, objectives and methodology of the study. The second chapter covers the review of some of the journal articles, proceedings and publications which were referred to during the course of the thesis. Also, in relation and comparison with previous works, what is done in this thesis will be stated. The mathematical and finite element modeling of the dynamic and thermal analysis during braking at different track level conditions were discussed in the third chapter. Multi body models representing rail track structure are presented. The results obtained from the static, modal, transient structural (ANSYS), transient structural (MBD), and thermo-mechanical analysis of the rail were included in the fourth chapter. Finally, the fifth chapter covers conclusions drawn based on the results of the analysis, and recommendations for future work.

CHAPTER-TWO: LITERATURE REVIEWS

2.1. Introduction

This is one of the portions of the paper that reviews the previous related works which are basic for this thesis works. Some of them may have a direct relation with this work whereas the others may have indirect relations, but it will add incredible values to the investigations. One must verify the value of the optimum vibratory impact forces resulting from the wheel - rail cooperation, which is related to maintaining vehicle stability in the new work conditions. [15], the railway track structure always starts to vibrate in lateral direction, following the vibration way of rails as simply supported beam. And, depending on the connection conditions between the track components, after reach certain frequency the vertical vibration modes get the domination. Also, the speed of the moving train has a significant dynamic effect on the track-bed. As the train speed increases, the displacement pattern of track-bed changes from symmetrical to asymmetrical.

The source to train-induced vibrations is the movement of the train along the track and the interaction occurring between wheel, rail, and track structure. According to [29] of the experimental investigation, the squeal noise in tramway occurs at the sharp curves. [35], studied the effect of lateral adhesion and rolling speed on wheel squeal noise and results showed that the sound pressure level and vibration velocity of the wheel increases substantially as the angle of attack reaches and exceeds the value around 8 mrad. The other study dealt with, the top rail friction control for curve noise mitigation and corrugation rate reduction. So, top of rail friction modifiers are designed, and controlled the frictional characteristics at the wheel-rail interface that influence noise, corrugations, and lateral forces, and wheel roughness increases the vibration levels generated at the wheel rail interface [13].

Vibration from trains manifests itself in two main ways. In some situations people can feel it and the effect can be exacerbated by floor resonances within a building. Secondary effects include noise radiation and disturbance of fixture and fittings [30]. [3], researched on an investigation into the use of time-frequency analysis of vibrations in railway vehicles for early detection of wheel flats and rail surface defects. It is used for identifying the content of a signal in the frequency domain without losing information about its time domain characteristics and the three analysis techniques: short-time-Fourier-transform, wigner-ville transform, and wavelet transform are investigated. The other studies presented that measurement of rolling

stock influence on railway vibrations and an overview of rolling stock mitigation measures [28].

According to [32], the flat is a serious fault of the rolling surface of the railway wheel. It appears when the wheel is blocked and slides on the rail at the rail joint (external tribology effect) and during braking process (internal effect) due to the wear. The rolling of the wheel flat is dangerous due to the impact force, which applies stresses both to the track and the wheel and generates impact noise. The study concluded that when the speed increases or the flat has larger dimensions, the wheel-rail contact might be lost during impact. As the vehicle speed increases, the impact force increases too. Although, a relative maximum may be observed, the frequency of 'passing over the flat' is a little higher than the wheel-rail first own frequency. If the rail pad stiffness is smaller, the impact force is small at low speeds and increases at high speeds. Combining this aspect with the one presented above, the conclusion is that the rigid rail pad is preferred. The time domain analysis of the flat wheel-rail interaction is interesting not only for determining the aggressiveness of the flat fault on the wheel-rail system, but also for the noise level calculation as well, starting with the spectra of the impact force. [2], a 3-dimensional finite element model for railway track analysis under impact forces by wheel flats are better approach to reality than the 2-dimensional finite element model. Also, it has found that the relationships between both incremental wheel-rail and sleeper impact forces and static wheel load are nonlinear, but monotonically increasing by increasing the static wheel load. According to the relationship between impact force and vehicle speed, the track engineers can realize that the maximum impact force occurs on sleepers at a critical speed but not the highest vehicle speed with specific static wheel loads under wheel flats. That critical speed may occur more frequently than the highest speed.

According to [5], the dynamic response of the wheel on irregular rail track can be analyzed with analytical approach using the method of Multiple Scales (MMS). The frequency of vibration and the dynamic motion of the center of the wheel were determined. From Comparisons, the analytical results are very close to those extracted by the numerical methods. Also, investigation on effects of preload on natural frequency has been shown that natural frequency increases by increasing the wheel-set preload. [6], the interoperability of the European rail transportation is affected by wheel profiles and the different rail inclination that varies between 1/40 and 1/20. This greater rail inclination leads to greater maximum pressures. Therefore, the rail inclination appears to be a major factor to influence the shape of the real contact

area and consequently the entire 3D elastic pressure distributions. The lateral displacement of the wheel alters considerably both, the shape of the real contact area and the maximum value of the pressure distribution. It has been noted that the more plain profiles wear, the less influence of the wheel-set lateral displacement appeared.

[24], provides an overview of the study of the rolling contact problem as it relates to railway wheel / rail interaction. It is focused on the development of ABAQUS models of the contact occurring at both the wheel tread/rail head and the wheel flange/rail head interface under a range of railway operating conditions that occur at these interfaces. The situation with heavy haul rail operations is that the payloads have been increasing to the point where the factors of safety used no longer accommodate this uncertainty in the magnitude of loads under extreme operating conditions. it is believed that the reverse approach may be more beneficial and the nature of the loads occurring in practice be determined by the development of a sound knowledge of the failure mechanisms and the propagating stress conditions.

[33], model the wheel and the rail as elastic deformable bodies and requires numerical solutions. In this section, results of the numerical analysis by finite element method (FEM) in rail-wheel collection under static loading are presented. Results shown that two critical and dangerous surfaces in collection of rail and wheel statistically. Elliptical, rectangular and circular contact surfaces were assumed for numerical stress analysis. These results show that stresses were similar to the exact analytical results by assumption of elliptical contact surface. As well as, results of contact stress with assumption of rectangular contact surface were more accurate than the contact stress results by assumption of circular contact surface. In addition stresses are approximately equal in small loadings unlike a high loads. These critical surfaces may be cause creation of micro and macro cracks. Eventually, good agreement was found between finite element method (FEM) and previous analytical results for determination of contact stress in rolling bodies.

[27], predicted train induced vibrations by a numerical model. The dynamic interaction between the wheel-sets and the rail is accomplished by using the non-linear Hertzian model with hysteresis damping. A sensitivity analysis is done to evaluate the variables affecting more the maintenance costs. The rail-sleeper contact is assumed extended to an area defined contact-zone, rather than a single point assumption which fits better real case studies. [25], investigated the effects of axle load and train speed at rail joint. The results from the present investigation are indicates that the axle load has a larger effect on the stresses and strain at the

constant speed. It indicated that the von mises stresses, the maximum shear stress and the Equivalent elastic strain are increases linearly with increasing axle load and the effect of train speed on above parameters is relatively weak. The results also indicate that the effect of train speed is relatively weak than to the axle load.

[36], study used an elastic-plastic and coupled temperature-displacement finite element model to investigate the effect of rail corrugation on the wheel-rail thermal contact pressure and temperature distributions during wheel braking. Contact elements were used to simulate the contact between a wheel and a corrugated rail. Various wavelengths and amplitudes of corrugated rail as well as braking speeds are considered in this study. The results indicate that, in the wheel-rail contact area, the rail corrugation affects the contact pressure and temperature distributions significantly. The corrugated rail can lead to a wavy contact pressure and temperature distributions on the rail surface. A larger corrugated wavelength and a smaller half-amplitude can both result in smaller amplitude of temperature fluctuation. A larger corrugated rail amplitude and a smaller wavelength results in a larger variation in the contact pressure peak p_{max}. In this study, a wheel and a corrugated rail contact is assumed as the contact of a cylinder and a plate. A function of $z(x) = [1+ \cos (2\pi x / L)]$ is used for the plate surface to simulate the corrugated rail.

The aim of this research is to investigate the dynamic and thermo-mechanical effects of the contacts between vehicles and rail track. It includes confirming the first cut-off vibration frequencies values and mode shapes with the standards, determining the frictional force and partitioned heat flux, verification of the thermal effect at the down grade braking and weigh transient structural(MBD) effects at the rail joints. The analysis would also be developed at different wheel-rail contact conditions. These are vehicle resistances at minimum curves, rail loading at continuum head and loading effect at rail-joints. The model of contacts would be figured with 3D by CATIA V-5 R-16 and simulation finite element analysis is done by using ANSYS-12 workbench.

2.2. The Rail

Rails are the longitudinal steel members that directly guide the train wheels evenly and continuously. They provide smooth running surfaces for the train wheels and guide the wheel-sets in the direction of the track. The rails also accommodate the wheel loads and distribute these loads over the sleepers or supports. Lateral forces from the wheel-sets and longitudinal

forces due to traction and braking of the train are also transmitted to the sleepers and further down into the track bed. The rails also act as electrical conductor for the signaling system. A modern steel rail has a flat bottom and its cross section is derived from an I-profile. The upper flanges of the I-profile have been converted to form the rail head [15].

Using mathematical modeling, the bending vibration of a free rail can be modeled as a beam with no support along it; the rail beam model is supported only at the boundaries. Also, a finite element discretization is used to model the rail. Considering insignificant the axial displacement, we discretized the rail with Timoshenko beam finite elements with two degrees of freedom: rotation and vertical displacement. The algorithm allows choosing the number of beam elements between two sleepers and the number of beam elements vertically connected to sleeper by pads. The motion equation for rail may be expressed as [26]:

$$M_r\ddot{Z}_r + C_p\dot{Z}_r + K_pZ_r = q_r + f \tag{2.1}$$

The force-deflection relation to the contact stiffness is assumed to follow the Hertz law and can be given by [26]:

$$f = C_H(x_w - x_r - r)^{3/2} \tag{2.2}$$

2.2.1. Rail Joints

Rail joint are used to connect the ends of two rails horizontally and vertically. Its length ranges from 11.8 meter to 25meter. The continuity of the railway track is breaks due to the existence of rail gap and difference in the height of the rail heads. Because of the above reasons rail joints are weaker than the rails and subjected to large stress. The joint bars prevent lateral or vertical movement of the rail ends and permit the longitudinal movement of the rails for expanding or contracting. Each rail section has a designated drilling pattern (spacing of holes from the end of the rail as well as dimension above the base) that must be matched by the joint bars. Although many sections utilize the same hole spacing and are even close with regard to web height, it is essential that the right bars are used so that fishing angles and radii are matched. Failure to do so will result in an inadequately supported joint and will promote rail defects such as head and web separations and bolt hole breaks [26].

Fig.-5 : Atypical bolt jointed rail

Rail joints provide discrete inputs to the wheel-rail system that induce quite large contact force variations. Rail joints can be characterized by a gap width and a step height (either up or down). Moreover, the rail often dips down to a joint on both sides. Such dips are also present at welds, and are usually characterized in terms of the angle at the joint [12].

2.3. Wheel-rail Contact Interactions

The dynamic behavior of railway vehicle is greatly affected by the rail-wheel dynamic interactions. The wheel-rail contact is a critical aspect of vehicle performance and railway system reliability and is influenced by many factors, such as vehicle suspension, track geometry, wheel and rail profiles. Differences in design parameters between railway networks create problems for interoperability.

2.3.1. Hertzian Theory Interactions

The wheel-rail contact problem was first solved regarding the contact as a cylinder rolling over a plane 2D problem. Three decades later, modeled the shape and size of the contact area and pressure distribution considering the Hertzian three-dimensional solution [6]. This work dealt with the Hertzian interactions of wheel and rail track.

2.3.2. Non-Hertzian Contact Theory

In reality, the wheel-rail contact is a non-Hertzian contact because of the following violations of the Hertzian assumptions:

- ✓ the surfaces within the contact regions cannot be expressed in quadratic form;
- ✓ the common generatrix has a finite length;
- ✓ the contacting surfaces are not smooth;
- ✓ friction is present in the contact area.

According to [15], assuming a circular contact area with a radius equal to the geometrical mean of the elliptical radii and an infinite radius of the transverse wheel profile, an approximate expression for the non-linear Hertzian contact stiffness is given by:

$$K_H = \sqrt[3]{\frac{3E^2 F_{stat}\sqrt{R_w R_r}}{2(1-v^2)^2}} \tag{2.3}$$

2.4. Contact Geometry

The wheel-rail contact can be described by the general case of an elliptic contact surface. This interaction (wheel-rail) mainly depends on wheel-rail contact geometry. The changes in contacting geometry of rail-wheel depends on different parameters like the variation of wheel and rail profile, track gauge, rail inclinations, railhead surface irregularities, and flexibility of rail support. The main parameters influencing the wheel rail contact geometry are the profiles of wheels and rails, rail inclination and track gauge.

The semi-axes (a, b) of the contact ellipse depend on the geometry of the wheel and the rail profile. According to Hertz's theory, the semi-axes can be calculated as [16]

$$a = m\left[\frac{3\pi N(K_1+K_2)}{4K_3}\right]^{1/3} \text{ and} \tag{2.4}$$

$$b = n\left[\frac{3\pi N(K_1+K_2)}{4K_3}\right]^{1/3} \tag{2.5}$$

$$K_1 = \frac{1-v_w^2}{\pi E_w}$$

$$K_2 = \frac{1-v_r^2}{\pi E_r}$$

$$K_3 = \frac{1}{2}\left[\frac{1}{R_1^w} + \frac{1}{R_2^w} + \frac{1}{R_1^r} + \frac{1}{R_2^r}\right] \tag{2.6}$$

$$K_4 = \frac{1}{2}\left[\left(\frac{1}{R_1^w} + \frac{1}{R_2^w}\right)^2 + \left(\frac{1}{R_1^r} + \frac{1}{R_2^r}\right)^2 + 2\left(\frac{1}{R_1^w} - \frac{1}{R_2^w}\right)\left(\frac{1}{R_1^r} - \frac{1}{R_2^r}\right)\cos 2\beta\right]^{1/2}$$

Where,β is the angle between the normal planes that contain $\frac{1}{R_1^w}$ and$\frac{1}{R_1^r}$. Coefficients m and n depend on the ratio$\frac{K_4}{K_3}$ and θ can be defined as:

$$\theta = \text{Cos}^{-1}\left(\frac{K_4}{K_3}\right) \tag{2.7}$$

The direction of the axes of the contact ellipse can be determined based on the radii of curvature and the rolling radii for the two bodies in contact:

If $\frac{1}{R_{1w}} + \frac{1}{R_{2w}} \geq \frac{1}{R_{1r}} + \frac{1}{R_{2r}}$: the transverse semi axis of the contact ellipse (y direction) is greater than or equal to the longitudinal semi-aixs.

If $\frac{1}{R_{1w}} + \frac{1}{R_{2w}} \leq \frac{1}{R_{1r}} + \frac{1}{R_{2r}}$: the transverse semi axis of the contact ellipse (y direction) is less than or equal to the longitudinal semi-axis.

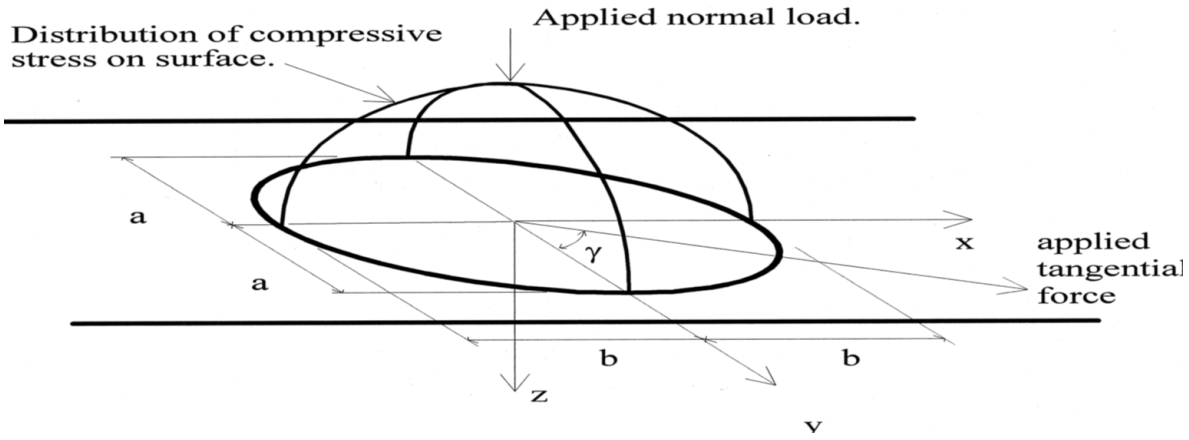

Fig.-6: Elliptical, Hertzian contact patch [16]

2.5. Wheel-rail Contact Vibrations

Vibration is a dynamic behavior of a physical system in which a system oscillates or repeats itself after an interval of time about a certain equilibrium position. A vibratory system is a dynamic system for which the variables such as the excitations (inputs) and responses (out-puts) are time-dependent. The response of a vibrating system generally depends on the initial conditions as well as the external excitations. It can be realized that the relationship between force and deflection is nonlinear. Modeling the system with a mass and a nonlinear spring, the vibration equation is obtained as [5]:

$$m\ddot{x} + K'x^{3/2} = F \tag{2.8}$$

Where, $F = K'\delta^{3/2}$ and $K' = \left(\frac{2\pi E K_a}{3C}\right)^{3/2}$ (2.9)

When the wheel rotates on the sinusoidal rail surface, the vibration equation can be rewrite as follow:

$$m\,\ddot{x} + K'(x - \varepsilon^2 a^2 \sin Vt)^{3/2} = F \quad (2.10)$$

$$\ddot{Z} + \lambda^2 (Z)^{3/2} = \varepsilon^2 a^2 V^2 \sin Vt + {}^{F}/_{m} \quad where, x = z + \varepsilon^2 a^2 \sin Vt \quad (2.11)$$

$$\lambda^2 = \frac{1}{m}\left(\frac{2\pi E K_a}{3C}\right)^{3/2} \quad (2.12)$$

Where**,** m is the equivalent mass and x is the vertical displacement of the center of the wheel and $\varepsilon^2 a^2$ is amplitude of rail irregularities and C is a function of the geometric and mechanical properties of the system.

2.6. Thermal Analysis during Braking

2.6.1. The Tramcar Braking Energy

During the process of braking, available energy of the tramcar that must be transformed into frictional heat. The energy of the tram will be dissipated by the work of the braking. Thus, the frictional dissipated heat energy by braking and resistance forces are equivalent to the total mechanical available energy (kinetic energy (E_k) and potential energy (E_p)) of the tramcar. But, the determination of effective braking energy depends up-on the different track conditions. The general energy equation is [6]:

$$E_k + E_p = \int_0^{S_b} F_b\, ds + \int_0^{S_b} R\, ds \quad (2.13)$$

$$\frac{1}{2}\boldsymbol{M v_{max}^2} + \frac{1}{2}\boldsymbol{I\omega_0^2} + \boldsymbol{M.g.S_b}\frac{\boldsymbol{\delta}}{\boldsymbol{1000}} = \int_0^{S_b} \boldsymbol{F_b\, ds} + \int_0^{S_b} \boldsymbol{R\, ds} \quad (2.14)$$

Where, v_{max} is maximum velocity, M is mass of the tramcar, I is polar inertial moment of rotating parts, ω_o is angular velocity of rotating parts, δ is track gradient [mm/m], S_b is braking distance, F_b is the maximum instantaneous braking force in [N] and R is the resistance forces in [N].

2.6.2. Transient Thermal

The wheel and rail dissipate the heat produced at the boundary between the rail and the wheel by convection and radiation. The heat dissipation from the free surfaces of the wheel and rail to the surrounding air is described by both convection and radiation as [22]:

$$q_d = -h(T - T_\infty) - \varepsilon\sigma\left(T^4 - {T_\infty}^4\right) \quad (2.15)$$

Where, h equals the convective film coefficient, ε is the material's emissivity, σ is the Stefan-Boltzmann constant ($5.67*10^{-8}$), and T_∞ is the temperature of the surrounding air.

The other main part of the transient model is the heat conduction through the rail and the wheel by the transient heat transfer equation as [22]:

$$\rho C_p \frac{\partial T}{\partial t} + \nabla(-K\nabla T) = Q - \rho C_p u \nabla T \quad (2.16)$$

Where, for materials of the wheel and the rail, ρ is the density, k is the thermal conductivity, Cp is the specific heat capacity, u is the velocity field, and Q is the heating power per unit volume of internal source, which in this case is set to zero. Thus, the above equation becomes:

$$\rho C_p \left(\frac{\partial T}{\partial t} + u\nabla T\right) = \nabla(-K\nabla T) \quad (2.17)$$

Where, $\nabla = \frac{\partial}{\partial x} i + \frac{\partial}{\partial y} j + \frac{\partial}{\partial z} k = \text{grad}$, which is vector operator and K is conductivity matrix

$$\rho C_p \left(\frac{\partial T}{\partial t} + u_x \frac{\partial T}{\partial x} + u_y \frac{\partial T}{\partial y} + u_z \frac{\partial T}{\partial z}\right) = \frac{\partial}{\partial x}\left(K_x \frac{\partial T}{\partial x}\right) + \frac{\partial}{\partial y}\left(K_y \frac{\partial T}{\partial y}\right) + \frac{\partial}{\partial z}\left(K_z \frac{\partial T}{\partial z}\right) \quad (2.18)$$

The temperature rise because of frictional heat at the contact patch was distributed to the wheel and rail according to the heat partitioning parameter. Thus**,** maximum temperature rise in the wheel rail interface is given by equation [6]:

$$T_{max} = \frac{1.276*(\Omega\mu)P_o}{\beta_r}\sqrt{a(v_s)} \quad (2.19)$$

CHAPTER-THREE: PYSICAL AND MATHEMATICAL MODELING

3.1. Physical Modeling

The 3D physical modeling and assembly is done by the software package of CATIA-V5-R16. The CATIAV5R16 is 3D mechanical design software for creating 3D prototypes, used to design, visualize and simulate of the analysis. The model assembly components are: wheel, continuous and bolt jointed rail, rail-pads, concrete sleepers and gravel ballast. The standard bolt jointed rail contains: the left and right rails, fish plates, bolts; nuts and washers that are used to secure the rail fastening assembly.

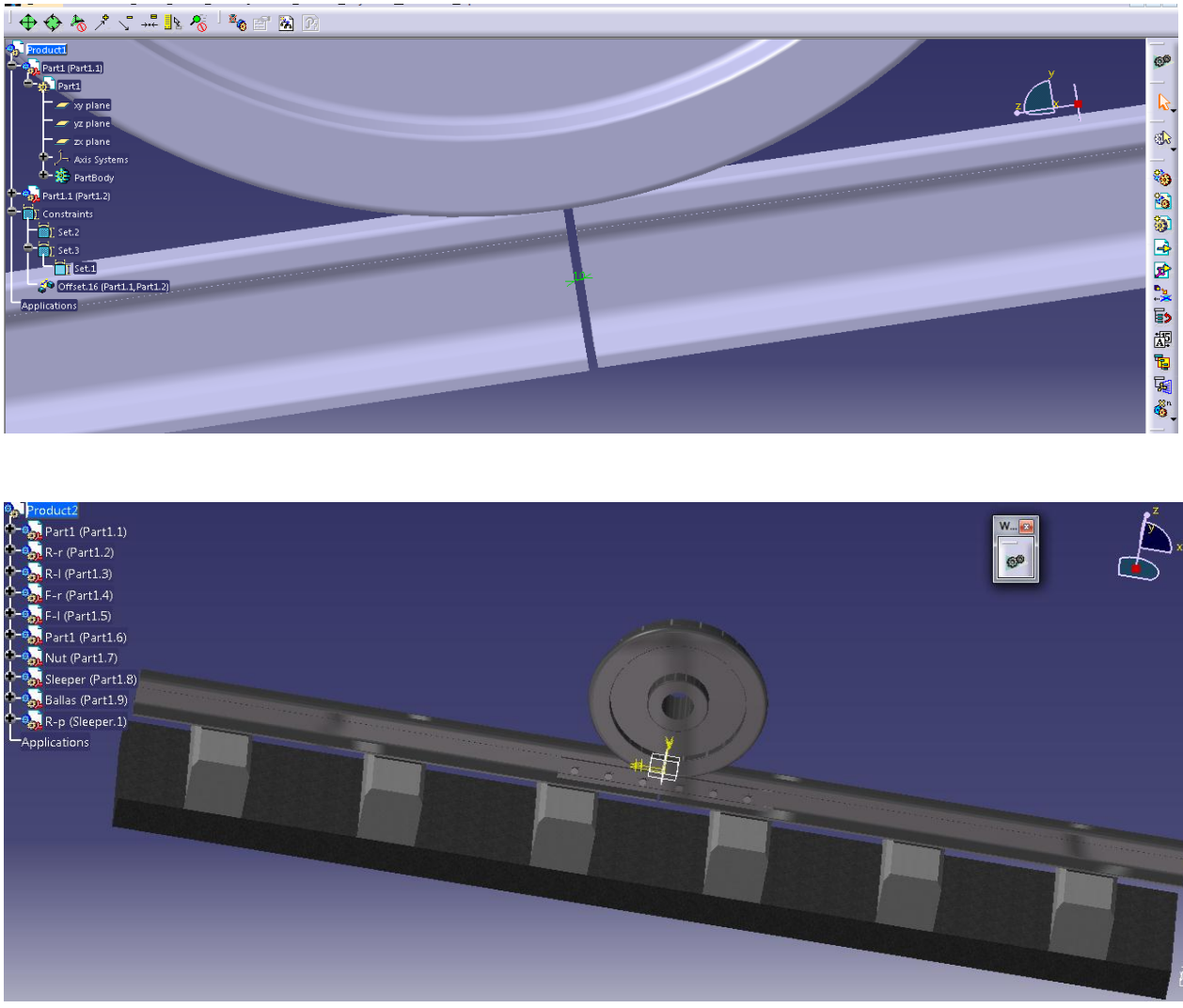

Fig.-7: 3D Catia modeling of wheel, bolt-jointed rail and track assembly

Fig.-8: Addis Ababa LRT track

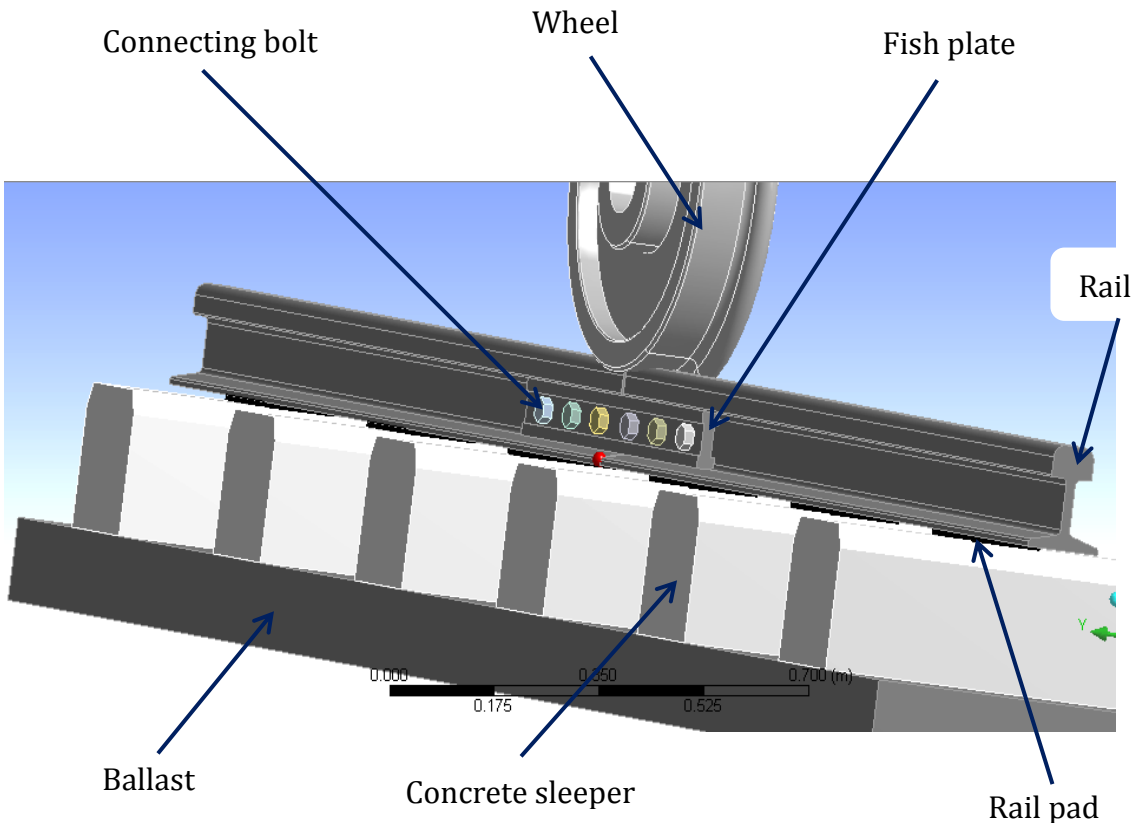

Fig.-9: Rail-joint components model

Table-1: Technical parameters used for the analysis [7, 8, 19, 23, 34]

Components	Parameters	Values
Wheel (ER9, EN13262)	Diameter	660 (mm)
	Young's modulus	210 (GPa)
	Poisson's ratio	0.3
	Mass density	7850 (kg/m)
Rail: 50Kg/m (GB2585 (2007); TB/T234(2003))	Young's modulus	210 (GPa)
	Poisson's ratio	0.3
	Mass density	7850 (kg/m)
	Mass Moment of Inertia	2037 (cm^4)
	Rail height	152 (mm)
	Web thickness	15.5 (mm)
	Head width	70 (mm)
	Apparent head width	46 (mm)
	Base width	132 (mm)
Rail Pad (Polyethylene)	Young's Modulus	1.1e+009 (Pa)
	Poisson's Ratio	0.42
	Stiffness	(50～70) MN/m
	Damping ratio	50 KN s/m
	Thickness	8 (mm)
Track	Gauge	1435 (mm)
Sleeper (Concrete)	Young's Modulus	3.e+010 (Pa)
	Poisson's Ratio	0.18
	Spacing	0.658 (m)
Ballast (Gravel)	Stiffness	120 M N/m
	Damping ratio	70 KN s/m
	Thickness	450 (mm)
Vehicle	Max. Operating Speed	≤ 70 (Km/hr)
	Rotational gravitation	9.81 (m/s^2)
	Axle load	≤11 （1+3%） [t]
Fish plate	Length	0.820 (m)
	Thickness	0.019 (m)
Bolt and Nut		M31

3.2. Mathematical Modeling

The mathematical model for the analysis contains: the inertia force, damping force and stiffness force together with externally applied force that will form the equation of equilibrium between them, which is called the 'equation of motion' that defines the dynamic behavior of the wheel-rail structure [20, 32].

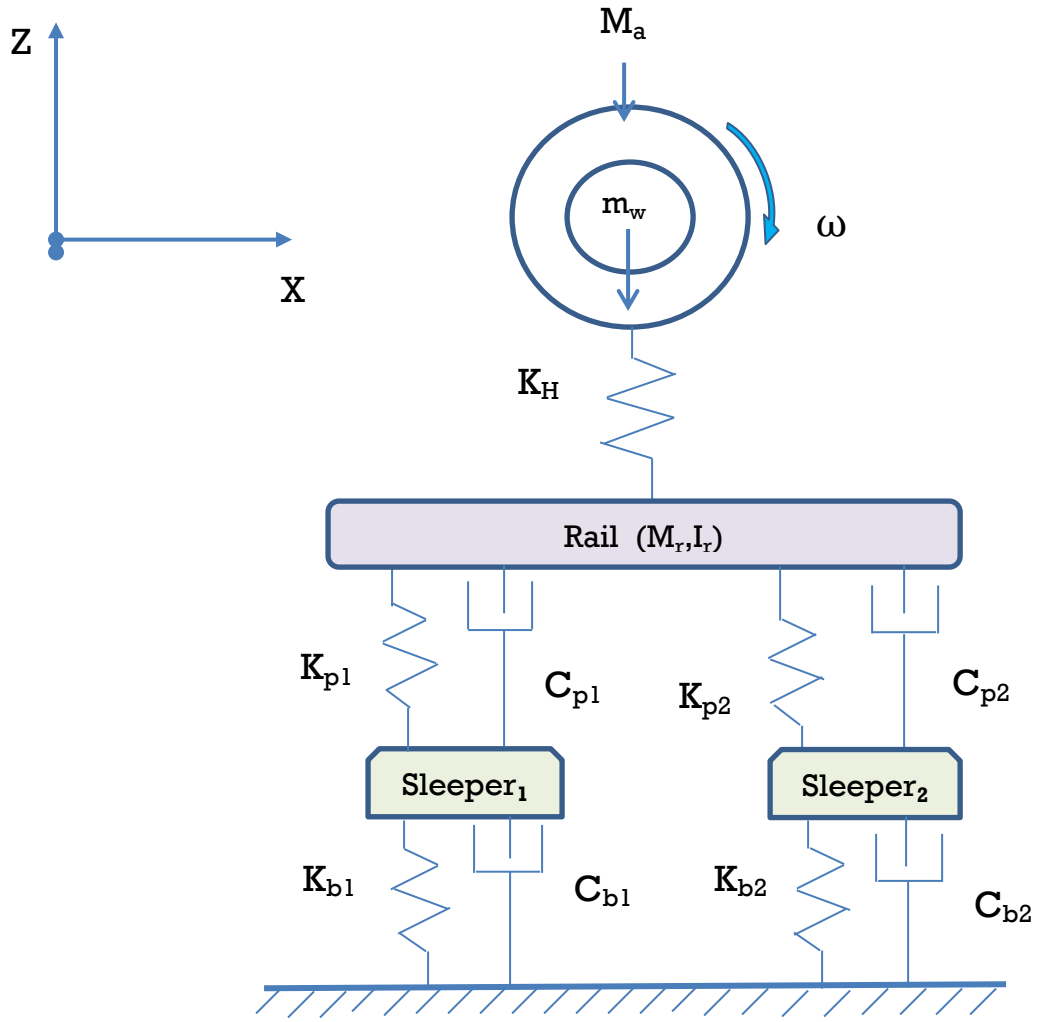

Fig.-10: Dynamic model for rail ballasted track

$$[\mathbf{M}]\{\ddot{u}\} + [\mathbf{C}]\{\dot{u}\} + [\mathbf{K}]\{u\} = \{\mathbf{F}\} \tag{3.1}$$

Where **M** is the mass matrix, **C** is the damping matrix, **K** is the stiffness matrix and {**F**} is the column vector of forces on the vehicle wheel loading area.

$$M = \begin{bmatrix} m_a & 0 \\ 0 & m_w \end{bmatrix},\ C = \begin{bmatrix} c_e & -c_p \\ -c_p & c_p \end{bmatrix},\ \mathrm{K} = \begin{bmatrix} k_e & -k_p \\ -k_p & k_p \end{bmatrix},\ \text{and}\ \{F\} = \begin{bmatrix} 0 \\ F_o - F(t) \end{bmatrix} \tag{3.2}$$

F(t) is the rail reaction in the contact point and the static load is $F_0 = g(M_a + M_w)$ with g as the gravitational acceleration. The {**F**} vector has this particular form because the elastic element from the suspension is pre-loaded by the car body weight. Supposing that the mass of sleepers are not considered and the stiffness and damping coefficient of rail pad and ballast is in series and parallel to the near-by assembled orientations [20]:

$$K_1 = \frac{K_{p1}K_{b1}}{K_{b1}+K_{p1}};\quad K_2 = \frac{K_{p2}K_{b2}}{K_{b2}+K_{p2}};\quad K_e = K_1 + K_2 \tag{3.3}$$

and

$$C_1 = \frac{C_{p1}C_{b1}}{C_{b1}+C_{p1}};\ C_2 = \frac{C_{p2}C_{b2}}{C_{b2}+C_{p2}};\quad C_e = C_1 + C_2 \tag{3.4}$$

Assuming a circular contact area with a radius equal to the geometrical mean of the elliptical radii and an infinite radius of the transverse wheel profile, an approximate expression for the non-linear Hertzian contact stiffness is given by [From equation(2.3)]:

$$K_H = \sqrt[3]{\frac{3E^2F_{stat}\sqrt{R_wR_r}}{2(1-v^2)^2}}$$

Thus,

$$K_H = \sqrt[3]{\frac{3(210e^{+09})^2 * 55551 * \sqrt{0.3 * 0.33}}{2(1-(0.3)^2)^2}} = \mathbf{1643.30M\ N/m}$$

3.3. Resonances

A condition known as resonance occurs, if the frequency of the external force coincides with one of the natural frequencies of the system. Resonant vibration is mainly caused by an interaction between the inertial and elastic properties of the materials within a structure. Resonance is often the cause of, or at least a contributing factor to many of the vibration. Several well damped resonances can be found in a track structure. At or near the natural frequency of a mode, the overall vibration shape ("operating deflection shape") of a structure will tend to be dominated by the mode shape of the resonance. As a consequence of discretely supporting beams like rails, the rail in the track 'frame-work' will obtain vibration modes related to this type of supporting. The most important vibration mode resembles a kind of bending between discrete points and pins. With some simplifying assumptions, the pin-pin vibration resonance occurs at a specific frequency (f_{pp}), which can be calculated by [15]:

$$f_{pp} = \frac{\pi}{2l^2}\sqrt{\frac{EI}{m}} \tag{3.5}$$

$$\text{Thus,} \quad f_{pp} = \frac{\pi}{2l^2}\sqrt{\frac{EI}{m}} = = \frac{\pi}{2(6.58)^2}\sqrt{\frac{2037e^{-8} * 2100^{+8}}{50}} = \mathbf{1035.6\ Hz}$$

A critical velocity of the rail-foundation system defined as 'a speed at which dramatic increases in the rail displacement is observed' has been presented [15]:

$$V_{cr} = \sqrt[4]{\frac{4KEI}{m^2}} \tag{3.6}$$

$$V_{cr} = \sqrt[4]{\frac{4KEI}{m^2}} = \sqrt[4]{\frac{4 * 120e^{+6} * 2100e^{+8} * 2037e^{-8}}{(50)^2}} = \mathbf{951.98\ m/s}$$

3.4. Modal Analysis

Modal analysis is the study of the dynamic character of a system which is defined independently from the loads applied to the system and the response of the system. The modal characteristics of the structure are used to determine the response of the system [25]. Modes are inherent properties of a structure, and are determined by the material properties (mass, damping, and stiffness), and boundary conditions of the structure. Each mode is defined by a natural (modal or resonant) frequency, modal damping, and a mode shape (i.e. the so-called "modal parameters"). If either the material properties or the boundary conditions of a structure change, its modes will change. A rigid body of rail has six degrees of freedom at the wheel-rail contact in 3D- modeling when the contact patch builds between the two supporting sleepers.

These are three degrees of freedom in translations (longitudinal-X, lateral-Y and vertical-Z): to define the position of the center of gravity from the inertial system and three degrees of freedom in angular movements (roll-Φ, pitch-Ω and yaw-ψ): to define the rotation of the rail about the longitudinal, lateral and vertical axes. The Cartesian coordinate orientations could be sated as:

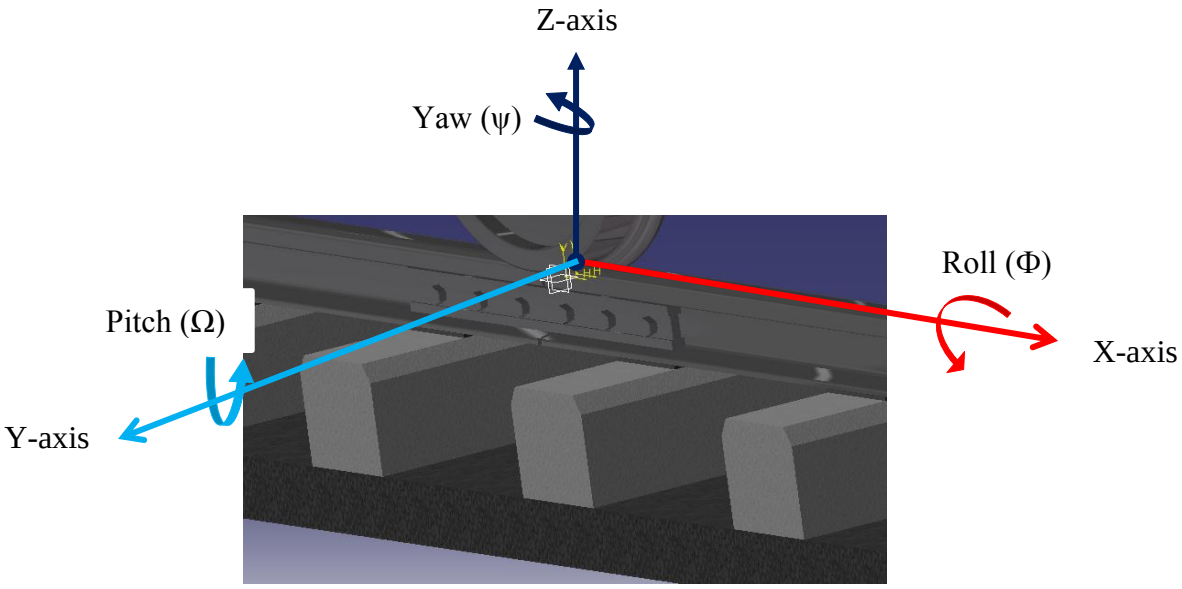

Fig.-11: Cartesian coordinate orientations

3.4.1. Modal Analysis Using ANSYS

Vibrational analysis of a rail can be done on ANSYS by providing structural data and load conditions on different supports. Modal analysis in ANSYS is used to find the rail's natural frequencies. The frequency response function represents the ratio of output over input signals. The frequency response is a function of frequency and reaches its maximum value at natural frequency. The modeling and analysis procedure is the following:

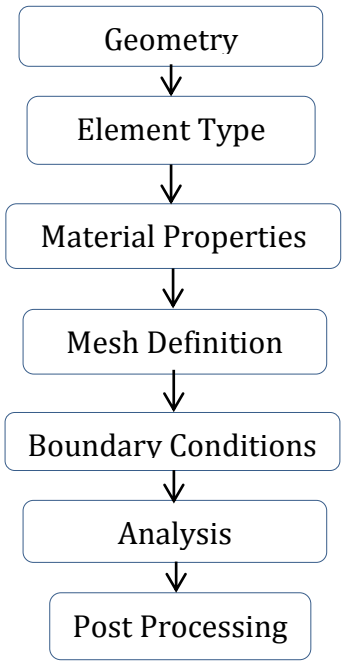

Fig.-12: Analyses frame work by ANSYS

3.5. Wear Rate of the Rail

The wear rate model is sensitive to vehicle characteristics through their effect on the wheel-rail contact patch, in particular contact patch size and shape, normal load and traction coefficient. The wear model of the rail U71Mn which its mechanical properties are equivalent to R260Mn on the dry contact was used to study the effect on rail of vehicle characteristics through their effect on the wheel-rail contact. The patch was assumed to be elliptical and the pressure distribution to be Hertzian; in addition, the contact was assumed to be on the top the rail, suitable for straight track, not curves, and the traction to be longitudinal only. To calculate profile area loss, the wear rate should be multiplied by the width of the contact. The wear rate equation is given as [17]:

$$w = 0.2\frac{t_c}{\mu}\left(3 - \frac{t_c}{\mu}\right)^2 (2.3\mathrm{p} - 0.68) \qquad (3.7)$$

Thus, $w = 0.2 * \frac{0.3}{0.35} * \left(3 - \frac{0.3}{0.35}\right)^2 * (2.3 * 1.14 - 0.68) = 1.53\ \mathrm{nm/cycle}$ and,

Area loss= 0.046*1.53=0.07nm^2/cycle

The quality of rails is prescribed by international standards: the European Union of Railways UIC 860 and EN13674. The new European standard EN 13674, which deals with issues of quality rail, takes into account the increasing demands for safety and economy of railway traffic. European standard EN 13674 includes symmetrical rails with wide rate of mass ≥46 kg/m. For a selection of different types of rails, the corresponding chemical composition and mechanical property requirements according to standard UIC 860 - 1. Carbon influences the mechanical properties through the volume fraction of cementite and the content of pearlite. Manganese influences the temperature decrease of the eutectoid reaction and the fineness of pearlite lamellae, that is, the reduction in the inter-lamellar distance. The wear rate for a rail of pearlite structure is [4]:

$$w = 0.1427\left(C + \frac{Mn}{4.72} + \frac{Si}{10}\right) \qquad (3.8)$$

Where: W represents the wear rate expressed as volume loss per unit of path over which sliding occurs, and C, Mn, Si represent the percentage contents of carbon, manganese and silicon respectively.

$$w = 0.1427\left(0.76 + \frac{1.4}{4.72} + \frac{0.35}{10}\right) = 0.1558\ (\mathrm{m^3/unit\ path})$$

3.6. Thermo-mechanical Analysis during Braking

An undoubted that the wheel-rail contact temperature rises much higher during braking than the normal traveling conditions. Thus, the thermo-mechanical analysis during braking is feasible and needed. But, the thermal analysis of wheel-rail contact depends up-on the different track level conditions. The following three cases (braking at downhill, straight track and curved track) are considered and the transient thermal analysis is done for maximum braking load on the rail.

Table-2: Technical data provided for the thermal analysis [7, 8, 11, 19]

Parameters	**Values**
Axle load(M)	≤11（1+3%）[t]
Start velocity(v_0)	19.44 [m/s]
Deceleration (a)	1.35[m/s^2]
Braking time (t_b)	14.40 [s]
Radius of the wheel (r_w)	0.33[m]
Maximum Gradient of the track (δ)	50[‰]
Minimum curvature of rail track	50 [m]
wheel-rail Coefficient of friction [μ]	0.35
Traction coefficient	0.3
Initial temperature (To)	22(℃)
Ambient temperature above the ground	+10℃～+30℃
Principal rolling radius of the wheel (R_1^W)	0.33 [m]
Transverse radius of curvature of the rail profile at the contact point (R_2^r)	0.30 [m]

3.6.1. Braking Energy at the Downgrade

During the process of braking, available energy of the tramcar that must be transformed into frictional heat, need to be determined accurately. This study considers the kinetic as well as the potential (while running on slopes) energy of the tram that must be dissipated by the work of the braking. Rail vehicles have important masses in rotation. Therefore, the contribution of

rotational kinetic energy is taken in to account. The initial kinetic energy imposed in to the tramcar is given by the sum total of translational and rotational [5]:

$$E_k = \frac{1}{2}Mv_0^2 + \frac{1}{2}I\omega_0^2 \quad (3.9)$$

And, the moment of inertia of the rotating parts can be calculated by using the equation below.

$$I = \sum_{i=1}^{n} m_i r_i^2 \quad (3.10)$$

Where,

m_i represents the masses of the rotating parts

r_i represents the rotation radius of the rotating parts from the center of rotation

For this case, all the rotating parts are fixed on the axle of the wheel set and the rotation axis could be taken as the tangent line joining the contact point of the rail heads with wheel set of the tramcar. It is the parallel to the axis of the wheel axle. Hence, the rotating radius is and equal to the radius of the wheel (r_w). But, in most analysis the contribution of the rotating masses are taken to be 10% the tare weight of the axle load of the train. Thus, the term $\frac{I}{Mr_w{}^2}$ accounts to the rotational masses involved and its value equals 0.1[11].

$$E_k = \frac{1}{2}Mv_0^2 + \frac{1}{2}I\omega_0^2 = \frac{1}{2}Mv_0^2\left[1 + \frac{I}{Mr_w{}^2}\right] = \frac{1}{2}(1.1)Mv_0^2 \quad (3.11)$$

The potential energy of the tramcar depends on the track gradient δ *[mm/m]* and on the travelled distance S_b. The exact definition of gradient is *tanα* where *α* is angle of inclination. According to EN 14531-6, for calculation of external forces that result from gradients in railway applications, the Simplification *sin α = tanα* is commonly used. Therefore the potential energy is expressed as [5, 11]:

$$E_p = M.g.S_b\frac{\delta}{1000} \quad (3.12)$$

Therefore, the total available braking energy of the tramcar is determined from the equation below.

$$E_b = \frac{1}{2}MV_0^2[1.1] + M.\mathrm{g}.S_b\frac{\delta}{1000} \quad (3.13)$$

When the tramcar begins to brake, the train lost power and will stop by frictional forces. The total work of brake force during the whole brake cycle equals with the total heat generated. The imposed mechanical energy theoretically transformed to frictional heat. According to EN

14531-6 [11], the frictional heat generated is the area under heat power versus braking time as shown below.

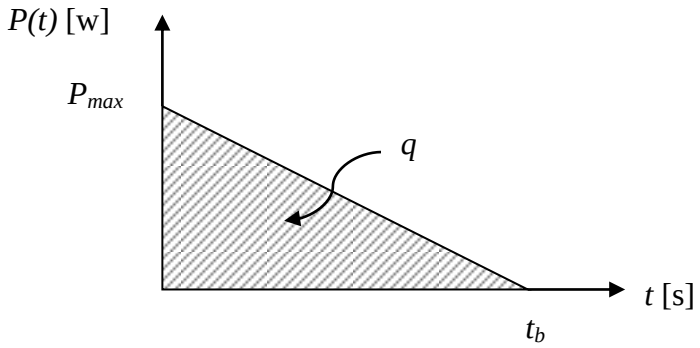

Fig.13: Heat input during braking

$$\frac{1}{2}Mv_0^2[1.1] + M.\mathrm{g}.S_b\frac{\delta}{1000} = \int_0^{t_b} P(t)dt \qquad (3.14)$$

$$\frac{1}{2}Mv_0^2[1.1] + M.\mathrm{g}.S_b\frac{\delta}{1000} = F_b\int_0^{t_b} v(t)dt \qquad (3.15)$$

The railway tramcar running with initial velocity (v_o) is supposed to stand still with constant deceleration (a). Its linear translational velocity as function of time (t) is given by:

$$v(t) = v_o - at \qquad (3.16)$$

The braking distance seems to be extremely appropriate for designating the braking capacity, because it is direct effect of braking forces and all other implied factors, being measurable and permitting comparisons for evaluating the braking efficiency. The total braking time and distance can also be calculated by the formula [13]:

$$S_b = v_o t_b - \frac{1}{2}at_b^2 \qquad (3.17)$$

$$t_b = \frac{V_0}{a} \qquad (3.18)$$

The vehicles shall be 70% low-floor articulated 6-axle modern trams, consisting of three modules, bi-directional driving. Two tramcars shall be able to operate with double heading.

Train formation: –Mc+Tp+Mc– Where,

- ✓ Mc module: motor car with driver's cab
- ✓ Tp module: trailer without driver's cab and with pantograph

- ✓ +: articulation device and -: Hidden folding coupler

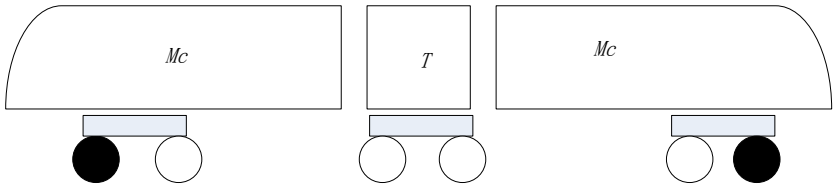

Fig.-14: Addis Ababa LRT tramcar model [8]

The tramcar stop braking on track derives from the physical model for determination of the heat transfer in dependency from the braking time. The weight distribution of the tramcar considered is equally distributed between on both the front and rear bogies, and each bogie consists of three six axles. Every axle is equipped with two wheel mounted hydraulic disc brakes. This means two disc brakes are fitted per axle. Hence, only 1/2 of the whole brake force is applied to one disc from the forward part of the carriage. The braking energy for one wheel considering constant deceleration is:

$$\frac{1}{2}\left\{\frac{1}{2}Mv_0^2[1.1] + M.\mathrm{g}.S_b\frac{\delta}{1000}\right\} = F_b\left[v_o t_b - \frac{1}{2}at_b^2\right] \tag{3.19}$$

$$\text{Braking Force } (F_b) = \frac{\frac{1}{2}\left\{\frac{1}{2}Mv_0^2[1.1] + M.\mathrm{g}.\left[v_o t_b - \frac{1}{2}at_b^2\right]\frac{\delta}{1000}\right\}}{\left[v_o t_b - \frac{1}{2}at_b^2\right]} \tag{3.20}$$

$$F_b = \frac{\frac{1}{2} * 11330 * \left\{\frac{1}{2} * (19.44)^2 * [1.1] + 9.81 * \left[19.44 * 14.40 - \frac{1}{2} * 1.35 * (14.4)^2\right]\frac{50}{1000}\right\}}{\left[19.44 * 14.40 - \frac{1}{2} * 1.35 * (14.4)^2\right]}$$

$$\mathbf{F_b = 11191.21\ (N)}$$

3.6.2. Braking Energy at the Straight Track

During the process of braking at the straight track, the total mechanical available energy of the tramcar that must be transformed into frictional heat is only the kinetic energy, not considering the other resistance forces. This study considers the kinetic energy of the tram that must be dissipated by the work of the braking. Rail vehicles have important masses in rotation. Therefore, the contribution of rotational kinetic energy is taken in to account. The initial

kinetic energy imposed in to the tramcar is given by the sum total of translational and rotational [5]:

$$E_k = \frac{1}{2}Mv_0^2 + \frac{1}{2}I\omega_0^2$$

Therefore, the total available braking energy of the tramcar; not considering an aerodynamic resistance effect is determined from the equation below.

$$E_b = \tfrac{1}{2}Mv_0^2 + \tfrac{1}{2}I\omega_0^2 \quad (3.21)$$

$$\tfrac{1}{2}Mv_0^2 + \tfrac{1}{2}I\omega_0^2 = F_b \int_0^{t_b} v(t)dt \quad (3.22)$$

$$\text{Braking Force } (F_b) = \frac{\frac{1}{2}\left\{\frac{1}{2}Mv_0^2[1.1]\right\}}{\left[v_o t_b - \frac{1}{2}at_b^2\right]} = \frac{\frac{1}{2}\left\{\frac{1}{2} * 11330 * (19.44)^2 * [1.1]\right\}}{\left[19.44 * 14.40 - \frac{1}{2} * 1.35 * (14.4)^2\right]}$$

$$F_b = \mathbf{8412.52(N)}$$

3.6.3. Braking Energy at the Curved Track

The determination of effective braking energy at the curved track**,** by considering the kinetic energy (*Ek*) of the vehicle/train that is dissipated by the work of the braking and resistance forces [5]. Because the rail vehicles have important masses in rotation, their rotation kinetic energy must not be neglected. Thus, the total mechanical energy is only kinetic energy and the energy equation is [5, 11]:

$$E_b = \frac{1}{2}Mv_0^2 + \frac{1}{2}I\omega_0^2$$

$$\tfrac{1}{2}Mv_0^2 + \tfrac{1}{2}I\omega_0^2 = \tfrac{1}{2}Mv_0^2[1.1] = \int_0^{s_b} F_b\, ds + \int_0^{s_b} F_c\, ds \quad (3.23)$$

Curve resistance (F_c) comprises force which is due to carvature of rail track. If c is curve resistance of train [11]:

$$c = \frac{700}{R} \text{ (kg/t)} \quad \text{and} \quad F_c = M*c \text{ (N)} \quad (3.24)$$

Where, M is mass of the train in tonne, c is in Newton per tonne train mass (N/t) and R is minimum radius of track in meters and the curve radii is ≤ 150m.

$$c = \frac{700}{R} = \frac{700}{50} = 14 \text{ (kg/t)} = \mathbf{137.34\ (N/t)}$$

$$F_c = M * c = 11.33(t) * 137.34\left(^{N}/_{t}\right) = \mathbf{1556}\ (\boldsymbol{N})$$

$$\text{Braking Force } (F_b) = \frac{\frac{1}{2}\left\{\frac{1}{2}Mv_0^2[1.1]\right\} - F_c * \left[v_o t_b - \frac{1}{2}at_b^2\right]}{\left[v_o t_b - \frac{1}{2}at_b^2\right]}$$

$$F_b = \frac{\frac{1}{2}\left\{\frac{1}{2} * 11330 * (19.44)^2 * [1.1]\right\} - 1556 * \left[19.44 * 14.40 - \frac{1}{2} * 1.35 * (14.4)^2\right]}{\left[19.44 * 14.40 - \frac{1}{2} * 1.35 * (14.4)^2\right]}$$

$$\mathbf{F_b = 6856.52\ (N)}$$

The possible maximum braking force is critical for the basic wheel/rail adhesion dependent braking systems. The wheel running along the rail will be necessarily accompanied with micro-sliding between wheel and rail and both wheel and rail will be rubbed locally. In the theory of railway traction and braking, the wheel-rail contact state with micro-sliding is called adhesion state and the technical term "adhesion" is used to replace the word "static friction" in the analysis of wheel-rail tangent force. Therefore, the friction braking force is equivalent to the adhesion tangent friction forces at the wheel-rail contact patch and the braking force obtained at the three track level conditions are used for the analysis.

3.7. Wheel-Rail Contact Parameters

Many head of the rail profile consists of three transverse radii of curvature (namely: 300 mm, 80 mm and 13 mm). But, the 50kg/m TB has two radii of contacts: 300 mm and 13 mm. Thus, the transverse radius of curvature of the rail profile at the contact point used is R=300mm. For this study, it is assumed that the wheel profile is cylindrical and the rail track is tangent, thus both the transverse radius of curvature of the wheel profile and the principal rolling radius of the rail (R_2^w and R_1^r) become ∞ . This means that it is reasonable to assume that: $\frac{1}{R_2^w} + \frac{1}{R_1^r} = 0$

$$a = m\left[\frac{3\pi N(K_1 + K_2)}{4K_3}\right]^{1/3} \text{ and}$$

$$b = n\left[\frac{3\pi N(K_1 + K_2)}{4K_3}\right]^{1/3}$$

$$\text{But, } K_1 = \frac{1-v_w^2}{\pi E_w} = \frac{1-(0.31)^2}{\pi * 210 * e^9} = \mathbf{1.37e^{-12}},$$

$$K_2 = \frac{1-v_r^2}{\pi E_r} = K_1 = \mathbf{1.37e^{-12}}$$

$$K_3 = \frac{1}{2}\left[\frac{1}{R_1^w} + \frac{1}{R_2^w} + \frac{1}{R_1^r} + \frac{1}{R_2^r}\right] = \frac{1}{2}\left[\frac{1}{0.33} + \frac{1}{\infty} + \frac{1}{\infty} + \frac{1}{0.3}\right] = \mathbf{3.18}$$

$$K_4 = \frac{1}{2}\left[\left(\frac{1}{R_1^w}\right)^2 + \left(\frac{1}{R_2^r}\right)^2 - 2\left(\frac{1}{R_1^w}\right)\left(\frac{1}{R_2^r}\right)\right]^{1/2}$$

$$= \frac{1}{2}\left[\left(\frac{1}{0.33}\right)^2 + \left(\frac{1}{0.3}\right)^2 - 2\left(\frac{1}{0.33}\right)\left(\frac{1}{0.3}\right)\right]^{1/2} = \mathbf{0.1515}$$

$$\theta = Cos^{-1}\left(\frac{K_4}{K_3}\right) = Cos^{-1}\left(\frac{0.1515}{3.18}\right) = 87.269(°)$$

From table appendix-A and by using interpolation: **m=1.033** and **n= 0.969**

$$N = \frac{1}{2}(\text{Maximum axle load}) * 9.81 = \frac{1}{2}\left(11(1+3\%)(ton)\right) * 9.81\left(m/s^2\right) = \mathbf{55551}\ (\boldsymbol{N})$$

Thus, $a = m\left[\frac{3\pi N(K_1+K_2)}{4K_3}\right]^{1/3} = 1.0333 * \left[\frac{3\pi * 55551 * 2\left(1.37e^{-12}\right)}{4*3.18}\right]^{1/3} = \mathbf{4.99}\ (\boldsymbol{mm})$ and

$$b = n\left[\frac{3\pi N(K_1 + K_2)}{4K_3}\right]^{1/3} = 0.969\left[\frac{3\pi * 55551 * 2(1.37e^{-12})}{4 * 3.18}\right]^{1/3} = \mathbf{4.68}\ (\boldsymbol{mm})$$

Therefore, since the major axis (a) is along the longitudinal direction, largest heat flux and the highest temperatures occur along the longitudinal axis which is parallel to the rolling direction.

3.8. Heat Energy

In braking system, the mechanical energy is transformed into heat energy. The total heat generated (Q_g) in the brake system equals with the total mechanical energy (E_b) lost from the tram. Hence, considering the energy balance [5]:

$$Q_g = E_b \qquad (3.25)$$

The heat power generated per unit contact area at the radius r of the wheel can be calculated as:

$$q_f = F_f * r * \omega \qquad (w) \qquad (3.26)$$

The heat flux evacuated of surfaces in contact (between rail and wheel) is equal to the power friction.

$$\text{Total heat flux } = \frac{Q_g}{A} = \frac{q_f}{\pi ab} \qquad \left(w/m^2\right) \qquad (3.27)$$

Amount of heat power flow to the wheel and rail with respect to braking duration is governed by the heat partitioning parameter (Ω) and in most analysis it was taken as 60-90 % of the total heat dissipated. Thus, the partitioned heat power flow through the rail, by taking partition factor 0.8 is calculated in the following table.

$$q_r = \Omega q_f \qquad (w) \qquad (3.28)$$

$$\text{Heat flux for the rail} = \frac{\Omega * q_f}{\pi ab} \qquad \left(\frac{w}{m^2}\right) \qquad (3.29)$$

$$\text{Maximum contact pressure}(P_{max}) = \frac{3N}{2\pi ab} \qquad (pa) \qquad (3.30)$$

Table-3: Summary for the thermal analytical results

Parameter	**Formula**	**Downgrade**	**Straight track**	**Curved track**
Braking force (F_b)-[N]		11191.21	8412.52	6856.52
Friction force (F_f)-[N]	$F_b * \mu_s$	3916.92	2944.38	2399.78
Total heat power (q_f)-[w]	$F_f * r * \omega$	76146.17	57239.67	46652.48
Total heat flux-$\left[\frac{w}{m^2}\right]$	$\frac{q_f}{\pi ab}$	$1.04e^{+09}$	$7.80e^{+08}$	$6.36e^{+08}$
Maximum contact pressure -[Gpa]	$\frac{3N}{2\pi ab}$	1.14	1.14	1.14
Rail heat power(q_r)- [w]	Ωq_f	60916.94	45791.74	37321.99
Rail heat flux - $\left[\frac{w}{m^2}\right]$	$\frac{\Omega * q_f}{\pi ab}$	$8.30e^{+08}$	$6.24e^{+08}$	$5.09e^{+08}$
Apparent rail heat flux-$\left[\frac{w}{m^2}\right]$	$\frac{\Omega * q_f}{wl}$	331070.33	248868.15	202836.90

3.9. Assumptions

The following assumptions were taken for the whole analysis:-

- ✓ Standard wheel threads are coned shapes. But, for simplicity the cylindrical shape is used for the analysis.
- ✓ In this analysis, only the thermal raise between wheel and rail is considered.
- ✓ However, in reality they have small clearance between them, the rail and fish plates are connected as bonded.
- ✓ The nominal surface of contact between the rail and the wheel in operation is equal to the apparent surface in the sliding motion.
- ✓ The contact pressure is uniformly distributed over all friction surfaces; the average of the intensity of heat flux into the rail on all the contact areas for the given length of rails is assumed to be equal and the heat transferred to the surrounding air, heat convection and heat radiation is neglected

3.10. Material Selection

From the common and inexpensive metals, steel has one of the highest values of elastic modulus (190-210) Gpa. For this reason, and because steel is relatively inexpensive and offers a very attractive combination of strength, ductility, and wear resistance, almost all wheels and rails worldwide are made from plain carbon-manganese pearlite steel, which has a lamellar structure of iron and iron carbide.

3.10.1. Wheel material

The following table illustrates the chemistries and mechanical property values of a typical wheel used for Addis Ababa LRT as ER9 and EN13262.

Table-4(a): Mechanical properties of the wheel material [8, 19]

Steel category		**Yield Strength (N/mm^2)**	**Ultimate Strength (N/mm^2)**	**Elongation (%)**	**Notch impact energy (J)**	
UIC 812-3	EN 13262	EN 13262	UIC/EN	UIC/EN	UIC 812-3 U-notch(RT)	EN 13262 V-notch(-20℃)
R9T,E	ER9	≥ 580	900-1050	≥ 12	≥ 10	≥ 8

Table-4(b): Chemical compositions of the wheel material

Grade (Steel)	**Main elements**					**Residual elements**				
	C	**Si**	**Mn**	**P**	**S**	**Cr**	**Cu**	**Mo**	**Ni**	**V**
ER9	0.60	0.40	0.80	0.04	0.04	0.03	0.30	0.08	0.30	0.05

3.10.2. Rail and Fish plate material

According to standard EN 13674, the U71Mn steel grade is the rail which mechanical properties are equivalent to R260Mn that introduce the qualified and accepted values. The following table shows the mechanical properties and chemical composition values with the heat treating residual elements of the rails and fish plate used for Addis Ababa LRT with standard code of GB2585-2007 and TB/T2344-2003[7, 8]. The increase in wear resistance is based on a theory of the mutual influence of certain elements. Carbon influences the mechanical properties through the volume fraction of cementite and the content of pearlite. Manganese influences the temperature decrease of the eutectoidal reaction and the fineness of pearlite lamellae, that is, the reduction in the inter-lamellar distance. So, the influence of residual alloying elements, such as carbon, manganese and silicon, on wear speed for a pearlite structure is much higher and the decimal composition values are shown in the following table.

Table-5(a): Mechanical properties of the rail and fish plate [7, 8, 23, 34]

Standard	***Type***	***Steel grade***	**Yield Strength (N/mm^2)**	***Ultimate Strength (N/mm2)***	***Extensibility A (%)***	***Hardness of Rail head (HBW10/3000)***
GB2585(2007) TB/T234(2003)	50 kg/m	U71 Mn	≥460	≥880	≥10	260-300
Rail type (kg/m)					50.00	
Section area (cm^2)					65.80	
Center of gravity from bottom of rail (cm)					7.10	
Center of gravity from ends of rail (cm)					8.10	
Moment inertia of Horizontal axis (cm^4)					2037.00	
Moment inertia of vertical axis (cm^4)					377.00	
Cross-section coefficient of bottom (cm^3)					287.20	
Cross-section coefficient of top(cm^3)					251.30	
Cross-section coefficient of bottom side edge (cm^3)					57.10	
Coefficient of Thermal Expansion					1.2e-005 C^-1	

Specific Heat	434 J kg^-1 C^-1
Thermal Conductivity	60.5 W m^-1 C^-1
Resistivity	1.7e-007 ohm m

Table-5(b): Chemical compositions of the rail and fish plate

Standard	Type	Steel grade	Main elements						Residual elements			
			C	Si	Mn	P	S	V	Cr	Cu	Mo	Ni
GB2585-2007; TB/T2344-2003	50kg/m	U71 Mn	0.65~0.76	0.15~0.35	1.10~1.40	≤0.030	≤0.030	≤0.030	0.15	0.15	0.02	0.10

3.11. Finite Element Modeling

Finite Element Method is a mathematical modeling tool involving discretization of a continuous domain using building-block entities called finite elements connected to each other by nodes for once and moment transfer. In this case, it is used to analyze the response of the wheel-rail contact effects on the rail at the continuous and jointed rail due to the static and dynamic loads.

The analysis is done by importing of 3D assembled model from CATIA V5-R16 to ANSYS-12 work bench that is then processed in order to clean up unnecessary details or components. The imported Model is then meshed to act like single entity. Finer mesh and close to exact solution can be achieved by controlling the mesh size to make the solution accurate.

The ANSYS software implements equations that govern the behavior of elements and solves them all; creating a comprehensive explanation of how the system acts as a whole. When the wheel is contact element and the rail is target element, the wheel and rail will be different. The wheel structure discretized into 24106, the rail-joint components 43658, the polyethylene rail-pad 72 and the concrete sleeper 1800 elements. The interval time for the dynamic analysis is 2.5 sec. and the maximum amount of time is 1sec. for the thermal finite element analysis.

3.12. Boundary Conditions and Load Applications

In the analysis, the situation considered is the standstill condition of the vehicle on a level road to the maximum wheel load with the +3% allowance payload. The other loads are: the displacement, rotational angular velocity, Standard earth gravity, frictional forces, initial temperature, contact pressure and heat flux. It is considered that the wheel and rail are initially at ambient temperature on coming into contact just before the brake application has started.

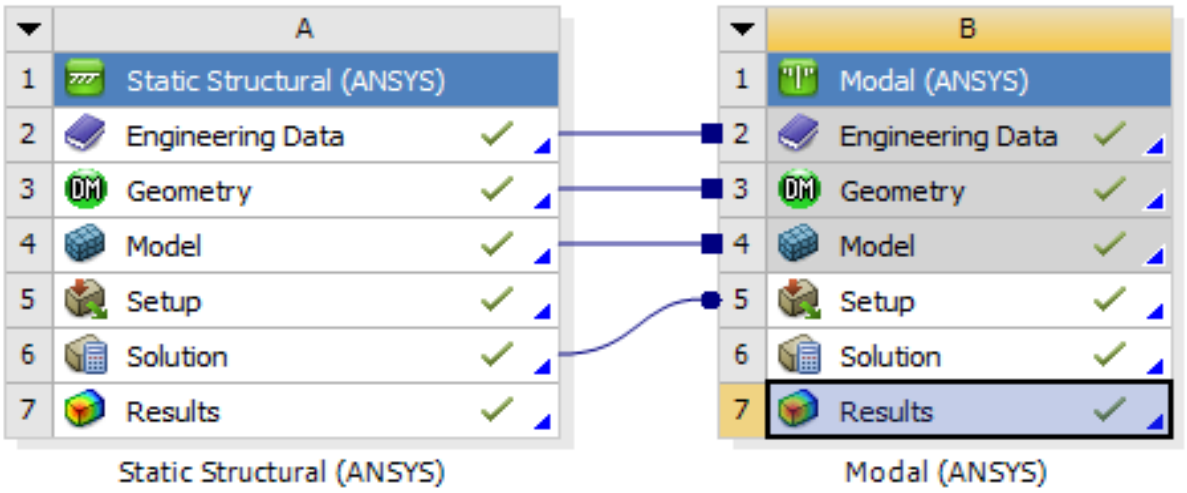

Fig.-15(a): Combining static and dynamic modal analysis

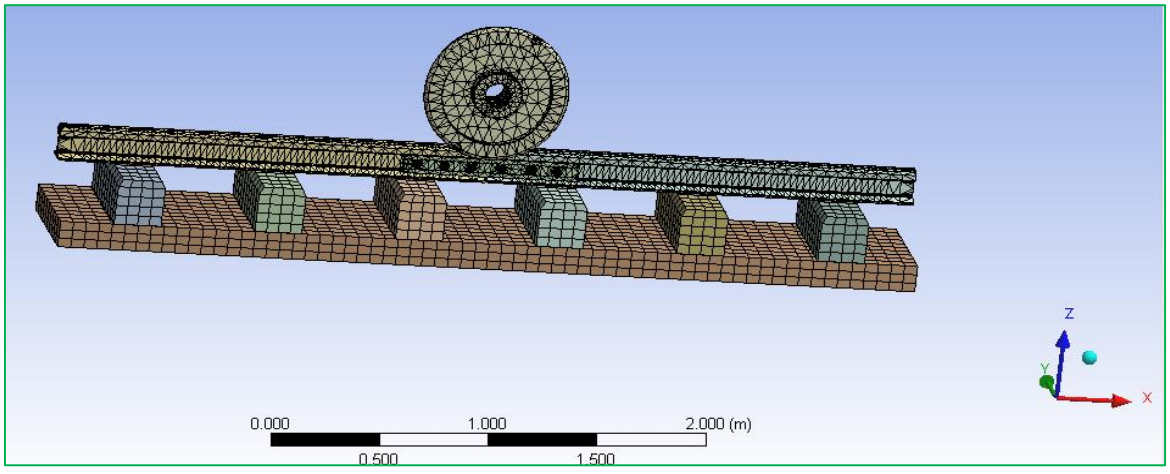

Fig.-15(b): The generated mesh model

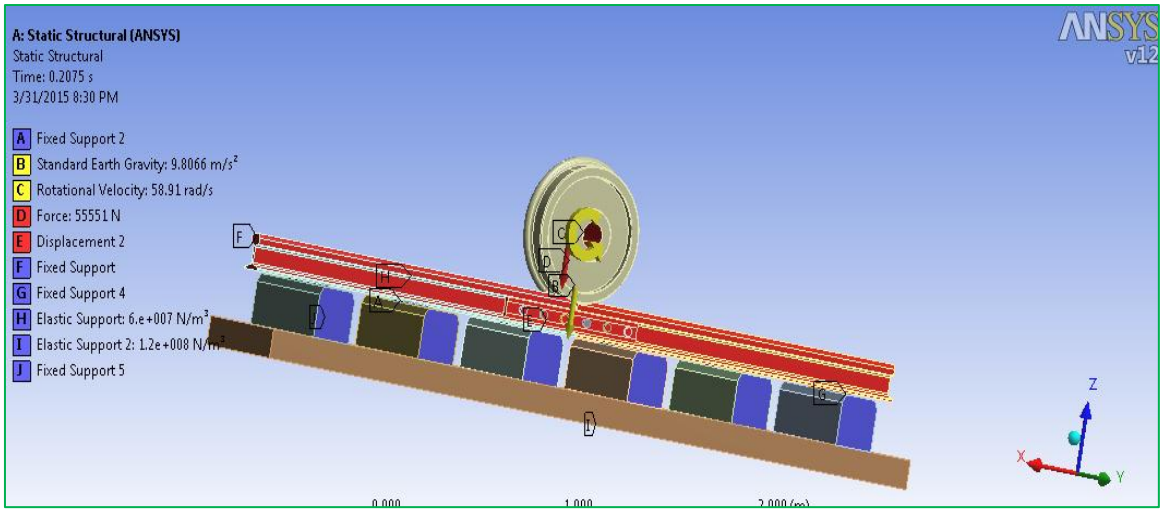

Fig.-15(c): Boundary conditions for modal analysis

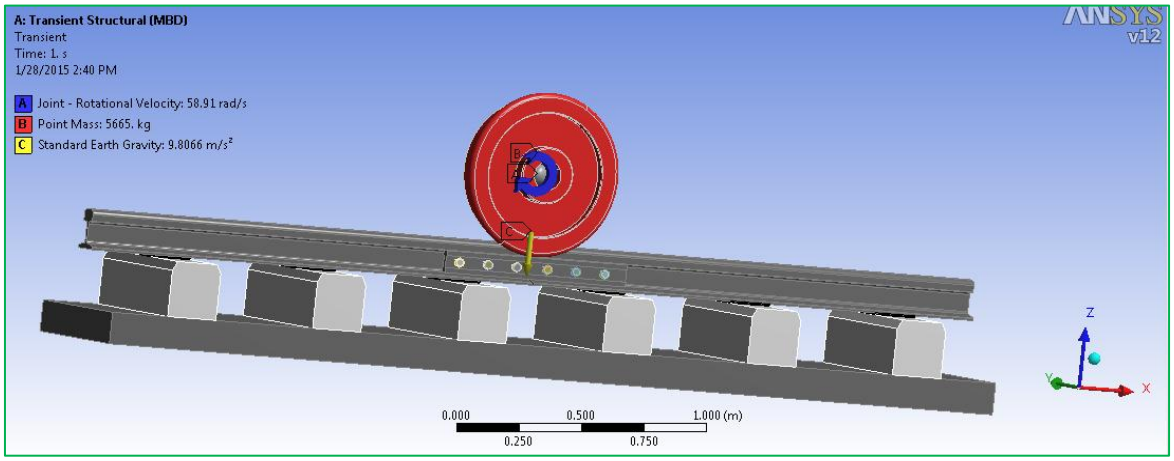

Fig.-15(d): Boundary conditions & load applications for transient structural (MBD) analysis

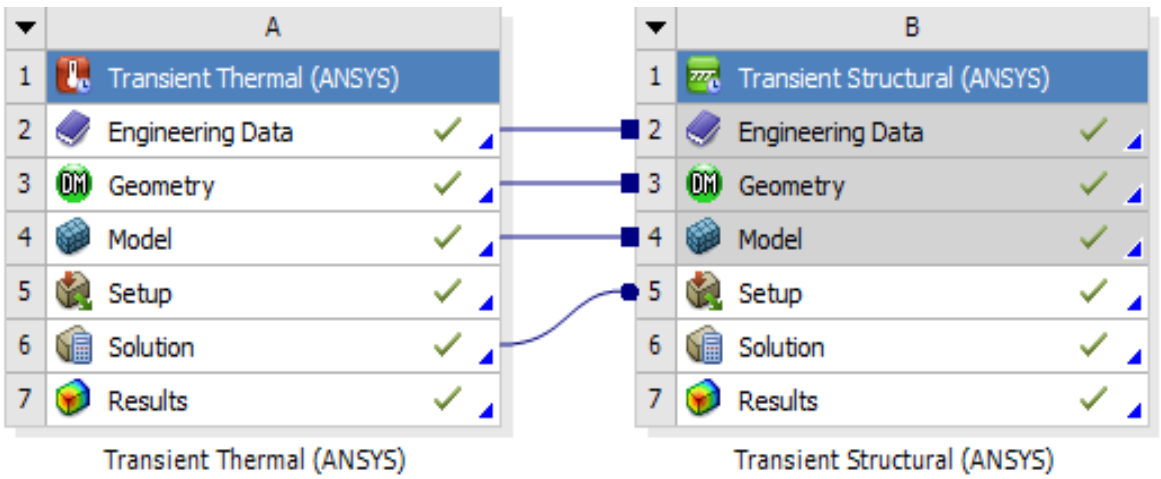

Fig.-15(e): Combining transient thermal and transient structural analysis

CHAPTER-FOUR: RESULT AND DISCUSIONS

4.1. Static and Modal Analysis

The static analysis is concerned with determination of the response of the rail to steady state loads. The corresponding stresses and strains are obtained using strain-displacement and strain-stress (constitutive) relations. The deflections between two nodes are determined using the assumed shape functions. The solution gives nodal translational and rotational displacements. A modal analysis determines the vibration characteristics of the structure. A modal analysis is performed on a pre-stressed structure. Thus, it requires performing a static structural analysis first. The natural frequencies and mode shape are important parameters in the design of the structure for dynamic loading conditions. In this section, the total deformation, maximum von-mises stress, the first five natural frequencies and its mode shapes for both continuous and jointed rail are discussed.

4.1.1. Continuous Rail

The continuous rail is the rail head surfaces where there is no the bolted joining edges and it may include the well welded rail ends. The results are maximum total deformations, the von-mises stress and the first five natural frequencies.

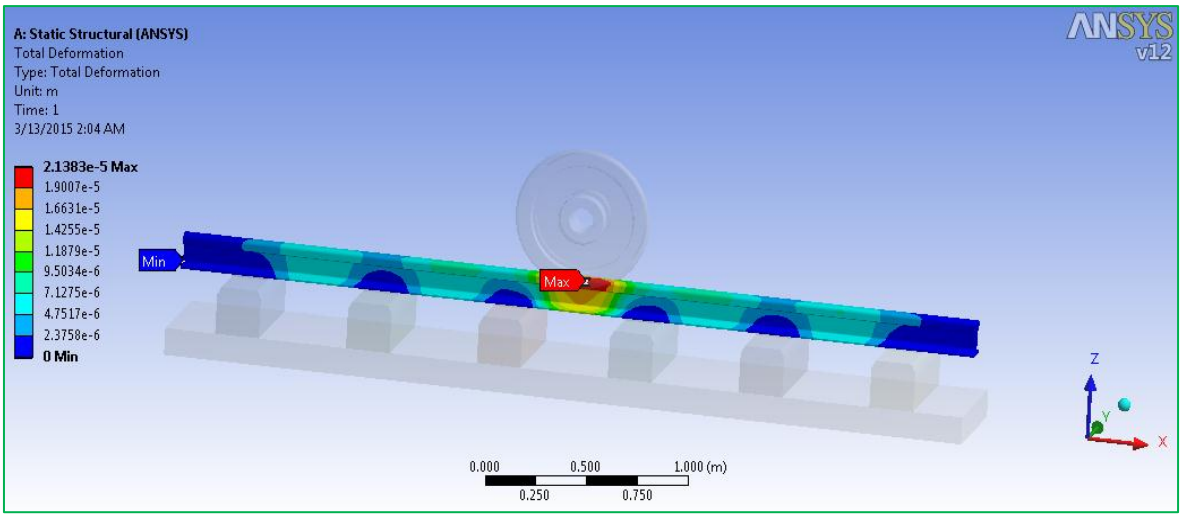

Fig.-16(a): Total deformation of the continuous rail (δ_{max}= 2.1383e-005m)

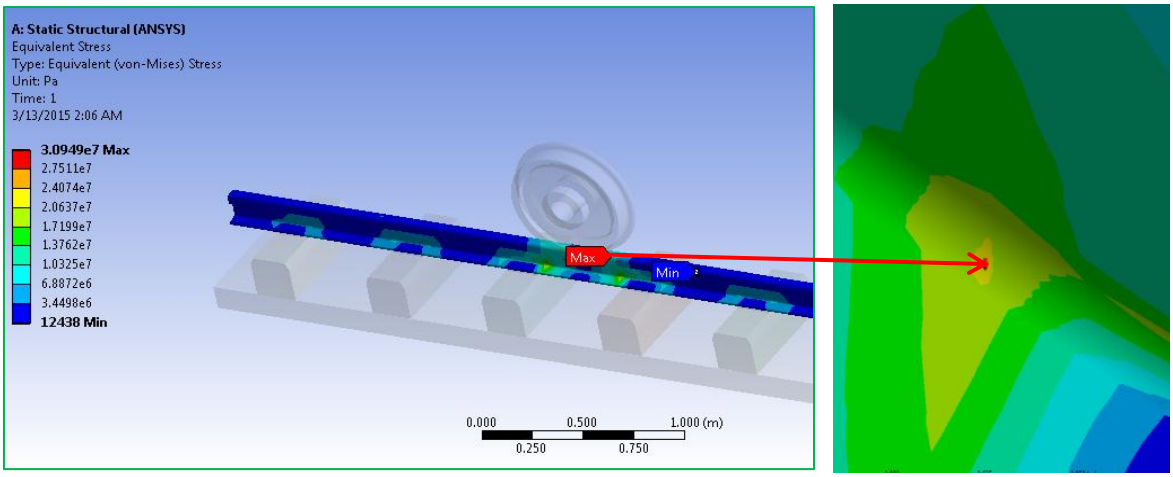

Fig.-16(b): Equivalent (Von-Mises) Stress of the continuous rail

✓ Since the yield strength of the rail material is 46.00e+007 Pa and the Equivalent (Von-Mises) Stress 3.0949e+007 Pa, the rail is safe to with stand the loading.

Table-6: Modal frequency and Maximum deformation results at the continuous rail

No.	Mode shape (DOF)	Natural frequency (Hz)	Max. deformation (m)
1	Lateral bending	42.136	1.1506e-002
2	Torsion along Y-axis	212.22	1.1544e-002
3	Torsion along Z-axis	259.08	1.1039e-002
4	Torsion along X-axis	371.5	6.3931e-002
5	Vertical bending	617.67	5.0965e-002

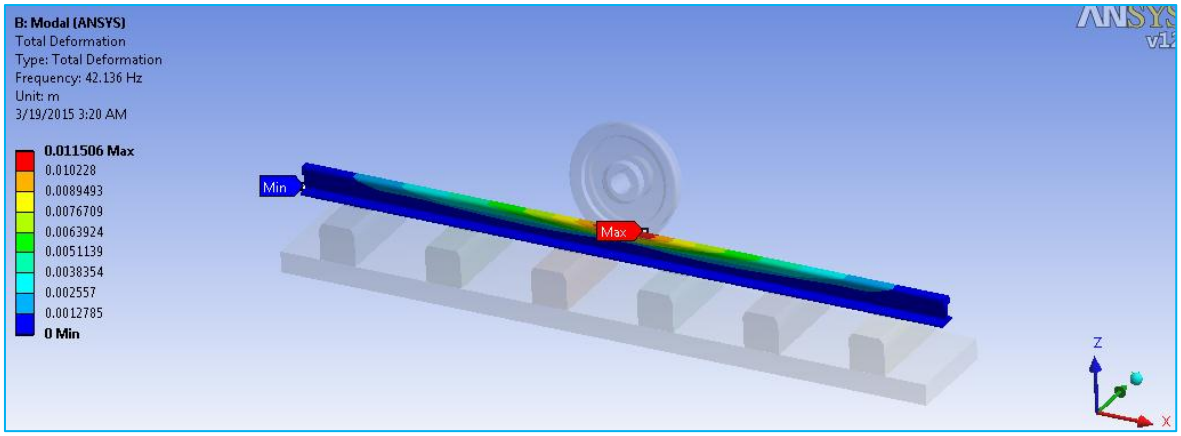

Fig.-16(c): Mode-1 of the Continuum rail: Lateral bending (*f = 42.136Hz*)

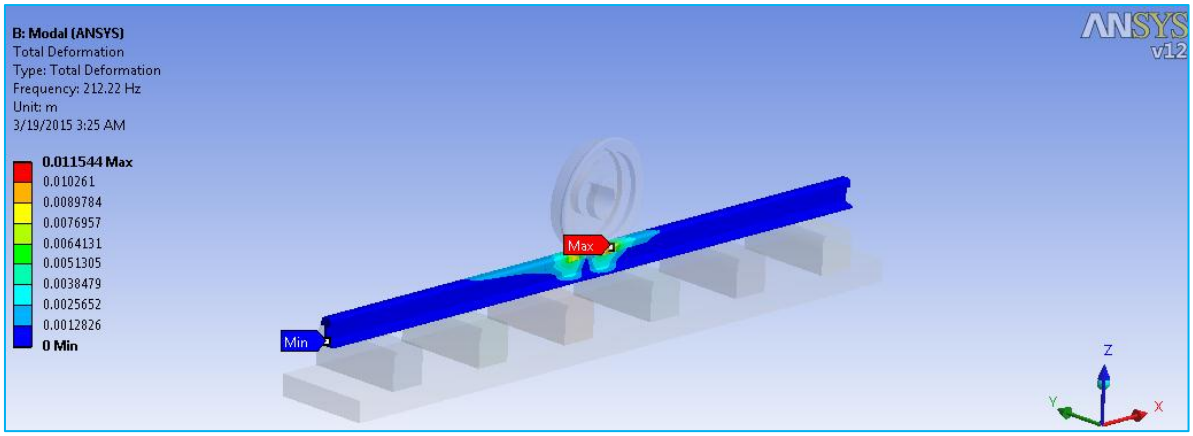

Fig.-16(d): Mode-2 of the Continuum rail: Torsion along Y-axis (*f = 212.220 Hz*)

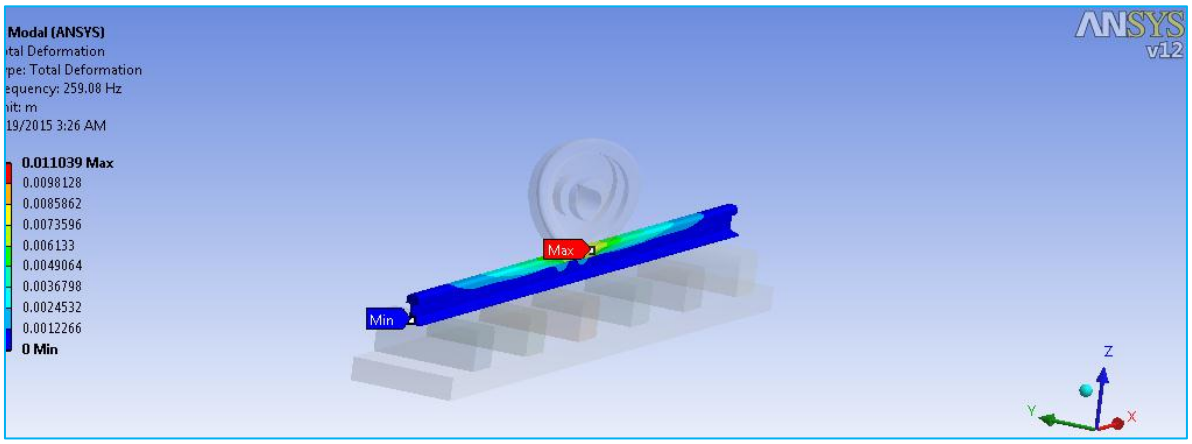

Fig.-16(e): Mode-3 of the Continuum rail: Torsion along Z-axis (*f = 259.080 Hz*)

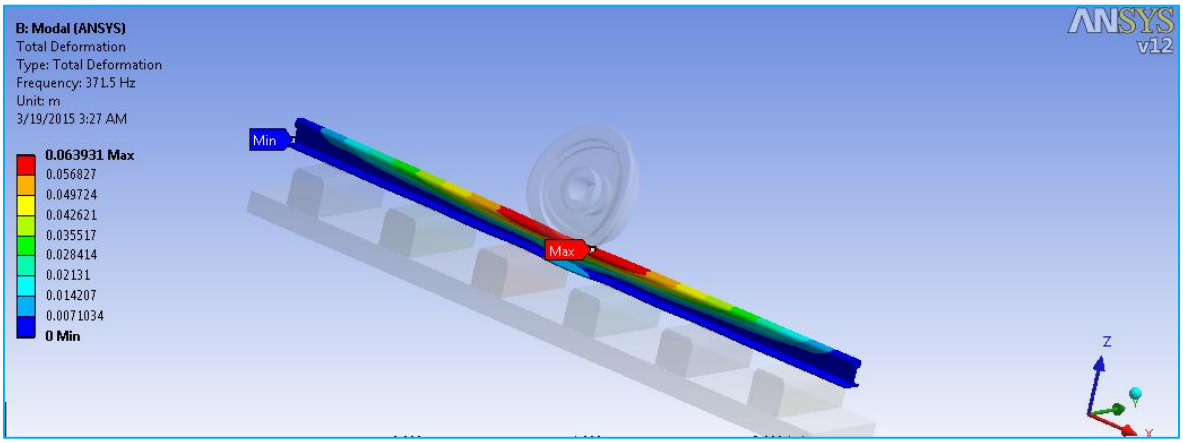

Fig.-16(f): Mode-4 of the Continuum rail: Torsion along X-axis (*f=371.500 Hz*)

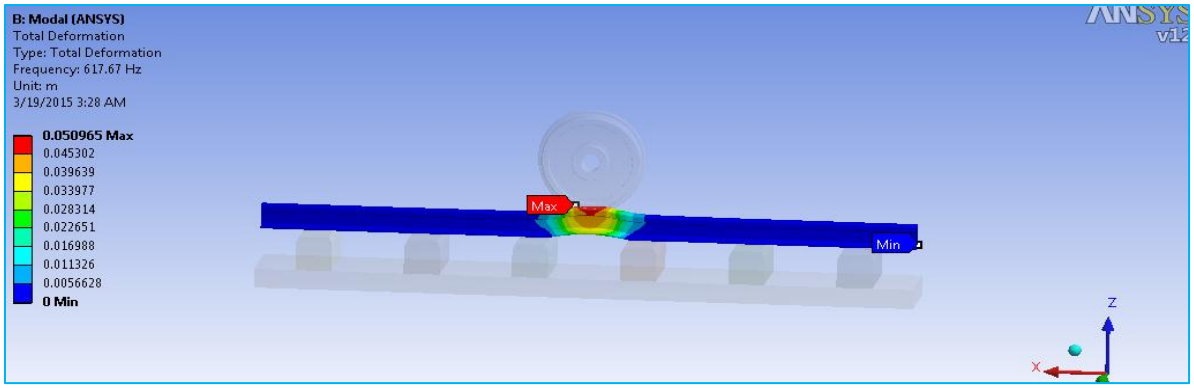

Fig.-16(g): Mode-5 of the Continuum rail: Vertical bending (*f= 617.670*)

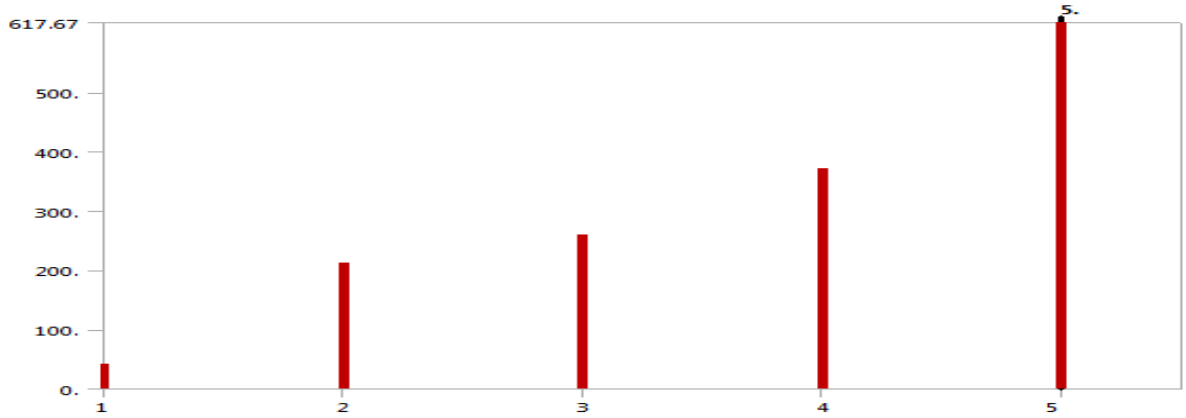

Fig.-16(h): The first five natural frequencies Vs. mode shape graph for a continuous rail

4.1.1. Jointed Rail

The continuity of the railway track is breaks due to the existence of rail gap and difference in the height of the rail heads. So, its continuity is kept by the rail end joining. These analyses may inferences whether the continuous or the jointed part of the rail couldn't withstand the loadings. The results retrieved and discussed are: the maximum total deformations, the von-mises stress, the first five natural frequencies and their corresponding mode shapes.

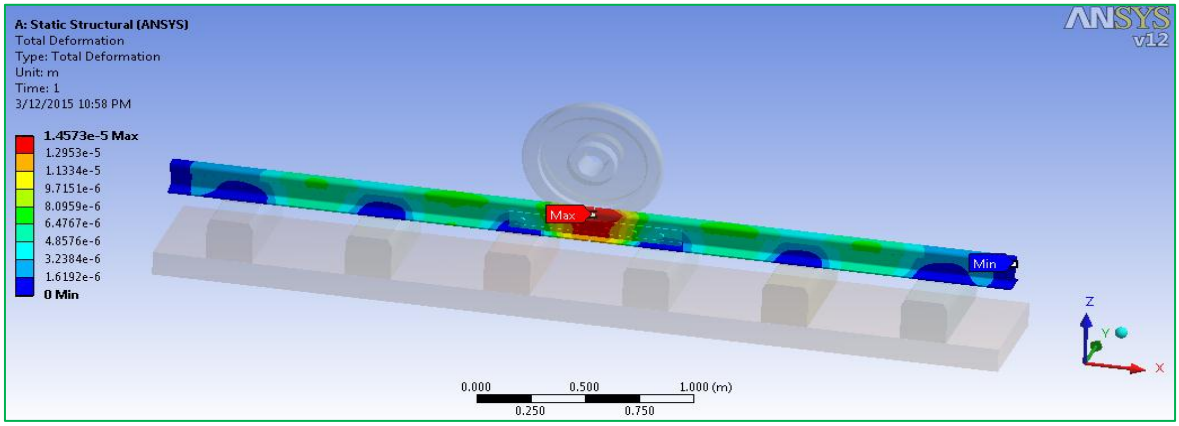

Fig.-17(a): Total deformation of jointed rail (δ_{max}= 1.4573e-005 m)

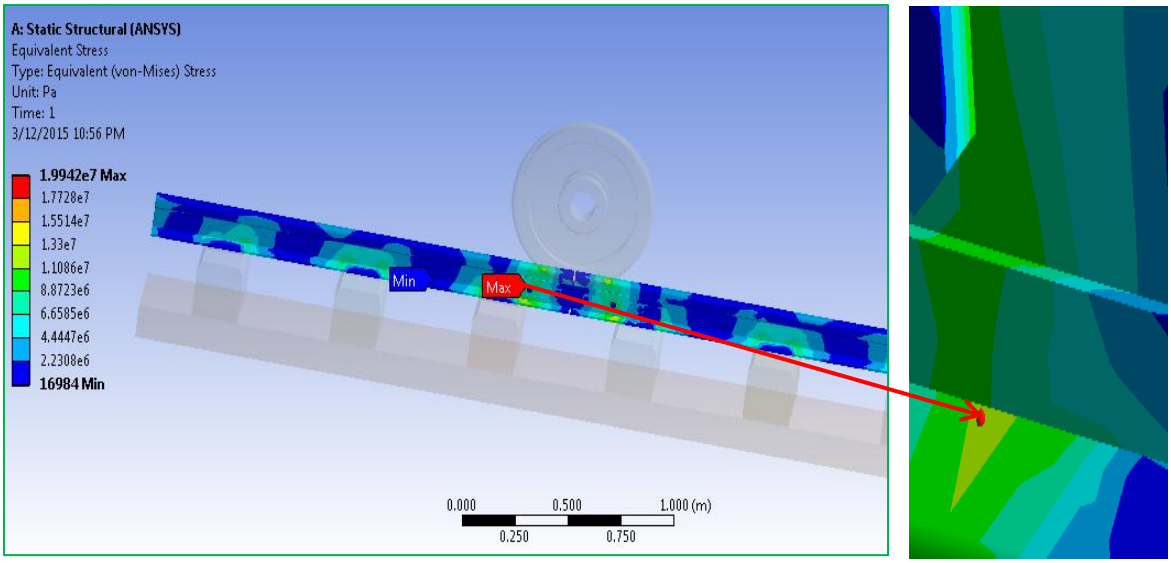

Fig.-17(b): Equivalent (Von Mises) Stress of the jointed rail

- ✓ Since the yield strength of the rail material is 46.00e+007 Pa and the Equivalent (Von-Mises) Stress 1.9942e+007 Pa, the rail-joint is safe to with stand the loading.
- ✓ From the result, the static total deformations and Von-mises stress at the continuum rail is larger than at the jointed rail
- ✓ As shown in table-6 and table-7, the maximum deformations and natural frequency at the rail-joint is larger than at the continuous rail track for the dynamic effects.

Table-7: The first five natural frequencies and maximum deformations at the rail-joint

No.	**Mode shape (DOF)**	**Frequency (Hz)**	**Max. deformation (m)**
1	Lateral bending	80.326	1.116e-002
2	Torsion along Y-axis	263.43	1.089e-002
3	Torsion along Z-axis	335.32	1.194e-002
4	Torsion along X-axis	513.47	5.4382e-002
5	Vertical bending	774.65	4.8243e-002

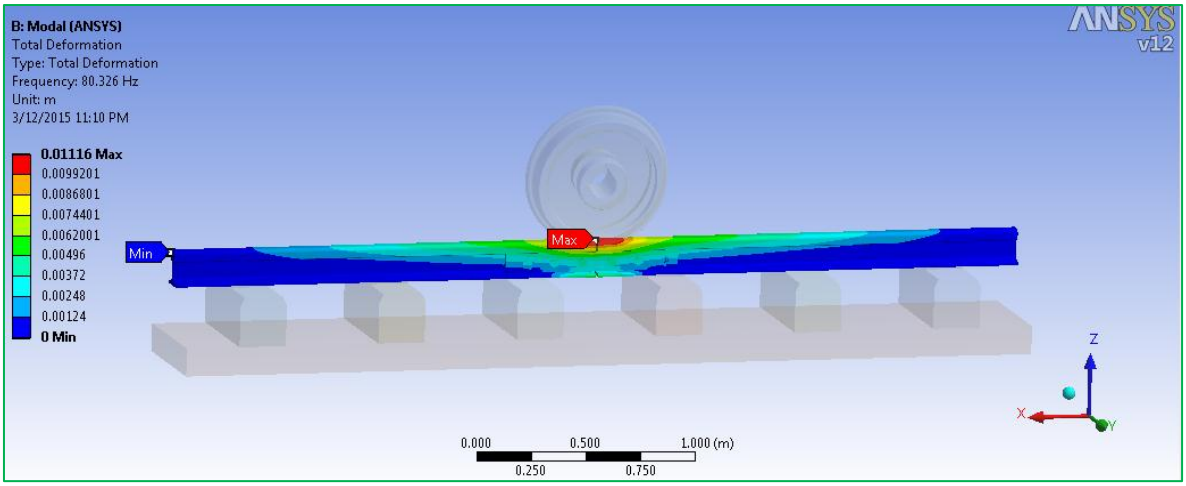

Fig.-17(c): Mode-1 of the jointed rail: Lateral bending (*f = 80.326Hz*)

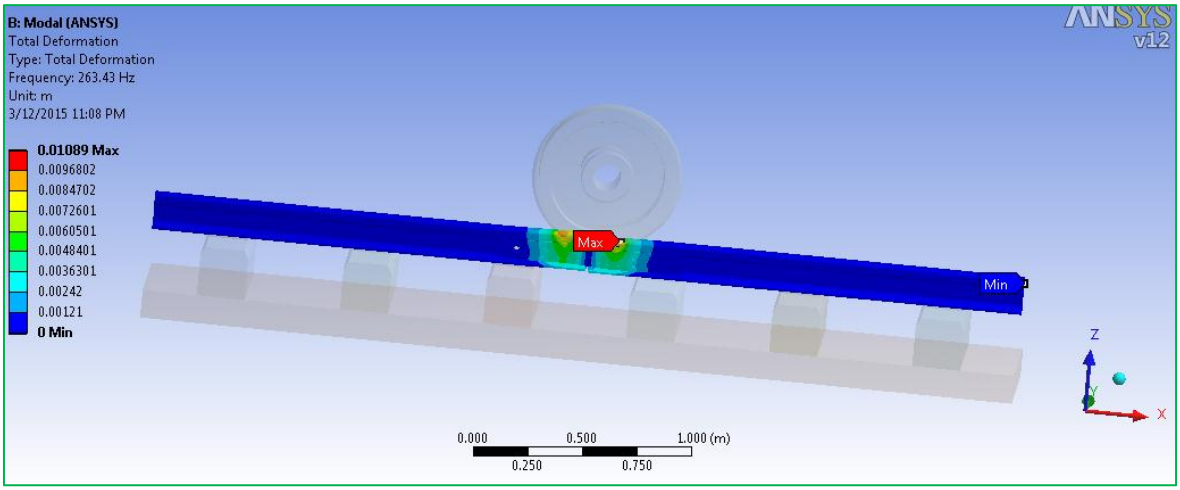

Fig.-17(d): Mode-2 of the jointed rail: Torsion along Y-axis (*f = 263.430 Hz*)

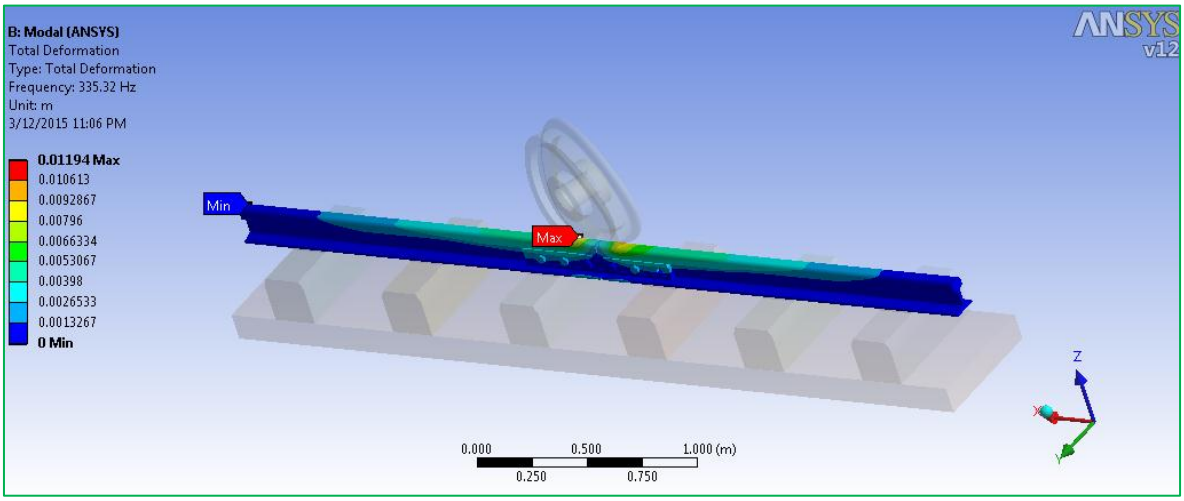

Fig.-17(e): Mode-3 of the jointed rail: Torsion along Z-axis (*f = 335.320 Hz*)

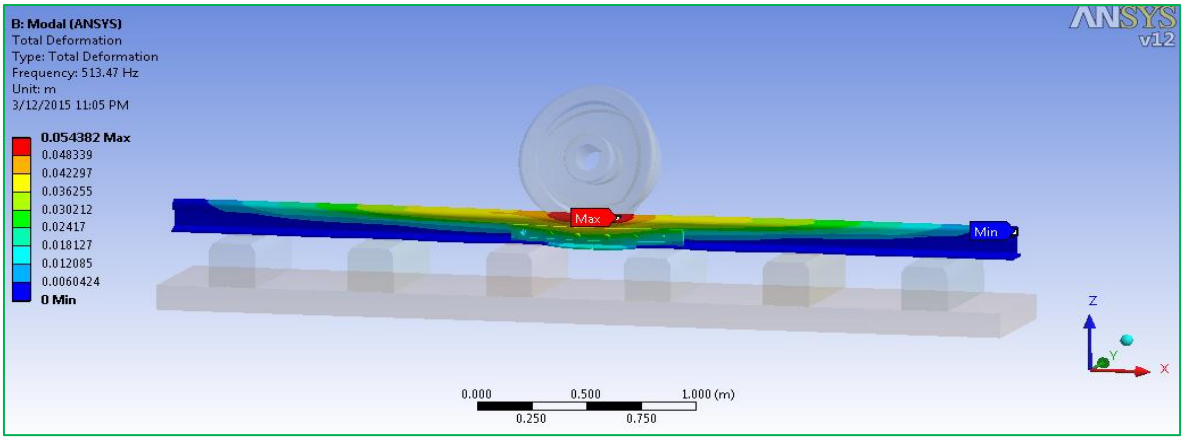

Fig.-17(f): Mode-4 of the jointed rail: Torsion along X-axis (*f=513.470 Hz*)

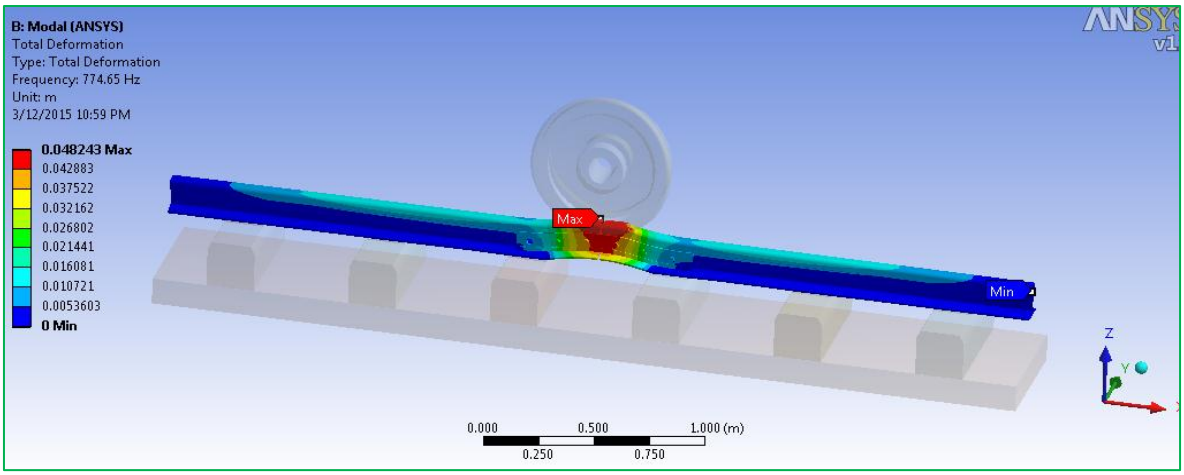

Fig.-17(g): Mode-5 of the jointed rail: Vertical bending (f= 774.650)

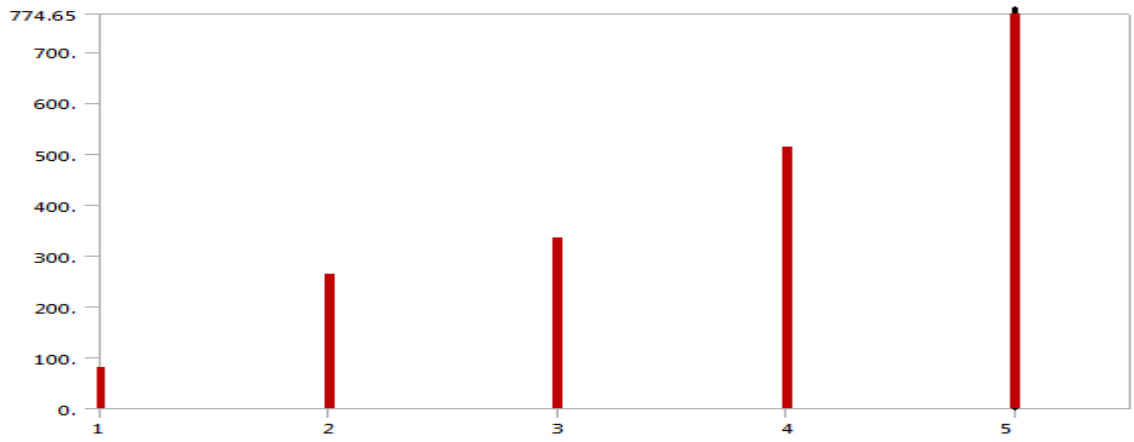

Fig.-17(i): The first five natural frequencies graph for a jointed-rail at each DOF

- ✓ For the static analysis, the maximum deformation and von-mises stress of the rail at the continuum is larger than at the jointed part and for both rail conditions the natural frequencies are smaller than the standard minimum limit (i.e. ≤ 1-1.5 kHz)

4.2. Transient (ANSYS) Analysis

Transient structural analysis is used to determine the dynamic response of a structure under the action loads. It determines the time –varying, strains, stress, and forces in a structure as it response to any transient effects under time dependent loads. In this analysis loading is such that the inertia or damping effect are considered. The damping effect is engaged from the rail-pad called polyethylene. In this paper the transient analysis was done on the continuous and jointed rail to show the dynamic impact by varying the applied load with very small time.

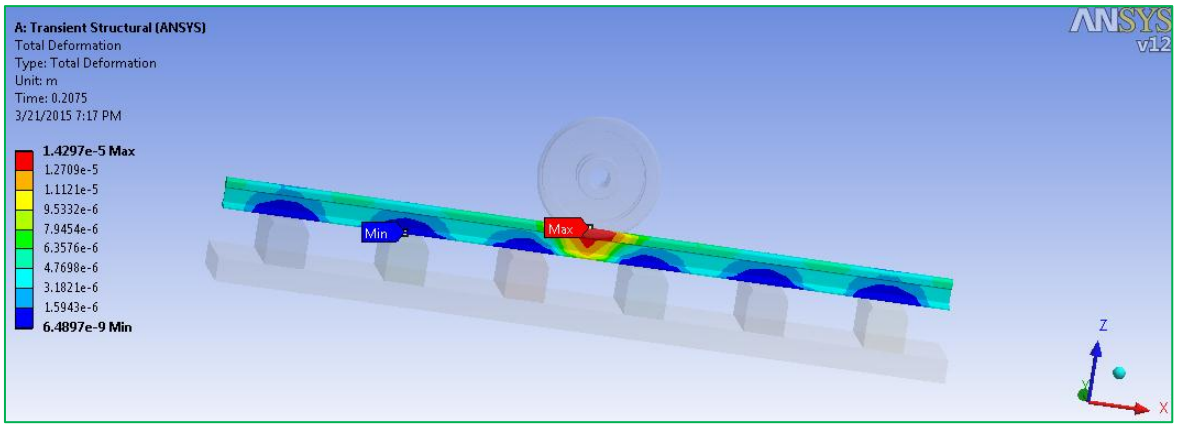

Fig.-18(a): Total transient deformation at the continuum rail

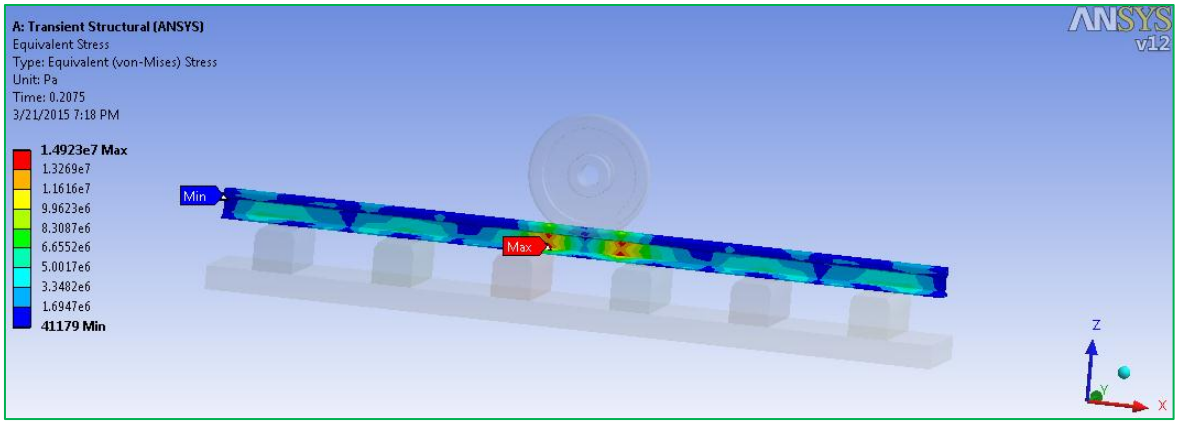

Fig.-18(b): Transient Von-mises stress at the continuum rail

- ✓ Since the yield strength of the rail material is 46.00e+007 Pa and the Transient Equivalent (Von-Mises) Stress 1.4923e+007 Pa, the rail at the continuous is safe to with stand the transient structural loading.

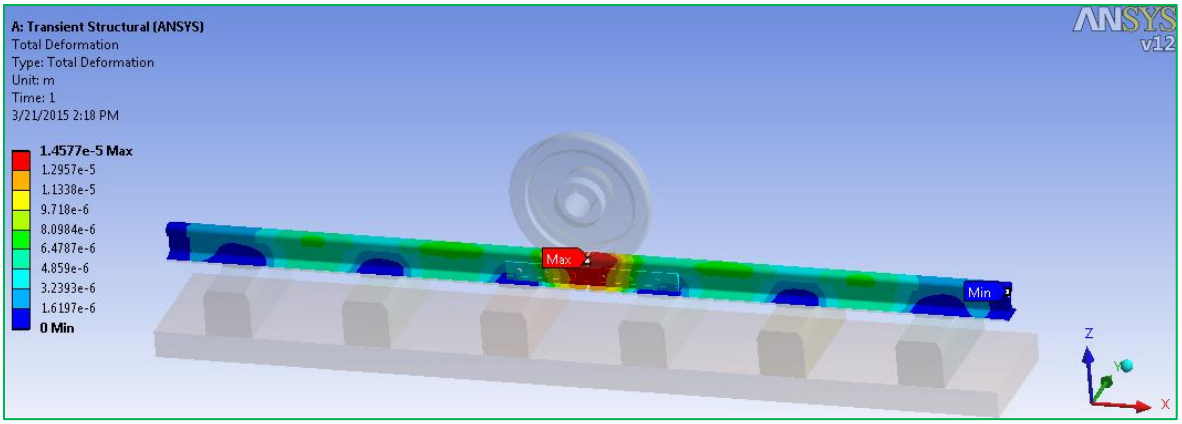

Fig.-18(c): Total transient deformation at the jointed rail

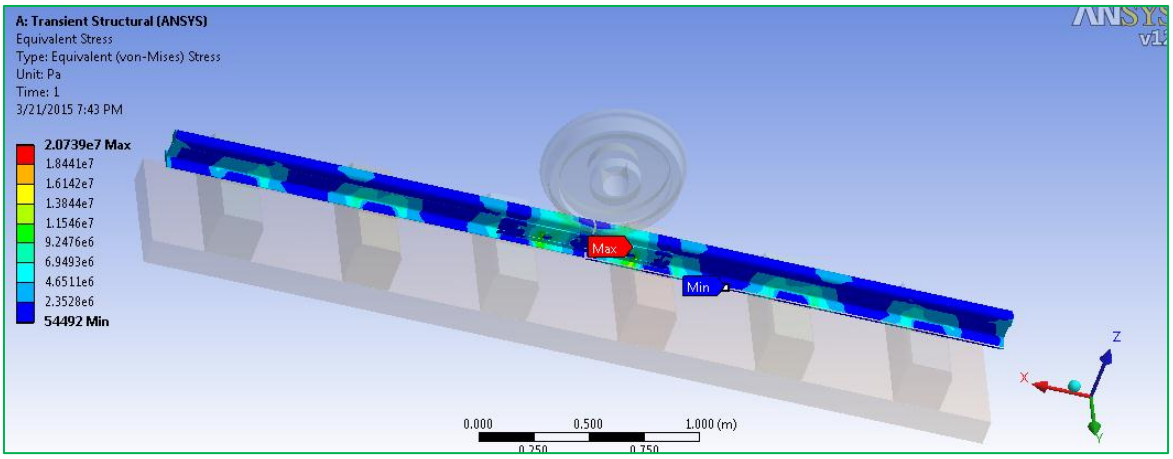

Fig.-18(d): Transient Von-mises stress at the jointed rail

- ✓ Since the yield strength of the rail material is 46.00e+007 Pa and the Transient Equivalent (Von-Mises) Stress 2.0739e+007 Pa, the rail-joint is safe to with stand the transient structural loading.

Table-8: Summary of the transient results for the continuous and the jointed rail

Transient parameter	**Maximum value over the time(1sec)**	
	Continuum rail	**Jointed rail**
Total deformation (m)	1.4297e-005	1.4577e-005
Von mises stress (Pa)	1.4923e+007	2.0739e+007

- ✓ For the transient analysis, the maximum deformation and von-mises stress of the rail at the joint is larger than at continuum part

4.3. Transient Structural (MBD) Analysis of the Jointed Rail

Transient structural multi-body dynamics (MBD) analysis in mechanical application uses the ANSYS Rigid Dynamics solver. This type of analysis is used to determine the dynamic response of an assembly of rigid bodies linked by joints and springs. In this analysis joint rotation are not cumulative with each additional step. All parts are assumed to be rigid such that there are no stresses and strain results produced, and only probe forces, energy, moments, displacements, velocities and accelerations are dealt with inputs and outputs.

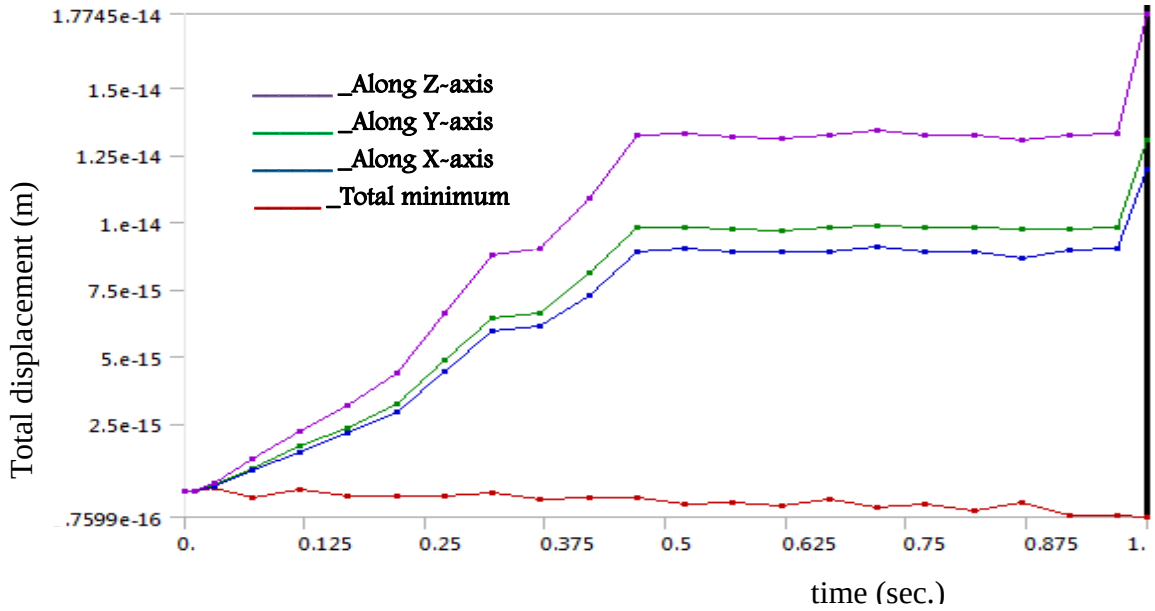

Fig.-19(a): Total displacement of the jointed rail

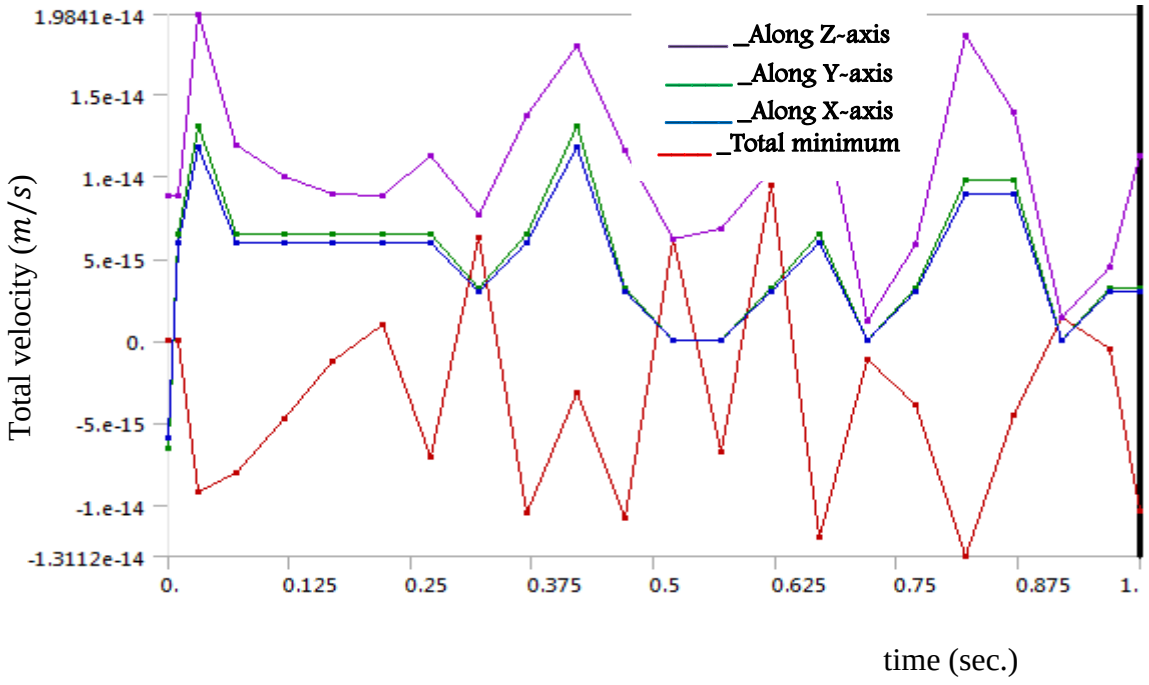

Fig.19(b): Total Velocity of the jointed rail

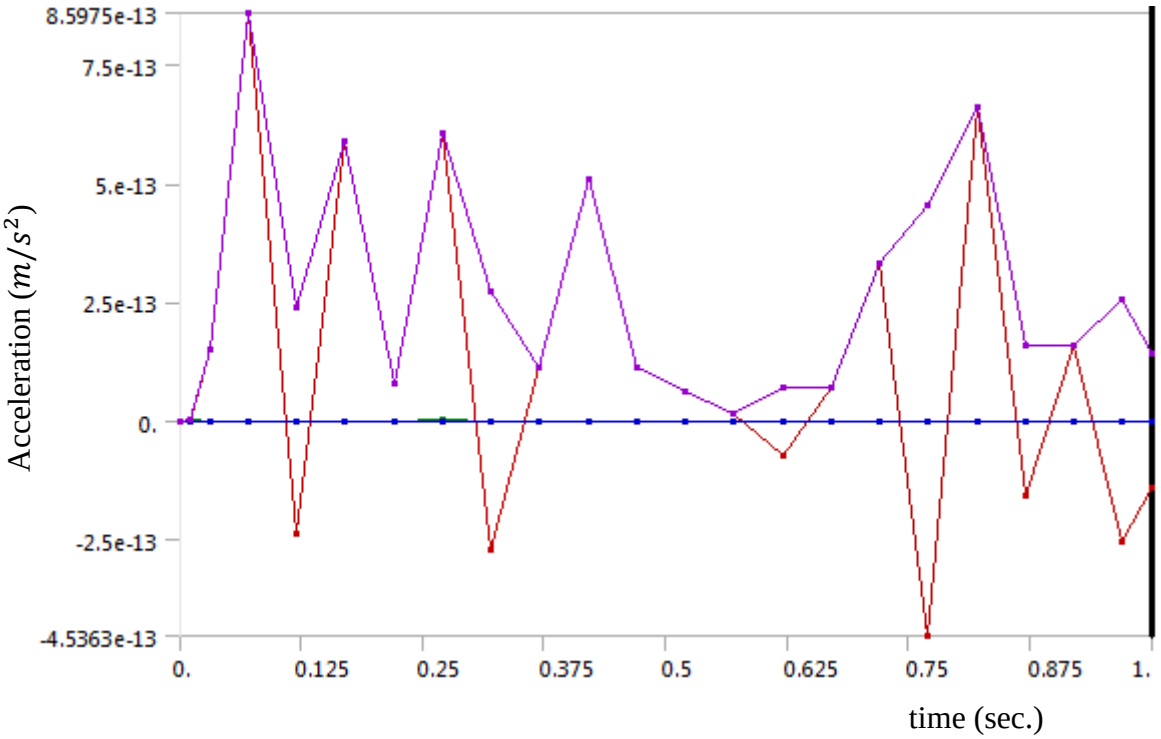

Fig.-19(c): Total Acceleration of the jointed rail

Table-9: Summary of the transient results for the jointed rail

Transient parameter	**Maximum value over the time(1sec)**			
	X-axis	**Z-axis**	**Y-axis**	**Total**
Displacement (m)	9.2903e-017	1.3045e-014	1.199e-014 m	1.7745e-014
Velocity (m/s)	9.4298e-015	1.303e-014	1.1838e-014	1.9841e-014
Acceleration (m/s^2)	8.5975e-017	5.081e-016	2.236e-016	8.5975e-013
Energy probe(potential)(J)	29740			
Energy probe(kinetic)(J)	30562			
Energy probe(External)(J)	5.8284			

- ✓ As it is seen from the result, the displacement and velocity along the Z-axis (the vertical direction) is larger than the other directions (Y-axis and X-axis).

4.4. Thermo-mechanical Analysis during Braking

Due to the application of brakes the heat generation takes place at the wheel-rail contact patch due to friction. The generated heat has conducted away and dispersed across the rail contact cross sections and the temperature of the rail rises. The condition of braking is very severe for the thermal effects that support the rail defects due to the mechanical loads. Thus why, the thermo-mechanical analysis is needed for long life and the structural stability of the rails.

Thermal stresses in the rail are developed due to the difference between the so-called neutral temperature and the service temperature. For service temperatures higher than the neutral temperature, compressive stresses are built up and there is the danger that these may be released by buckling in the rail, with risk of train derailment, an effect on the rail which sometimes is called "sun twists". At temperatures lower than the neutral temperature, tensile thermal stresses raise which act as an additional static loading component together with the wheel loads and the residual stresses.

After verification of the model and boundary conditions, the calculation was started for the time of braking t_b = 14.40 sec, in order to stop the tramcar. The time dependent solver was used for solving. The time set for software is 1 second. The thermal and structural results obtained from ANSYS are deformation, Von Mises stress, thermal flux and temperature gradient.

The types of loads applied in a thermo-mechanical analysis include:

- ✓ Initial temperature
- ✓ Heat flux
- ✓ Wheel load (forces)
- ✓ Standard earth gravity
- ✓ Rotational velocity
- ✓ Elastic stiffness support
- ✓ Boundary conditions and
- ✓ Imported body temperature

4.4.1. During Down-grade Braking

During the process of braking at the downhill, the total mechanical available energy of the tramcar that must be transformed into frictional heat is both kinetic and potential energy. The resisting load for stopping the tramcar is the braking force that is not considering the aerodynamic effects. Thus, the largest braking force is needed at this rail track conditions from the other track level conditions. The thermo-mechanical results are: temperature rise, heat flux variations, thermo-mechanical Von-mises stress and deformations.

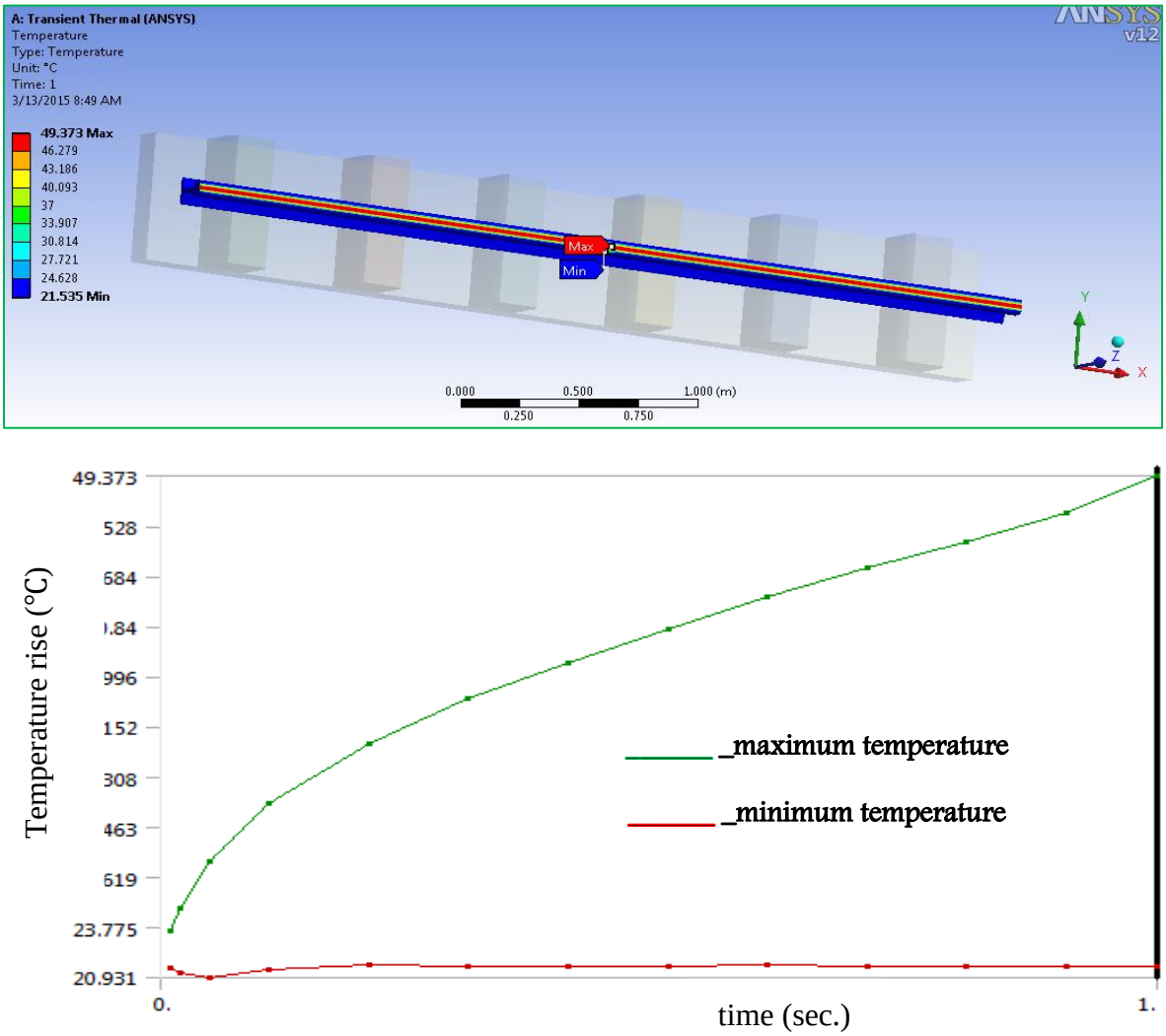

Fig.-20(a): Global rail temperature rise during down-grade braking

- ✓ The global maximum temperature during down-grade level tack braking is 49.373°C
- ✓ Thus, since the melting point of structural steel (1510°C) and the pearlite rail material microstructure change temperature (about 700°C) are much larger than this temperature the rail can withstand the thermal loading.

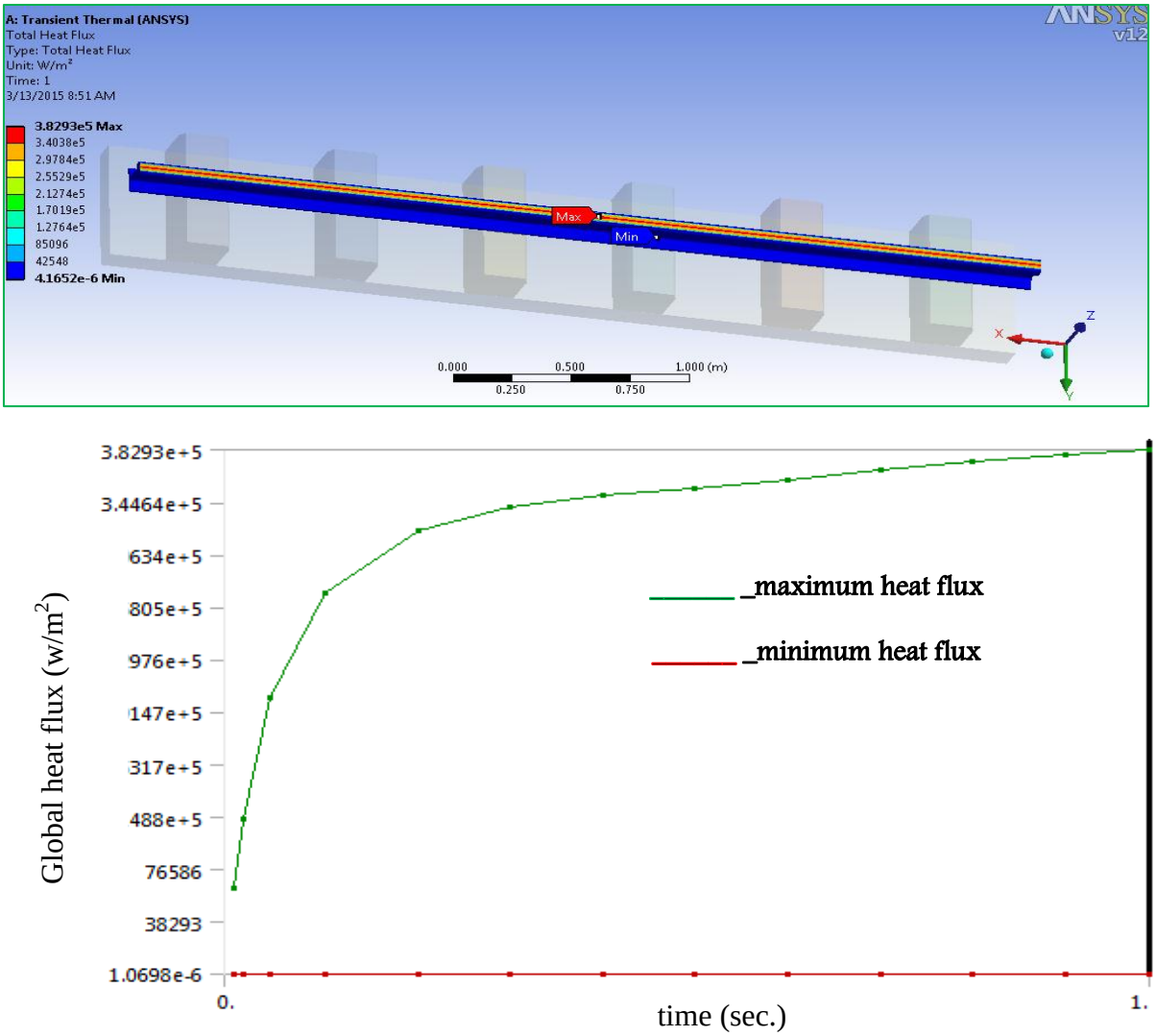

Fig.-20(b): Global heat flux for the down-grade braking

✓ The global residual maximum heat flux is 3.8293e+005 W/m²

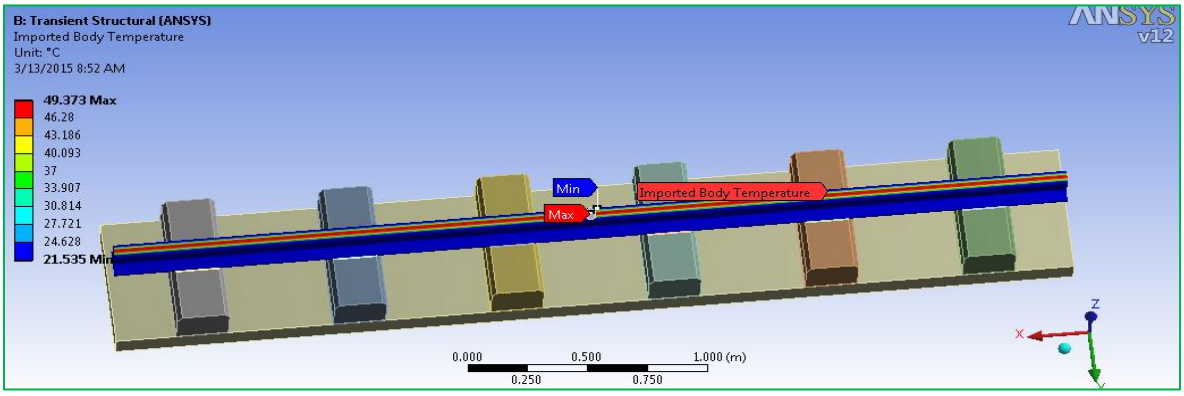

Fig.-20(c): The imported rail body temperature for the down-grade braking

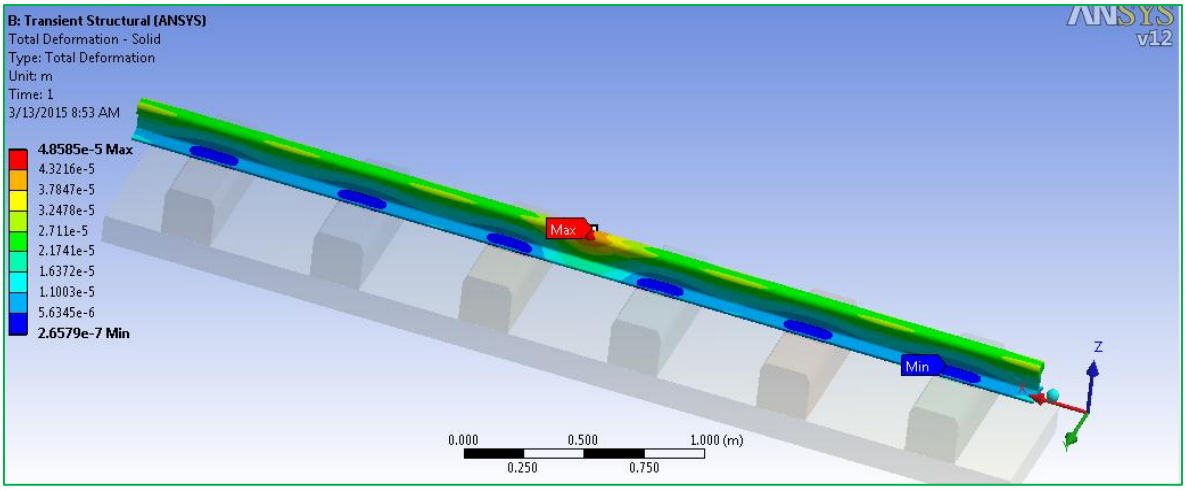

Fig.-20(d): Thermo-mechanical total deformation at the down-grade braking

- ✓ The thermo-mechanical maximum deformation during the down-grade braking is 4.8585e-005 m

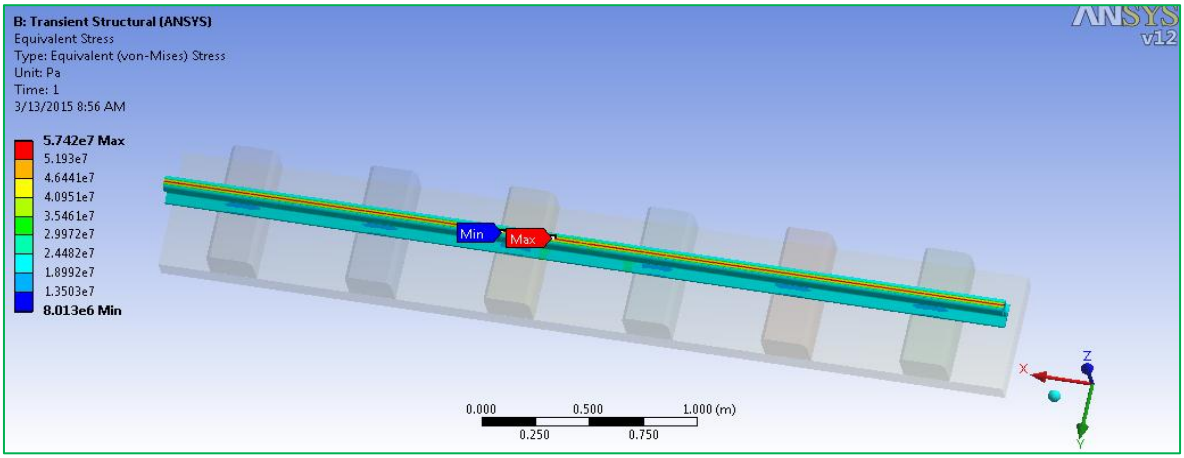

Fig.-20(e): Equivalent (von-Mises) thermo-mechanical Stress at the down-grade braking

- ✓ Since the yield strength of the rail material is 46.0e+007 Pa and the Equivalent (Von-Mises) thermo-mechanical maximum Stress 5.742e+007 Pa, the rail is safe to with stand the thermo-mechanical loading, during braking, at the down-grade.

4.4.2. During the Straight Track Braking

During the process of braking at the straight track, the total mechanical available energy of the tramcar that must be transformed into frictional heat is only the kinetic energy. But, the aerodynamic resistance load which may cause powerful effects if its direction is the opposite of motion is not considered. Thus, the thermo-mechanical results are: maximum temperature rise, heat flux variations, thermo-mechanical Von-mises stress and deformations.

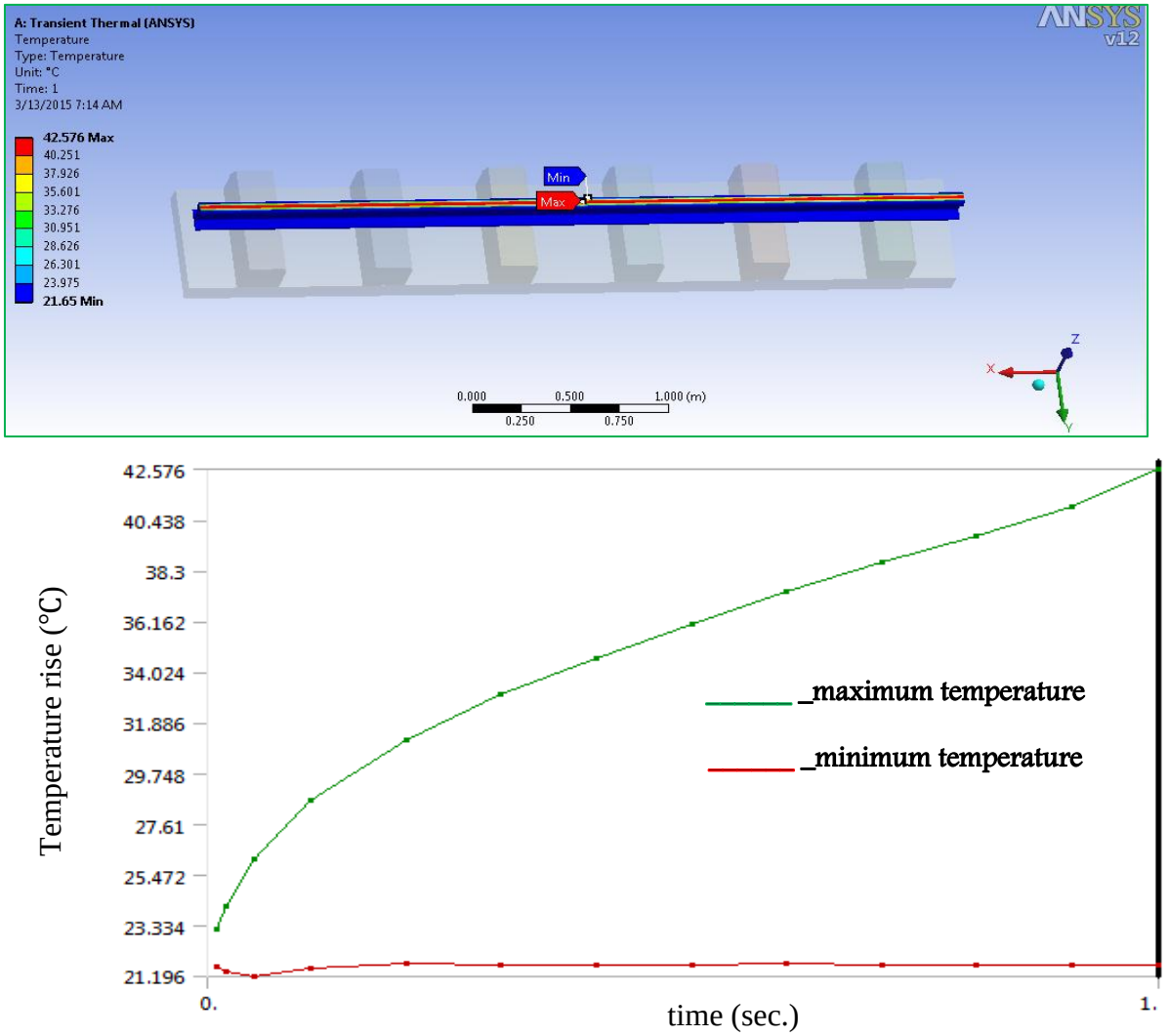

Fig.-21(a): Global rail temperature rise at the straight track braking

- ✓ The global maximum temperature at the straight track braking is 42.576 °C
- ✓ Therefore, since the melting point of structural steel (1510℃) and the pearlite rail material microstructure change temperature (about 700℃) are much larger than this temperature the rail is safe to withstand the thermal loading.

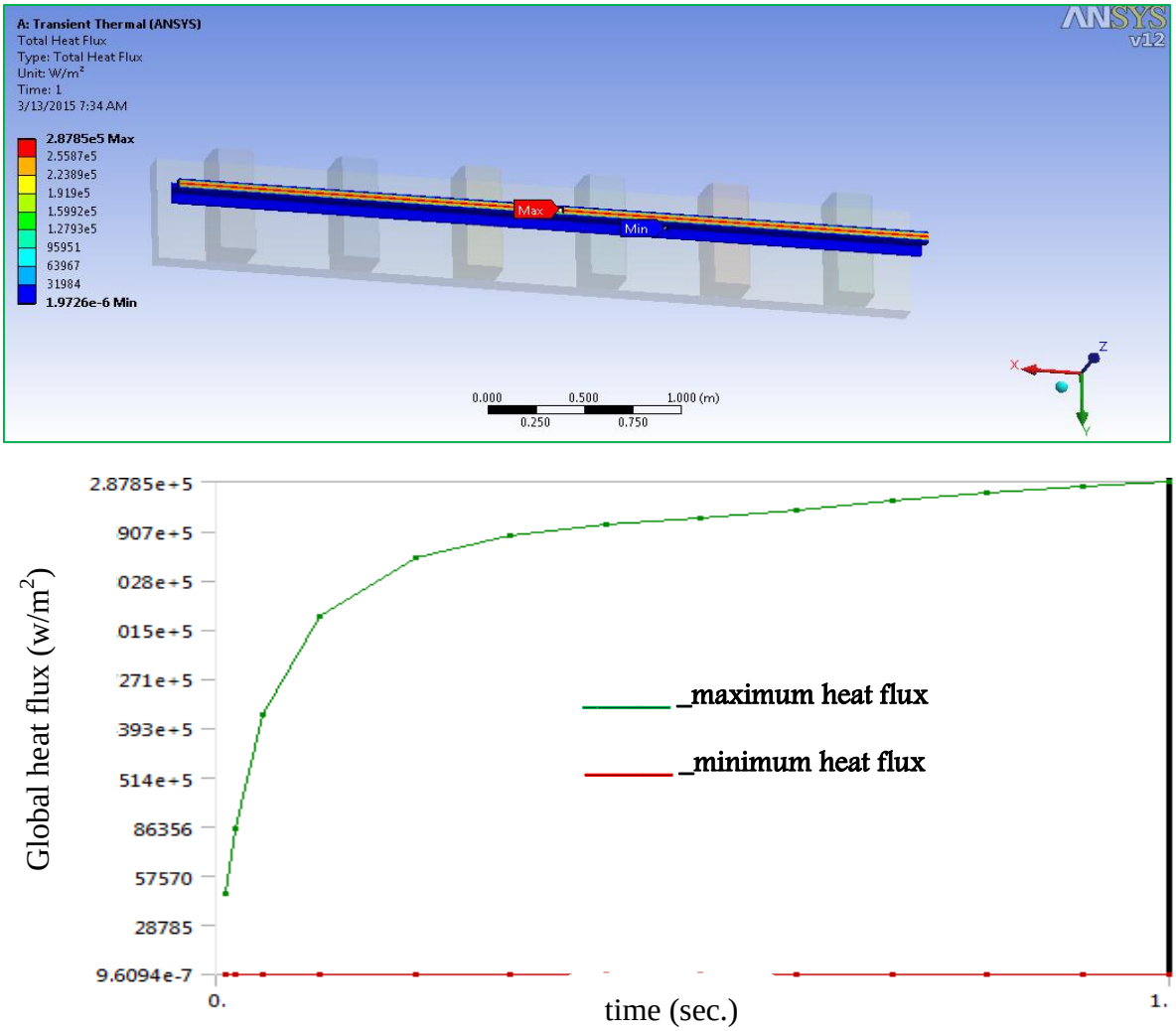

Fig.-21(b): Global heat flux for the straight track braking

✓ The global residual maximum heat flux is 2.8785e+005 W/m²

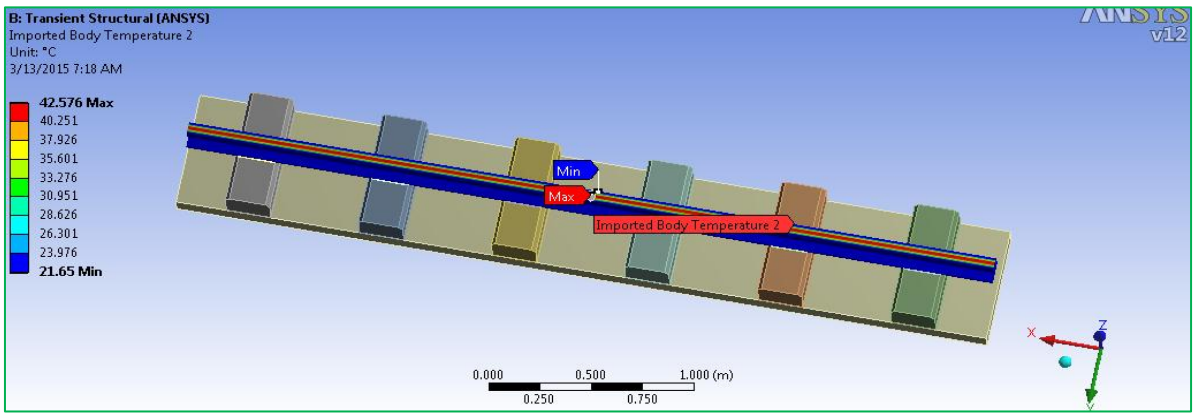

Fig.-21(c): The imported rail body temperature for the straight track braking

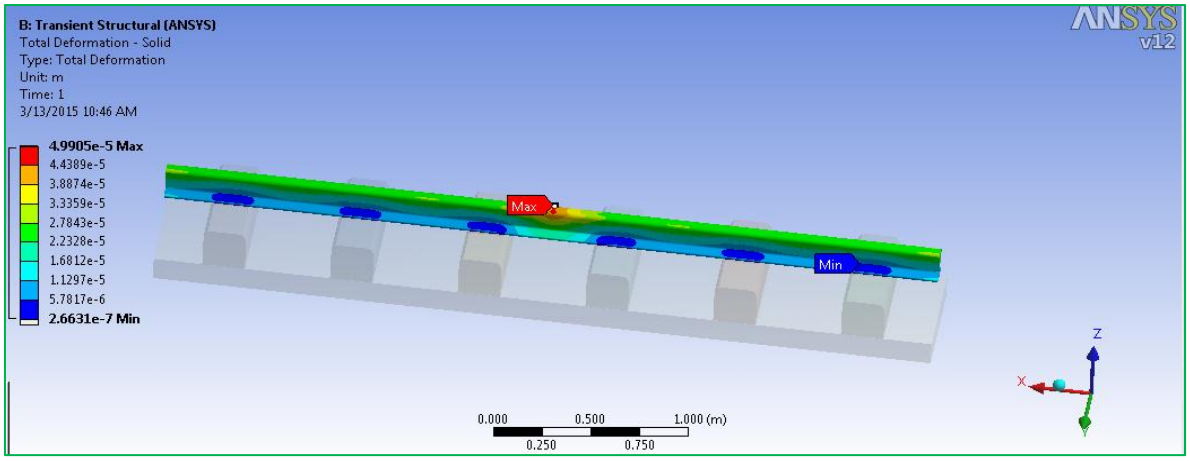

Fig.-21(d): Thermo-mechanical total deformation of a rail at the straight track braking

- ✓ The thermo-mechanical maximum deformation of a rail at the straight track braking is 4.9905e-005 m

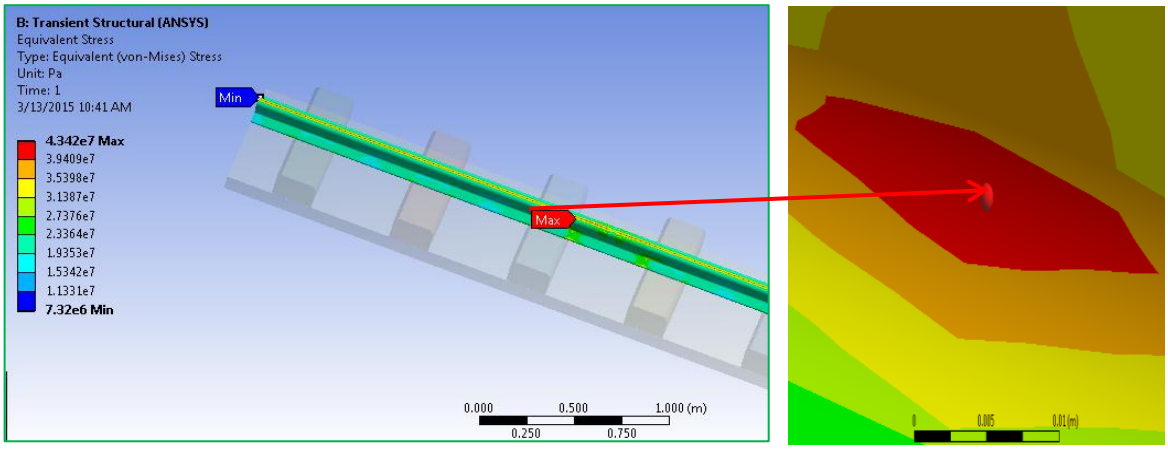

Fig.-21(e): von-Mises thermo-mechanical Stress of a rail at the straight track braking

- ✓ The Equivalent (Von-Mises) thermo-mechanical maximum Stress of the rail during braking at the straight track is 4.342e+007 Pa
- ✓ Hence, since the yield strength of the rail material is 46.0e+007 Pa, the rail can with-stand the thermo-mechanical loading during braking at the straight track.

4.4.3. During the Curved Track Braking

During the process of braking at the curved track, the total mechanical available energy of the tramcar that must be transformed into frictional heat is only the kinetic energy and the resisting loads are instantaneous braking force and the curve resistance forces. The aerodynamic resistance effect is not considered. Thus, the thermo-mechanical results are: temperature gradient, heat flux variations, thermo-mechanical Von-mises stress and deformations.

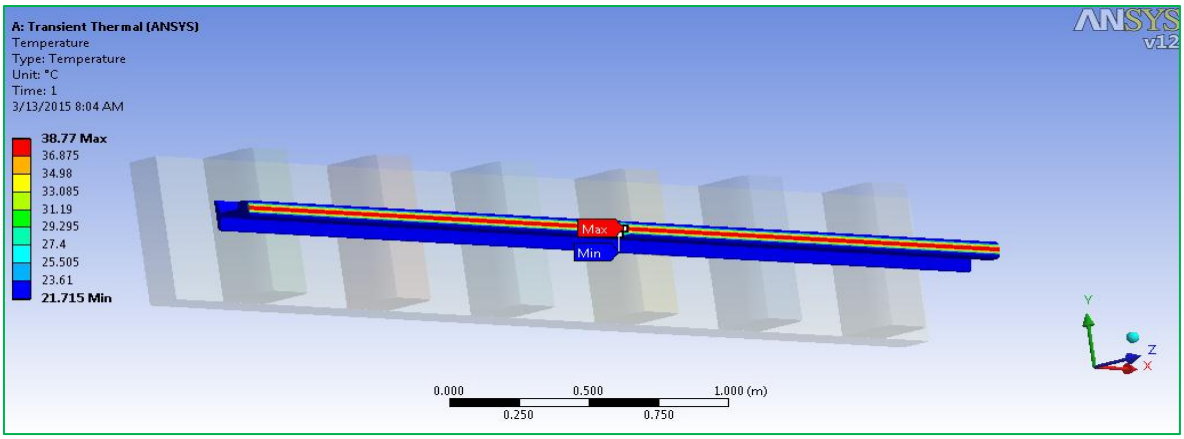

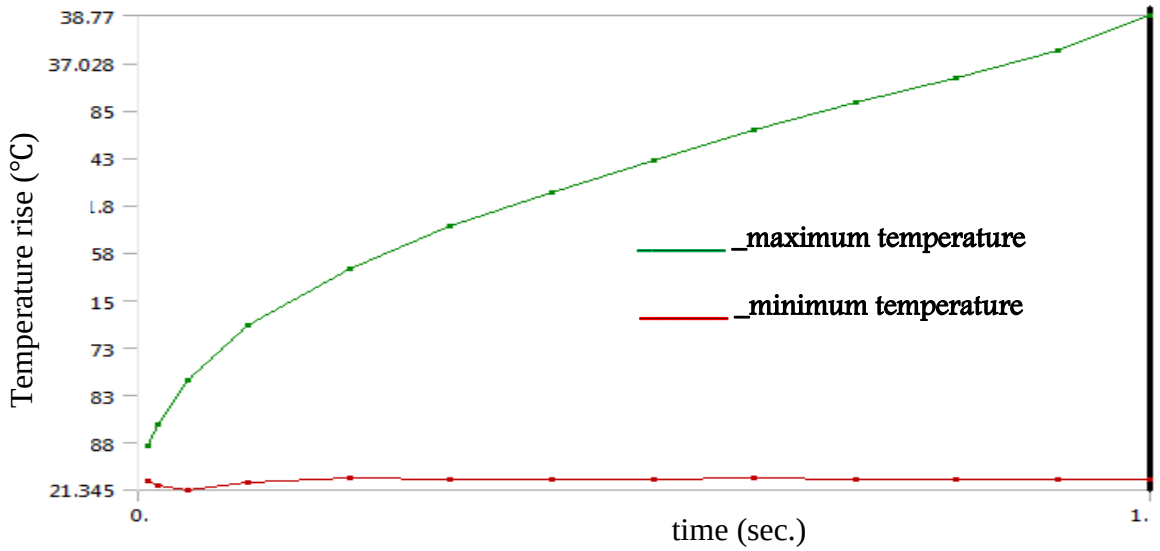

Fig.-22(a): Global rail temperature rise for the curved track braking

- ✓ The global maximum temperature at the straight track braking is 38.77°C
- ✓ Hence, since the melting point of structural steel (1510℃) and the pearlite rail material microstructure change temperature (about 700℃) are much larger than this temperature the rail is safe to withstand the thermal loading during braking at the minimum radius curvature (50m) of the track.

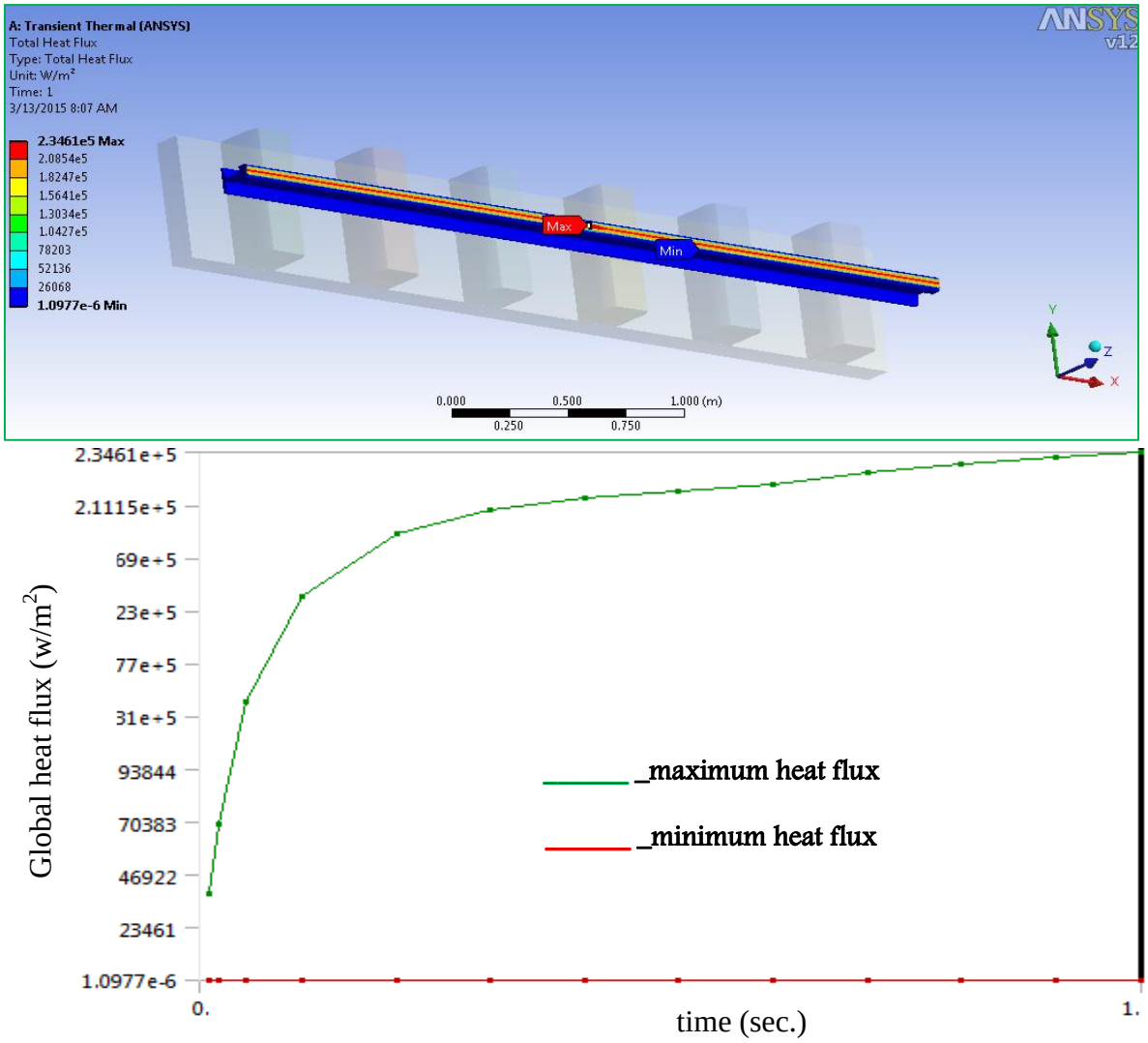

Fig.-22(b): Global heat flux for the curved track braking

✓ The global residual maximum heat flux is 2.3461e+005 W/m²

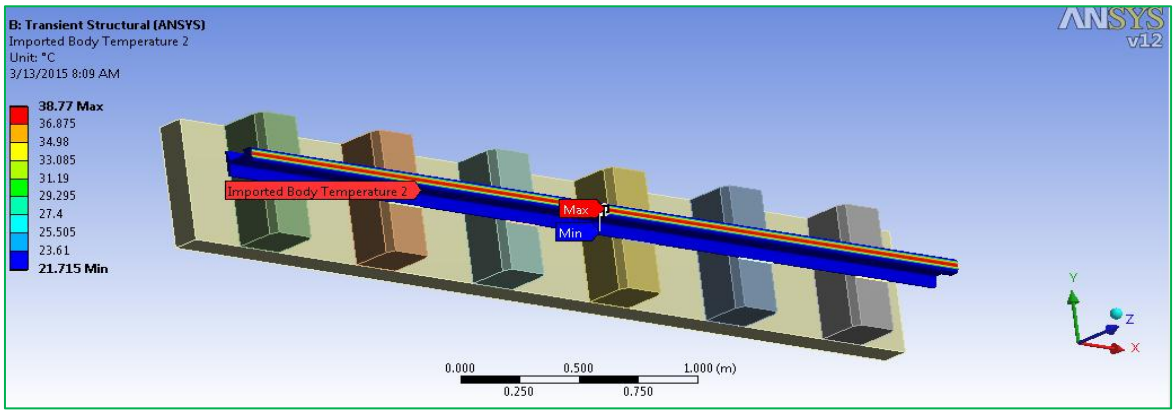

Fig.-22(c): The imported rail body temperature for the curved track braking

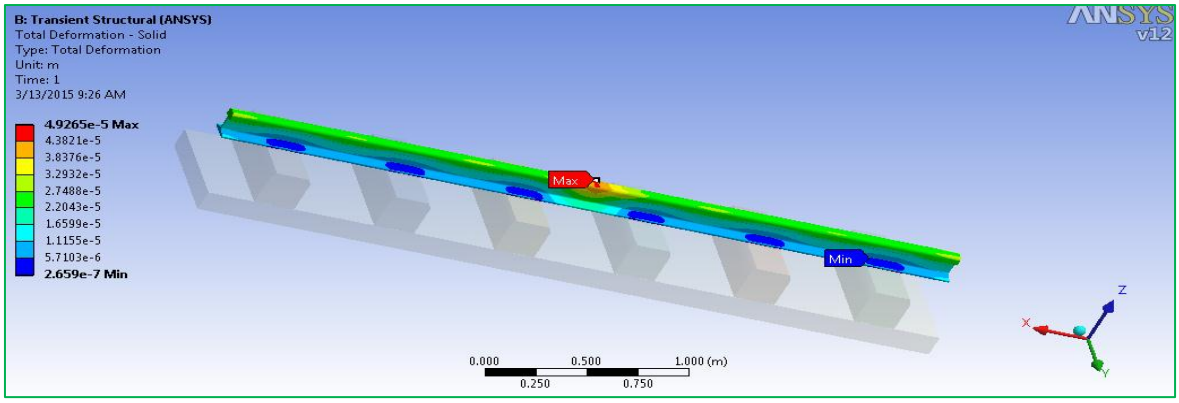

Fig.-22(d): Thermo-mechanical total deformation of a rail at the curved track braking

- ✓ The thermo-mechanical maximum deformation of the rail during braking at the minimum curved track is 4.9265e-005m.

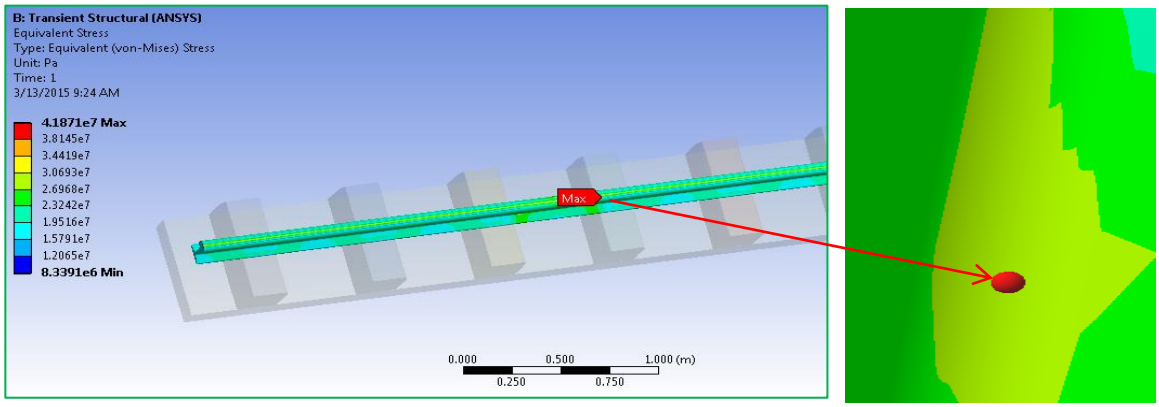

Fig.-22(e): von-Mises thermo-mechanical Stress of a rail during braking at the curved track

- ✓ The Equivalent (Von-Mises) thermo-mechanical maximum Stress of the rail during braking at the minimum radius of curvature (50m) of the track is 4.1871e+007 Pa.
- ✓ Thus, since the yield strength of the rail material is 46.0e+007 Pa, the rail can withstand the thermo-mechanical loading at the 50m radius of curvature of the rail track.

Table-10: Summary of the thermo-mechanical effects on the rail during braking

Parameter per 1sec loading	**Unit**	**Downgrade**	**Straight track**	**Curved track**
Maximum temperature rise	°C	49.373	42.576	38.77
Maximum heat flux	*W/m²*	3.8293e+005	2.8785e+005	2.3461e+005
Maximum deformation	m	4.8585e-005	4.9905e-005	4.9265e-005
Maximum von-mises stress	Pa	5.742e+007	4.342e+007	4.1871e+007

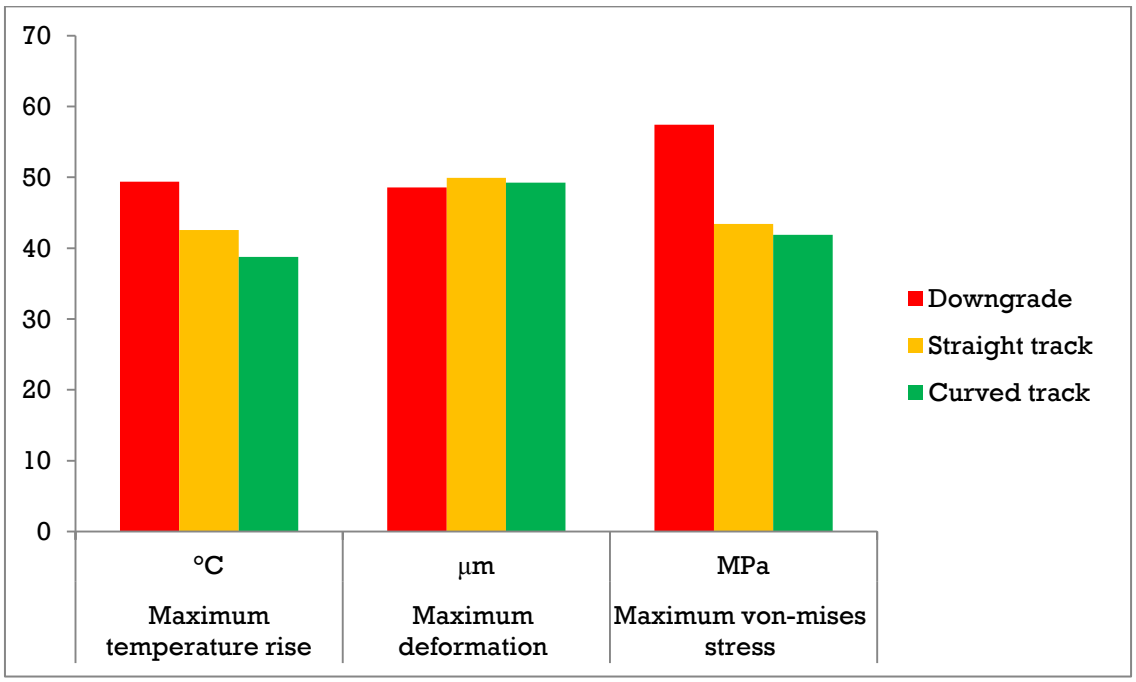

Fig.-23: Thermo-mechanical effect results at downgrade, straight and curved track

In these investigations, the static maximum deformation and von-mises stress result of the rail at the continuum is larger than at the joint while, for the transient analysis, the maximum deformation and von-mises stress of the rail at the joint is larger than at continuum part. For combined thermal and mechanical loads, the maximum deformations and Von-mises stress is much larger than the static and transient results due to the temperature rise. Also, the temperature rise is much smaller than the melting point and microstructure changing temperature of the pearlite steel rail material, and for all cases, the Von-mises stress is less than the rail material yield stress. Hence, the rail can withstand the dynamic, static, thermal and thermo-mechanical loadings. The vertical displacement, velocity and accelerations are larger than in the other directions. From the modal results of the continuum and jointed rail conditions the natural frequencies are much smaller than the standard frequency limits.

CHAPTER-FIVE: CONCLUSIONS AND RECOMMENDATIONS

5.1. Conclusions

This study focused on two loading effects on the rail. The first is the investigation of dynamic effects and the second is thermo-mechanical effects of the contacts between vehicles and rail track during braking. In dynamic analysis, the modal and mechanical transient effects are investigated. Since, a modal analysis is performed on a pre-stressed structure; the static loading effect was first validated. Then, the maximum deformation, the first five natural frequencies and its mode shapes for both continuous and jointed rail were discussed. In the transient structural(MBD), the total displacement, total velocity, total acceleration, freedom effects in three axes (along-X, Y, and Z) and the energy probe (both kinetic and potential) are also investigated. In this study, the stiffness and damping effect of the polyethylene rail-pads and ballast were considered. Further, the retrieved results were discussed and validated. The result shows that the rail can with-stand both static and dynamic load effects. Also, the first five natural frequencies results are much less than frequency limit (1-1.5KHz) for the standard rail.

The thermo-mechanical analysis entailed the transient thermal effects on the rail, in addition to the static mechanical loads. In this case, the rail body temperature that is generated during braking was imported to the mechanical loading and the combined effects were explained. Due to the friction force, thermal power penetrant at the continuous rail surfaces increased. The transient mechanical effect also increased due to the contact body temperature rises. The thermo-mechanical braking effects developed on the three rail track level conditions: during the downgrade braking, at the straight track braking and at the curved track braking. As shown in results, the combined thermal and mechanical effects are the highest at the downhill braking.

5.2. Recommendations

The rail of the track shall be designed as stiff as possible to resist the incoming compressive, vertical, quasi static, vibration stress, dynamic loads, and thermal effects and at the same time it should provide better guidance to the wheel of the train. So, this study recommends giving attention for design and care of the rail. The rail joint needs especial design and handling of the dynamic effects (the vibration and transient structural effects) while the continuum rail requires notable consideration of the static loads with track alignments. The rail-pad, sleeper and ballast should be selected and well equipped with rail to reduce the static and dynamic effects. This paper also recommends that the dynamic loads, friction wear rate and heat power penetrant should be considered in design and treatment of the rail in addition to the mechanical loads.

5.3. Future works

However, there are some better achievements obtained here, there are many ways in which the present work could be continued. Here some topics are presented that would be of interest to investigate in the near future. These would be:

- Explicit dynamic effect of the rail joint components
- Fatigue analysis and rail life predictions on the different rail track level conditions
- Rail burn defect and crack initiation at the tip end and continuous rail heads
- Optimization of rail contact loading along the principal coordinate the rail profiles
- The effect of rail end gap on the wheel at the rail joints

References

[1] Ajay Kapoor, F. Schmid , David I. Fletcher, K.J. Sawley and M. Ishida (2001), Tribology of Rail Transport, University of Sheffield, Transportation Technology Centre and Railway Technical Research Institute, CRC Press LLC.

[2] Bian, Jian, Gu, YuanTong, & Murray, Martin Howard (2013), Numerical study of impact forces on railway sleepers under wheel flat. Advances in Structural Engineering, 16(1), pp. 127-134.

[3] Bo Liang, Simon Iwnicki, Gu Feng, Andrew Ball, Van Tung Tran, Robert Cattley (2013), Railway wheel flat and rail surface defect Detection by time-frequency analysis, Chemical Engineering Transactions,745-750, DOI: 10.3303/CET1333125

[4] Branislav, Miloš and Milica (2011), New Requirements for the Quality of Steel Rails, Association of Metallurgical Engineers of Serbia AMES, Vol 17, p. 213-219

[5] B. Soleimani1, M.M. jalili (2013), Analytical Approach to Vibration Analysis of the Wheel-rail contact**,** Department of Mechanical Engineering, Faculty of Engineering, Yazd University, Yazd, Iran, Vol. 3, N. 3.

[6] Cătălin Cruceanu (2012), Train Braking, Reliability and Safety in Railway, Dr. Xavier Perpinya (Ed.), ISBN: 978-953-51-0451-3.

[7] China, ICS (2012), Technical specifications of 43kg/m-75kg/m rails,TB/T 2344-07-01

[8] China Railway Group (CRECG) Project Manager Office (2013), Technical Specifications of Vehicles, Light Rail EPC Project of Addis Ababa, Ethiopia, 07.

[9] Constantin-Ioan Barbinta, Cristian Ulianovb, Francis Franklin and Spiridon Cretu (2014), Wheel-rail contact modelling and analysis by considering profiles types and lateral displacement, Transport Research Arena, Paris.

[10] David Thompson (2006), Understanding and Controlling Noise and Vibration from Railways, Institute of Sound and Vibration Research, University of Southampton

[11] David Thompson and Chris Jones (2005), Noise and Vibration from the Railway Vehicles, Taylor and Francis Group, LLC.

[12] David Thompson, Tianxing Wu and Tristan Armstrong (2003), Wheel/Rail Rolling Noise - The Effects Of Nonlinearities in the Contact Zone**,** Institute of Sound and Vibration Research University of Southampton.

[13] D.T. Eadie and M. Santoro (2003), Top of Rail friction control for curve noise mitigation and corrugation rate reduction, Kelsan Technologies Corp., 1140 West 15th St., North Vancouver, B.C., Canada.

[14] European Committee for Standardization; (CEN) (2009), Methods for calculation of stopping and slowing distances and immobilization braking - Part 6: Step by step calculations for train sets or single vehicles, EN 14531-6.

[15] Huan Feng (2011), 3D-Models Of Railway Track for Dynamic Analysis, Department of Transport Science School of Architecture and the Built Environment Royal Institute of Technology, Stockholm.

[16] Husain Abdulrahman Ahmad (2013), Dynamic Braking Control for Accurate Train Braking Distance Estimation under Different Operating Conditions, Blacksburg,USA.

[17] Innotrack (2009), Improved model for the influence of vehicle conditions (wheel flats, speed, axle load) on the loading and subsequent deterioration of rails, Newcastle University, Innotrack Tip5-CT-031415

[18] Jens Nielsen, Eric Berggren, Thomas Lölgen, Roger Müller, Bert Stallaert, Lise Pesqueux (2013), Overview of Methods for Measurement of Track Irregularities Important for Ground-Borne Vibration, Chalmers University of Technology, Trafikverket, DB, SBB, D2S International, Alstom, Rivas_Chalmers_ WP2_D2_5

[19] Katrin Madler and Manfred Mannasch, materials used for wheels on rolling stock, Germany, EN 13262

[20] Liang Bo., Iwnicki Simon, Zhao Yunshi and Crosbee, David (2013), Railway wheel-flat and rail surface defect modeling and analysis by time–frequency techniques, University of Huddersfield Repository, pp. 1403-1421. ISSN 0042-3114

[21] Maksym Spiryagin, Kwan Soo Lee, Hong Hee Yoo, Valentyn Spiryagin and Yuriy Vivdenko (2008), Experimental and Theoretical Investigation of Adhesion Based on Analysis of Wheel-Rail Noise, School of Mechanical Engineering, Hanyang University, Seoul, 133-791, Korea and Department of Informatics, East Ukrainian National University named after Volodymyr Dal, Lugansk, 91034, Ukraine.

[22] Miloš S. MILOŠEVIĆ*, Dušan S. STAMENKOVIĆ, Andrija P. MILOJEVIĆ, and Miša M. TOMIĆ(2012), Modeling Thermal Effects in Braking Systems of Railway Vehicles, Faculty of Mechanical Engineering, University of Niš, Niš, Serbia, Vol. 16, Suppl. 2, pp. S515-S526

[23] National Standards of the People's Republic of China (2007), Hot-rolled steel rails for railway, General Administration of Quality Supervision, Inspection and Quarantine of the People's Republic of China, GB 2585-07-12

[24] Paul Boyd, Manicka Dhanasekar (2002), Wheel / Rail Contact Analysis, Central Queensland University, Australia, QLD 4702.

[25] Peter Avitable, Mechanical Vibrations of Experimental Modal Analysis, University of Massachusetts Lowell

[26] Prachi Katheriya, Veerendra Kumar, Anshul Choudhary and Raji Nareliya (2014), An Investigation of Effects of Axle Load and Train Speed at Rail Joint Using Finite Element Method**,** M.P., India.

[27] Riccardo Ferrara, Giovanni Leonardi and Franck Jourdan (2013), A Contact-Area Model For Rail-Pads Connections In 2-D Simulations: Sensitivity Analysis of Train Induced Vibrations, HAL.

[28] Roger Mueller (2011), Measurements of rolling stock influence on railway vibrations and an overview of rolling stock mitigation measures, Rail Environmental Center, SBB, Hochschulstrasse 6, CH-3000 Bern 65.

[29] R. Corradi, P. Crosio, S. Manzoni and G. Squicciarini (2011), Experimental investigation on squeal noise in tramway sharp curves, Politecnico di Milano, Department of Mechanical Engineering, Via La Masa, 1133.

[30] Sinan Al Suhairy (2000), Prediction of Ground Vibration from Railways**,** SP Swedish National Testing and Research Institute Acoustics.

[31] Slawomir Duda(2010), Simulation Of Railway Vehicle Motion On the Straight Track, Silesian University Of Technology, Department Of Applied Mechanics,Vol. 17, No. 1

[32] Traian Mazilu (2007), A Dynamic Model For The Impact Between the Wheel Flat And Rail**,** Department of Railway Vehicles, University "Politehnica"of Bucharest, Romania, Vol. 69, No. 2

[33] Vahid Monfared (2012), Contact Stress Analysis in Rolling Bodies by Finite Element Method (FEM) Statically, Department of Mechanical Engineering, Zanjan Branch, Islamic Azad University, Zanjan, Iran, 2(2): 12-16

[34] WISCO China (2013), Steel rail products, Railway Standards TB/T2344 and National Standard GB2585.

[35] Xiaogang Liu and Paul A Meehan (2013), Investigation of the effect of lateral adhesion and rolling speed on wheel squeal noise, Proceedings of the Institution of Mechanical Engineers, Part F: Journal of Rail and Rapid Transit 2013 227: 469, DOI:10.1177.

[36] Yung-Chuan Chen, Li-Wen Chen, Sing-You Lee and Jao-Hwa Kuang(2007), A wheel and a corrugated rail thermal contact simulation during braking sliding, 12th IFToMM World Congress, Besançon (France), NPUST Pingtung, Taiwan.

Appendices

Appendix-A

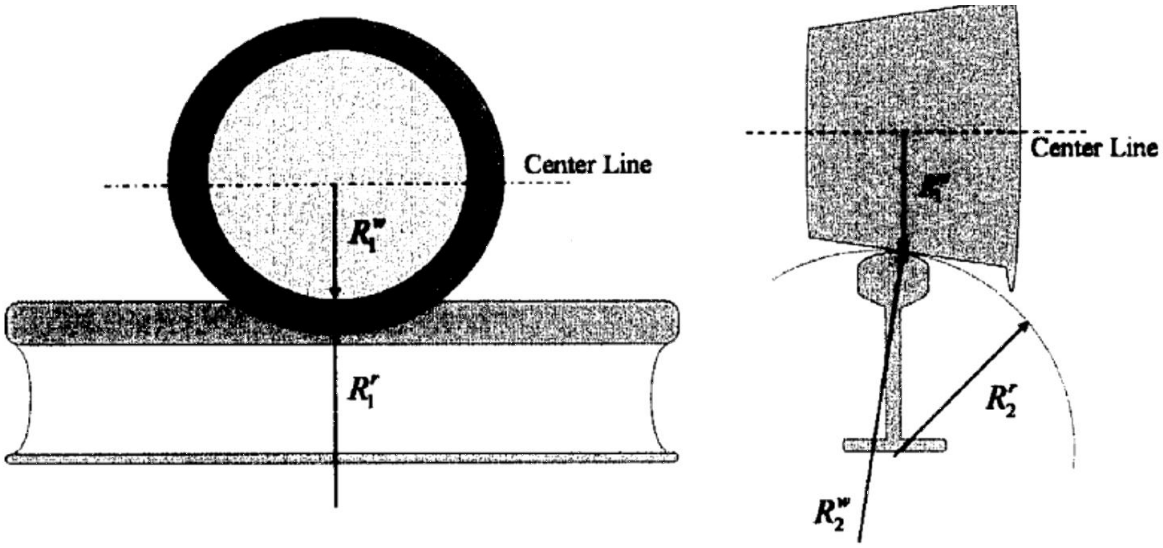

Fig.-24: Principal radii of curvature for wheel and rail

Table-11: Coefficients m and n for different values of θ

Θ (°)	m	n	Θ (°)	m	n	Θ (°)	m	n
0.5	61.400	0.1018	55.0	1.611	0.678	130.0	0.6410	1.754
1.0	36.890	0.1314	60.0	1.486	0.717	135.0	0.6040	1.926
1.5	27.480	0.1522	65.0	1.378	0.759	140.0	0.5670	2.136
2.0	22.260	0.1691	70.0	1.284	0.802	145.0	0.5300	2.397
3.0	16.500	0.1964	75.0	1.202	0.846	150.0	0.4930	2.731
4.0	13.310	0.2188	80.0	1.128	0.893	160.0	0.4123	3.813
6.0	9.790	0.2552	85.0	1.061	0.944	170.0	0.3112	6.604
8.0	7.860	0.2850	90.0	1.000	1.000	172.0	0.2850	7.860
10.0	6.604	0.3112	95.0	0.944	1.061	174.0	0.2552	9.790
20.0	3.813	0.4123	100.0	0.893	1.128	176.0	0.2188	13.310
30.0	2.731	0.4930	105.0	0.846	1.202	177.0	0.1964	16.500
35.0	2.397	0.5300	110.0	0.802	1.284	178.0	0.1691	22.260
40.0	2.136	0.5670	115.0	0.759	1.378	178.5	0.1522	27.480
45.0	1.926	0.6040	120.0	0.717	1.486	179.0	0.1314	36.890
50.0	1.754	0.6410	125.0	0.678	1.611	179.5	0.1018	61.400

Appendix-B

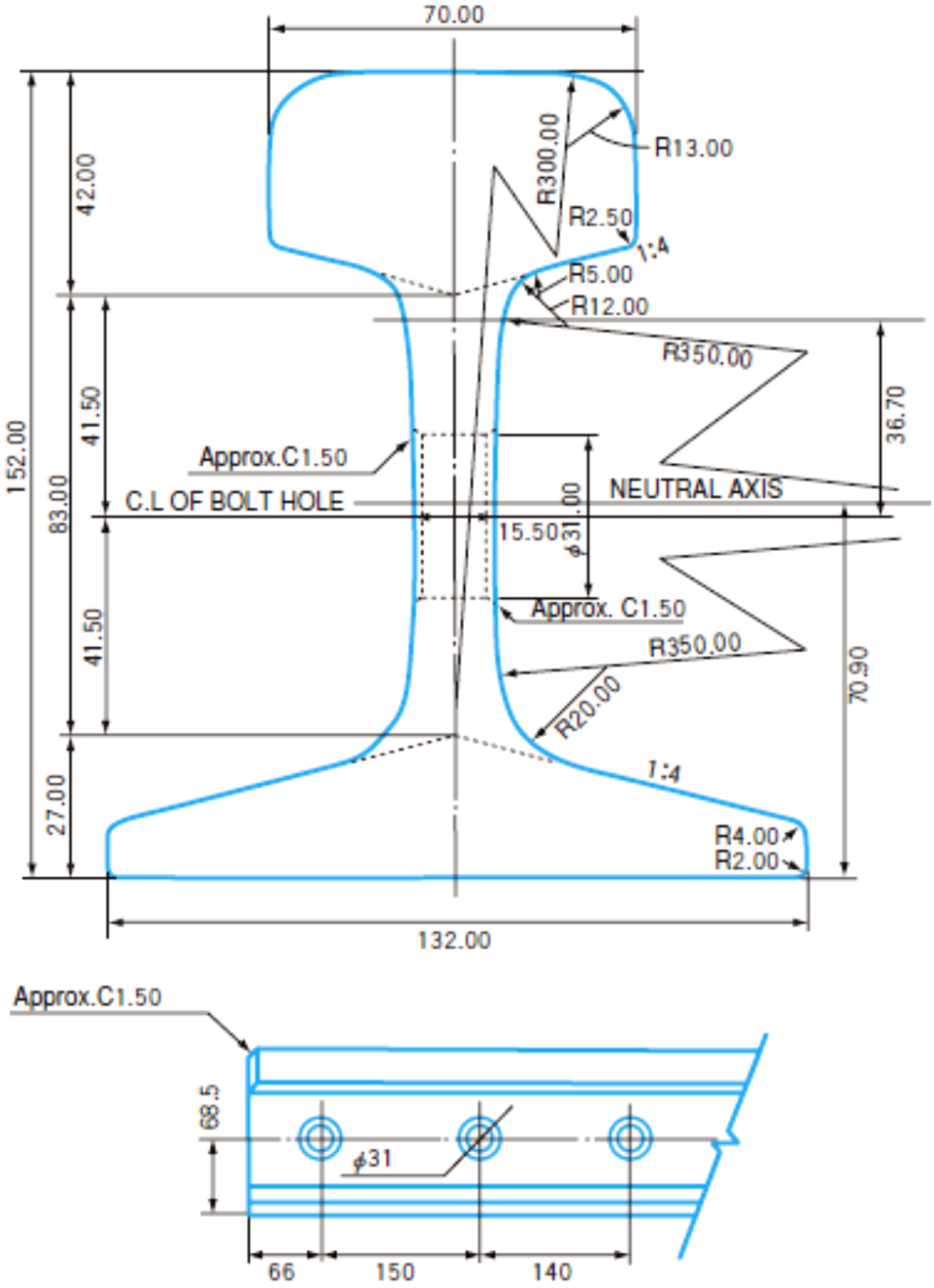

Fig.-25: Rail profile for 50kg/m

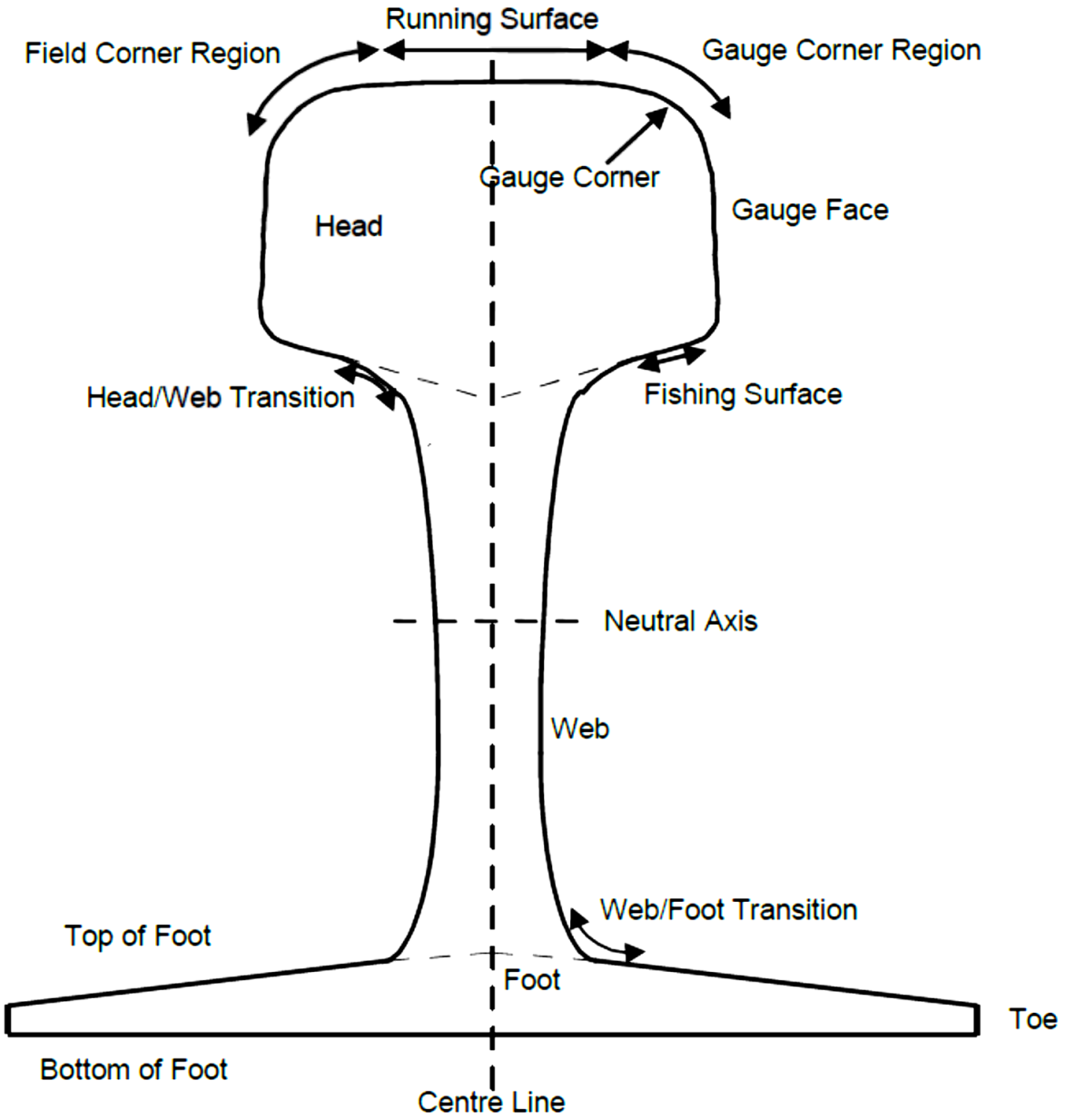

Fig.-26: Terminology used for rail profiles

Table-12: The typical values of K in computing curve resistance coefficient

Rail System	The Value of K
SNCF	800
Japan	800
AREMA	700
China	700
Department of Rapid Transit Systems, Taipei City Government	700
Taiwan Railway Administration (TRA)	600
IR Universalformel	516
RFFS Universalformel	505